Title page

Specialisation: Chemical Engineering, Environmental Nanotechnology
Title: Investigation of Fouling Formation during H_2S Scavenging with 1,3,5-tri-(2-hydroxyethyl)-hexahydro-s-triazine
University: Esbjerg Institute of Technology – Aalborg University
Supervisor: Erik G. Soegaard
Collaborators: Maersk Oil and Dansk Shell
Project period: 1/2-2011 - 6/6-2011
Semester: 10
Date of hand in: 6/6-2011

Henrik Taekker Madsen

Preface

The project is a master thesis that concerns the issue of fouling formation during the refining of oil at Shell in Fredericia, Denmark, and how the fouling relates to Maersk Oil's use of the H_2S scavenger 1,3,5-tri-(2-hydroxyethyl)-hexahydro-s-triazine. It has been an intriguing subject to work with, and the problem has been a real challenge. Still, no matter how exciting this project has been, I am quit sure that I will not miss the foul smell of H_2S and triazine.

At the end of the report a nomenclature list is found. Words included in the nomenclature list will be marked with a star (*) the first time they appear in the report.

Sources are referred to with a number in square brackets, [X], indicating their placement in the bibliography. In the bibliography, the sources are listed alphabetically by the surname of the author. For books author, title, volume, editor and year of publication are given. For articles author, title, journal, and year of publication are given. For web pages author, url and the date for when the information was retrieved from the web page are given.

After the conclusion, a number of appendixes are found. These cover background theory for the experimental methods used in the project, raw eperimental data and experiments deemed non-essential to the main report.

On the attached CD an Excel file with the mass balance and a M-file with the script for the kinetic model are found.

I would like to thank Flemming Egebjerg from Dansk Shell A/S for valuable information about the fouling problem at Shell, as well as for providing physical and chemical data for the refining process. The laboratory personal at Esbjerg Institute of Technology also deserves great thanks for their help with the experimental analyses. Special thanks to Dorthe Spangsmark, Linda Madsen and Heidi Thomsen. Last but not least, many thanks to Kenneth Andersen from Maersk Oil for supply of triazine, spent scavenger, and oil samples, for being most helpful with supplying process data, and for good discussions.

I hope you will find the subject as intriguing as I have.

Henrik Tækker Madsen
Esbjerg, June 2011

Abstract

During the refining of oil, Shell in Fredericia, Denmark, has encountered a fouling rich in carbon and sulphur, which clogs up their water treatment system. The fouling is suspected to be linked to the H_2S scavenger 1,3,5-tri-(2-hydroxyethyl)-hexahydro-s-triazine used by Maersk Oil. Here the final product, s-trithiane, could explain the high content of sulphur and carbon. The scavenging reaction and the structure of the fouling are investigated in this project, which aims at documenting whether two processes are connected, as well as understanding how the fouling is formed, to find a way of either avoiding or removing it.

With information supplied by Maersk a mass balance was made, and with data from litterature a kinetic model for the reaction system was constructed. The scavening reaction was investigated by measuring the composition of the reaction mixture at different times with ESI-MS. This was done for three reactions: HS^-/triazine, H_2S/triazine and H_2S/spent scavenger, to investigate if experiments with HS^- are representative for the real reaction between the spent scavenger and H_2S. Also, the effect of heating and the reaction between MEA and H_2S were investigated. The fouling was analysed with IR and XRD, and compared to pure trithiane. Furthermore, a TS/VS analysis and a HSP analysis was made.

The mass balance indicated strongly that the bulk of the spent scavenger is discharged with the produced water, but that during maintenance the amount of spent scavenger in the oil may increase with factor of 43. The kinetic model showed the scavening reaction to be much faster than the hydrolysis of the triazine, which should ensure only low amounts of formaldehyde in the reactiom mixture. The experiments with the scavenging reaction demonstrated that the triazine is first converted to thiadiazine, and then to dithiazine where the reaction terminates. Trithane was not detected. Also, the experiments demonstrated that by overspending the scavenger with H_2S a precipitate identical to the Shell fouling is formed. The fouling was found to be semicrystalline, and the IR analysis showed it to contain different C-S bonds, and also indicated a ring opening. The fouling was found to be very difficult to dissolve, although being affected most by solvents with HSP values of δH = 0-9 and δP = 5-11. In a reaction between MEA and H_2S, a small amount of disulphide was detected with GC-MS.

The fouling at Shell has been proven to be a direct result of the use of H_2S scavenger by Maersk. The reaction terminates at dithiazine, which then most likely reacts in a polymerisation reaction, where a polymer consisting of dithiazine molecules connected by chains of carbon and sulphur is formed.

Contents

Introduction

During the production of natural gas it is sometimes necessary to clean the gas for impurities to reach existing standards. One such impurity is hydrogen sulphide, H_2S; an undesireable compound in the final product because of its toxicity and foul smell. Also, H_2S causes problems with wear and tear on the equipment because it is a corrosive chemical.

In the effort of removing H_2S, the Danish oil and gas company Maersk Oil has used 1,3,5-(2-hydroxyethyl)-hexahydro-s-triazine, which is a known H_2S scavenger. However, this has apparently led to problems further downstream during the refining of the oil. Here Shell, who purchases crude oil from Maersk, has experienced severe fouling at several locations in their refinery. The fouling is found in the water treatment system, where it clogs up the system, making it necessary to shut down the refinery to remove the fouling.

Via elemental analyses, the fouling has been found to consist heavily of carbon and sulphur, and Shell therefore suspects the fouling to be related to the presence of reaction products from the scavenging process in the crude oil they receive from Maersk. Especially the final reaction product from the scavenging reaction, s-trithiane $C_3H_6S_3$, has received much attention since the chemical structure could explain the high content of carbon and sulphur in the fouling.

To avoid fouling, it is necessary to understand the processes leading to its formation, and these processes might very well be the scavenging reaction. The literature on the scavenging with triazines is scares, but a Norwegian study indicates that trithiane is not formed during the scavenging of H_2S with 1,3,5-(2-hydroxyethyl)-hexahydro-s-triazine. This might therefore question whether the fouling really is trithiane; if not, the fouling might possibly originate from another process than the scavenging reaction. As a result, the initiating problem for this project is:

> *How does the H_2S scavenger system with 1,3,5-(2-hydroxyethyl)-hexahydro-s-triazine function, what is the nature of the fouling, and why is it created?*

To answer these questions, a theoretical study of the scavenger system will be made alongside with experiments. The theoretical study will focus on understanding the concept of H_2S scavenging as well as the specific scavenger system. Also, models will be created to investigate the plausibility of the scavenger being the source for the fouling. The experiments will focus on investigating the reaction mechanism of the scavenging process and the nature of the fouling, to see if these may be linked.

Chapter 1

H_2S in natural gas

Natural gas is primarily made up of methane, CH_4, together with smaller amounts of the other short chained alkanes, but also contains a variable amount of impurities. Table 1.1 gives an overview of the composition of natural gas, which may vary significantly depending on where in the world the gas is produced.

To comply with existing quality demands, the H_2S level must not exceed certain threshold limits. For natural gas in Denmark, a maximum of 5 $\frac{mg}{m^3}$ H_2S and a maximum total sulphur of 150 $\frac{mg}{m^3}$ is allowed, and should the average values exceed 3 $\frac{mg}{m^3}$ H_2S and 50 $\frac{mg}{m^3}$ total S for longer periods of time, then it must be reported to the DGP (Danmarks Gasmateriel Prøvning) [24].

Table 1.1: Constituents of natural gas [27]

Name	Formula	Vol.%
Methane	CH_4	>85
Ethane	C_2H_6	3-8
Propane	C_3H_8	1-5
Butane	C_4H_{10}	1-2
Pentane $\leq$	$C_5H_{12}^{\dagger}$	1-5
Carbon dioxide	CO_2	1-2
Hydrogen sulphide	H_2S	1-2
Nitrogen	N_2	1-5
Helium	He	<0.5

[†] Pentane and higher aliphatic hydrocarbons including benzene and toluene

1.1 Formation of natural gas in the underground

Underground hydrocarbon deposits are associated with sedimentary rocks*, indicating that the hydrocarbons originate from microscopic plant and animal life that have been entrained by sediment during the history of the Earth. In time, the organic material and the clastic rock*, among which it was entrained, turned into a sedimentary source rock, where hydrocarbons were formed.

If the life forms became covered with sediment rapidly after dying, aerobic decay processes were avoided, and instead a reducing environment was created. As the layer of rock above the organic material increased, so did the pressure and temperature, allowing liquifaction and gasifaction processes to occur. During these processes, the organic material in the reservoir was transformed into hydrocarbons. For significant amounts of hydrocarbons to be present at a specific location, the amount of organic material originally deposited there has to be high, and so does the sediment input. Therefore, many deposits are found at sea on the continental shelves, where life flourished early and where rivers could bring large amount of sediment to the basins [20].

A source rock is the rock from where the hydrocarbons originate; however, because of gravitational diffusion, the hydrocarbons does not remain here. Since pressure is increasing with depth, the hydrocarbons have a natural tendency of moving towards the surface. The rate of diffusion depends on the rock type through which the fluids move. Very porous rock types, like limestone and sandstone, gives high diffusion, whereas layers with low porosity, such as shale*, limits the diffusion. In certain situations, this difference in porosity between the types of rock creates pockets where the hydrocarbons may become trapped, creating a reservoir. An example of such a hydrocarbon trap is shown in figure 1.1.

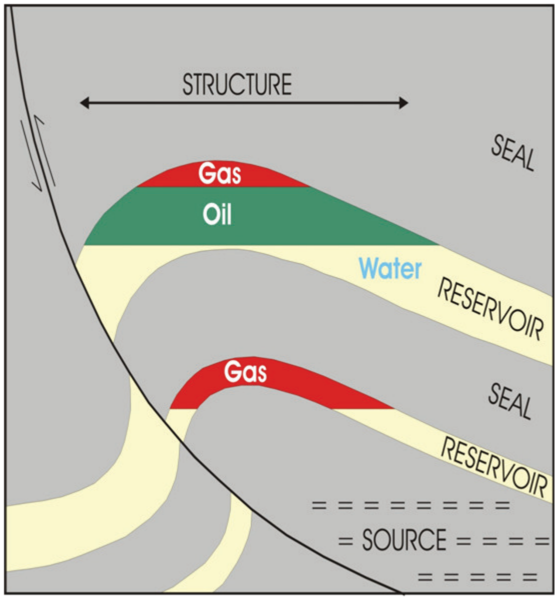

Figure 1.1: Anticlinal hydrocarbon accumulation [20]

The reservoir consists of a reservoir rock and a cap rock. The reservoir rock have a high permeability, while the cap rock is an impermeable rock that encloses the reservoir rock, and in this way inhibits the hydrocarbons from further diffusion. Because of the difference in density between the gas, oil and water, a multiphase solution will form in the pocket with gas on top followed by oil saturated by gas and finally water.

Part of the H_2S found with the hydrocarbons originates from the sulphur containing parts of the organic material, such as the two amino acids cysteine and methionine, while minerals like anhydrite ($CaSO_4$) also contribute to the total amount of sulphur. There exist several natural processes from which H_2S may be formed, and these include thermal cracking, indigenous sulphate-reducing bacteria (SRB's), and thermochemical sulphate reduction [16].

Through thermal cracking, the larger organic molecules containing sulphur may be broken down into smaller compounds, which eventually may convert into H_2S. Sulphate ions present in the reservoir may be converted either biologically, through specialised bacteria who obtain their energy via oxidation of organic compounds while reducing sulphate to H_2S, or via thermal processes. If the temperature is sufficiently high, above 140 °C [16], hydrocarbons may be thermally oxidised while sulphate is reduced with H_2S as a by-product.

Because sulphate is a contributor to H_2S formation, reservoirs where seawater has been injected may show high concentrations of H_2S. This is because seawater naturally contains around 2,800 ppm sulphate [16], which after injection may be converted to H_2S as described above. The reason for injecting seawater into a reservoir is to maintain a high pressure. When gas and oil are retrieved from a reservoir, the pressure in the reservoir drops, and it will be increasingly difficult to extract the remaining gas and oil. Therefore, by injecting water into the reservoir the pressure may be maintained, but as mentioned earlier this will add sulphate to the reservoir when seawater is used [20].

There are several reasons for removing H_2S from natural gas. First of all, it is a very toxic compound as seen in table 1.2. Because of the toxicity of H_2S, the human sensory organ has evolved in such a way that even concentrations down to 0.003 ppm can be

Table 1.2: H_2S toxicity data [21]

Concentration (ppm)	Effects
0.003-0.02	Clearly detectable by smell
3-10	Very unpleasant smell
20-100	Distinct smell of rotten eggs
50-100	Stinging pain in eyes and irritation of respiratory organs
100-200	Sedation of olfactory sense
250-500	Fluids in lungs, cyanosis, bloodstained cough, pneumonia
500-	Headache, vertigo, paralysis of respiratory muscles, unconsciousness
500-1000	Stop for respiration, immediately collapse, death

detected, and the gas is associated with an obnoxious smell. H_2S and other sulphur compounds may also give problems further downstream the processing of the oil/gas if not removed. Many of the catalysts used in the refining process are poisoned by sulphur, making it necessary to remove sulphur prior to the catalytic processes. Furthermore, H_2S will be very harsh for the equipment. In an anhydrous environment the corrosive ability is very low, but in a wet gas, H_2S becomes a very corrosive agent. In natural gas both CO_2 and H_2S will give rise to an acidic environment. To distinguish between different types of natural gas, where the acidic environment is either caused by CO_2 or H_2S, natural gas with only CO_2 is called ”sweet gas” and natural gas with H_2S is called ”sour gas” [16]. The differentiation is made because H_2S is more corrosive than CO_2. In an acidic environment the cathodic and anodic reactions will be:

$$2\mathrm{H}^+ + 2e^- \rightleftharpoons \mathrm{H}_2 \qquad \text{cathode} \tag{1.1}$$

$$\mathrm{Fe} \rightleftharpoons \mathrm{Fe}^{2+} + 2e^- \qquad \text{anode} \tag{1.2}$$

When H_2S is present, the hydrogen atoms may be inhibited from forming diatomic hydrogen, and will instead enter the metal matrix, making the metal increasingly brittle and eventually leading to what is known as sulphide stress cracking [16].

The complete deprotonation of H_2S will yield sulphide ions, S^{2-}, which may give further problems since they willingly react with metal ions like Fe^{2+} to form sulphide scales, which are only sparingly solubility in water.

$$\mathrm{Fe}^{2+} + \mathrm{S}^{2-} \rightleftharpoons \mathrm{FeS}_{(s)} \tag{1.3}$$

The scales will attach to the surface of the equipment and the well, and may in this way end up blocking the flow through the well. At the same time, corrosion may occur beneath or around the scale deposition due to formation of oxygen gradients [16].

In total, there are plenty of reasons for removing sulphur, especially H_2S, and for that purpose different techniques have been developed.

Chapter 2

H_2S scavenging - gas sweetening

The process of removing H_2S from the natural gas is also called gas sweetening, and which method to use depends on both the amount of natural gas that has to be treated, as well as the concentration of H_2S in the natural gas. Further factors that can influence the choice of method are whether the scavenger is to be specifically directed at H_2S, and if the sulphur is to be used after separation. In general there are two categories of scavenging methods:

1. Regenerative
2. Non-regenerative

2.1 Regenerative scavengers

In the regenerative methods the absorption of H_2S is reversible, and the absorbent may therefore be reused after having been re-separated from the H_2S. By choosing this type of scavenging method H_2S may be reused; often via a Claus process where H_2S is converted into elemental sulphur. The absorbent is often alkanolamines mixed with an activator. Some of the most commonly used alkanolamines are shown in table 2.1.

Alkanolamines are very suitable for acid gas absorption because of their two functional groups; the hydroxy and amino group. The hydroxy group enables the alkanolamines to make hydrogen bonds between the molecules, hereby lowering the vapour pressure. A low vapour pressure is desirable because the separation process usually depends on heating the H_2S/amine mixture, whereby the solubility of the gas in the liquid is lowered. The hydroxy group may also form hydrogen bonds with water molecules, which increases the water solubility of the alkanolamine. The lone pair on the amino group allows the alkanolamine to function as a base, and this way increase the pH of the solution, which will allow acid gasses to be dissolved in the solution. Primary amines, like MEA, are the most alkaline while tertiary amines, like MDEA, are the least alkaline. Furthermore, primary and secondary amines can react with CO_2 to form carbamate [18]. In equation 2.1 the reaction for a primary amine is shown.

$$\mathrm{RNH_2 + CO_2 \rightleftharpoons RNHCOO^- + H^+} \tag{2.1}$$

Table 2.1: Alkanolamines [18]

Name	Abbreviation	Formula
Monoethanolamine	MEA	
Diethanolamine	DEA	
Methyldiethanolamine	MDEA	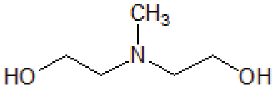
2-(2-aminoethoxy)ethanol	DGA	

Tertiary amines do not participate in this reaction, which makes them less good at absorbing CO_2. The other reaction with CO_2 is carbonate formation, but this reaction path is slow compared to the carbamate formation, and it requires a pH high enough to form CO_3^{2-}. For selective H_2S absorption, a molecular structure that suppresses carbamate formation should be chosen since it lowers the CO_2 absorption rate without affecting the rate of H_2S absorption [18].

Of the alkanolamines, MEA was for many years used almost exclusively as absorbent for H_2S and CO_2 removal. Since then, it has been replaced by other more efficient solutions, but is still widely used because it gives a high pH, and relatively easily can be regenerated. However, it does form irreversible products with carbonyl sulphide, COS, and carbon disulphide, CS_2. In cases with COS and CS_2 in the gas stream, DEA may be used instead. Secondary amines are much less reactive towards these compounds, but on the other hand, DEA may form irreversible and corrosive products with CO_2, and it may be necessary to apply vacuum distillation for reclaiming the DEA. DGA is a compound which in many ways resemble MEA, but because of its increased molecular weight and an extra oxygen atom, it has a lower vapour pressure and may therefore be used in more concentrated solutions (up to 40-60 %). MDEA is a tertiary amine, which makes it relatively selective towards H_2S. Furthermore, it is highly resistant to thermal and chemical degradation, it is noncorrosive, has a low specific heat and heat of reaction with CO_2 and H_2S, and it is only sparingly miscible with hydrocarbons [18]. In figure 2.1, a general regeneration plant is shown.

As seen from figure 2.1, the use of a regenerative absorbent will demand the construction of absorption and stripping towers alongside with the additional equipment. Furthermore, the separated H_2S cannot just be released to the atmosphere and will therefore require extra facilities capable of handling the gas. If the concentration of H_2S in the natural gas is sufficiently low, a few hundred ppm [16], it is more economic to use a non-regenerative H_2S scavenger.

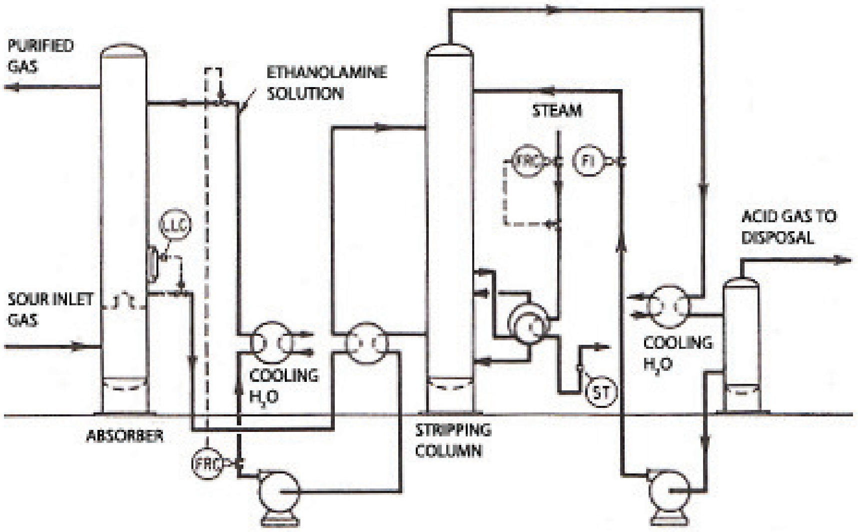

Figure 2.1: Alkanolamine plant for acid gas removal. The natural gas is fed into the absorber, which removes the acid gasses. The spent solution is then pumped over to the stripper tower where the gasses are released via heating of the solution, which then can be pumped back to the absorber tower [18].

2.2 Non-regenerative scavengers

Non-regenerative scavengers may be divided into the following categories:

(a) Solid basic metallic compounds

(b) Oxidising chemicals

(c) Aldehydes and aldehyde-related products

(d) Metal caboxylates and chelates (may be regenerative)

(e) Amine based products

(f) Triazines

One of the oldest methods of removing sulphur from natural gas involves the use of metal oxides such as ferrous oxide or zinc oxide. The metal oxide absorbs the hydrogen sulphide forming metal sulphide compounds.

$$2\mathrm{Fe_2O_3} + 6\mathrm{H_2S} \rightleftharpoons 2\mathrm{Fe_2S_3} + 6\mathrm{H_2O} \tag{2.2}$$

If the process takes places in an aerated environment, the iron sulphide may be regenerated under the formation of elemental sulphur; however, this will interfere with bed porosity. Because of its porosity and absorbing capabilities, this method is also commonly known as the iron sponge. Today the iron sponge is almost exclusively used when the amount of gas that needs treatment is very small [18, 16].

Another way of removing H_2S is by oxidation, where the sulphur atom in H_2S is converted into a higher oxidation state, from where it is more easily removed. Two oxidising agents that are often used are $KMnO_4$ and $K_2Cr_2O_7$, used in concentrations of 5-10 % in buffered solutions.

$$8MnO_4^- + 5H_2S + 14H^+ \rightleftharpoons 8Mn^{2+} + 5SO_4^{2-} + 12H_2O \tag{2.3}$$

Via this method, it is possible to achieve a complete removal of H_2S, either as elemental sulphur, SO_2 and/or SO_4^{2-}, but due to the high cost of the oxidising chemicals, the method is only used when very small amounts of H_2S are present in the gas, and when the gas must be absolutely free of H_2S [18]. Other oxidising compounds may be chlorites, bromates/iodates, nitrites and persalts [16].

H_2S and aldehydes react in rapid reactions, which can be used to remove H_2S from natural gas. Typical aldehydes includes formaldehyde, gluteraldehyde, acrolein, and glyoxal, with formaldehyde being the most used [16]. The chemistry of formaldehyde/H_2S reactions are quite complex, and will lead to the formation of cyclic carbon-sulphur compounds, such as trithiane, and also to a lesser extent mercaptans. The reaction system may be represented by equation 2.4.

$$3HCHO + 3H_2S \rightleftharpoons C_3H_6S_3 + 3H_2O \tag{2.4}$$

Although formaldehyde systems have been reported to remove 100 % of the H_2S from natural gas [18], they are only used to a lesser extent. This is due to the toxicity of formaldehyde, and problems with the reaction products. They retain the foul smell of sulphur compounds, are often poorly soluble in water, and have a tendency to polymerise and flocculate, which may give problems with clogging of the equipment [18].

There exists numerous methods which use suspensions of metal ions with chelating groups to keep the metal ions suspended in the solution, to scavenge H_2S. Examples of commercial products that use this method are the Wheelabrator Clean Air System, LO-CAT, SulFerox, Cataban, and Sulfint processes. The metal ions used are most often either iron(III) or zinc(II), while examples of the chelating agents are EDTA, polyaminodisuccinic acid, and gluconate. In these processes, the metal ion is reduced, while H_2S is oxidised to elemental sulphur.

$$2Fe^{3+} + H_2S \rightleftharpoons 2Fe^{2+} + S + 2H^+ \tag{2.5}$$

$$4Fe^{2+} + O_2 + 2H_2O \rightleftharpoons 4Fe^{3+} + 4OH^- \tag{2.6}$$

As seen from reaction 2.6, the metal ions may be regenerated via oxidation by oxygen. However, because of the low solubility of oxygen in water, good contact between the solution and air is required for this to be a viable possibility [18, 16].

Besides the regenerative alkanolamines that have already been mentioned, several other classes of amines may be used to scavenge H_2S. Examples are amidines ($RC(=NH)NH_2$), which can be modified to be both water and oil soluble, piperazinone, and mixtures of amine oxides with specific enzymes. These systems are reported to be more selective towards H_2S, but little field knowledge is reported and the use of these solutions are not widespread [16].

The most commonly used H_2S scavenger today is triazines. Triazines have the advantage that they can be modified to become more or less hydrophilic by using different side groups on the nitrogen atoms. Often a hydroxylethyl-side group will be used, but triazines with purely non-polar alkyl side groups have also been investigated. The reasons why triazine based scavengers are so widely used are that they are H_2S selective because of their tertiary nitrogen atoms, the reaction products are water soluble (depending on the original triazine), the reaction products are corrosion inhibitors, and the spent material has a low toxicity making disposal easier [18, 16]. Furthermore, the reaction between triazines and H_2S is faster than the rapid aldehyde/H_2S reaction, and triazines remove H_2S down to a concentration of 5 ppm, which is the threshold limit for natural gas in Denmark [24]. It is also a triazine based scavenger that is being used by Maersk for H_2S scavenging.

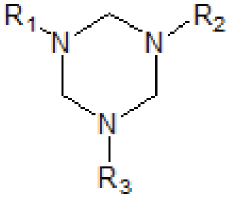

Figure 2.2: s-Triazine

Chapter 3

Actual scavenging - problems

Maersk has chosen to use a triazine system, with 1,3,5-tri-(2-hydroxyethyl)-hexahydro-s-triazine as the main component, for removal of H_2S. They apply the scavenger at their production platforms offshore, but it is first when the crude oil reaches Shell's refining plant in Fredericia that the problems with fouling arise. Here specific parts of the system become clogged, requiring a complete stop in the production from time to time. This chapter describes how the actual scavenging process is carried out by Maersk, and the problems experienced at the Shell refining plant.

3.1 Maersk scavenging process

Maersk has several operating platforms in the North Sea, see figure 3.1 for an overview, but it is not on all of these platforms that H_2S removal is necessary. The Tyra platforms only produce gas, which contains no significant amounts of H_2S, while Dan, Gorm and Halfdan produce both oil and gas, and here removal of H_2S is necessary. An interesting observation is that the H_2S in the fields seems to originate from bacterial activity in the oil rather than thermal conversion processes. At present the sour gas from Halfdan is being exported for treatment at Gorm, meaning that the scavenging process only takes place at Dan and Gorm.

At Dan the scavenging process takes place on three platforms, Dan FF, Dan FC and Dan FG. The systems are connected across the platforms, and each scavenging system cannot be considered completely independent. In figure 3.2 a general process diagram for the part of the Maersk facility that handles the scavenging process at Dan is shown. First the raw oil from the well is led into a high pressure three phase separator where oil, gas and water are separated. The gas is taken out in the top, where additional liquid is knocked out, after which the gas is compressed. At this point the concentration of H_2S is high, and it is here the triazine is injected into the gas stream. The triazine will react with the H_2S forming water soluble products. The gas/scavenger mixture is then cooled down and sent into a gas/liquid separator. In some of the coolers Maersk has experienced deposition of a black solid, which possibly could be related to the fouling problem at Shell. In the gas/liquid separator, the treated gas has a low H_2S content, and it is sent for further treatment, while the liquid containing the spent scavenger is sent to

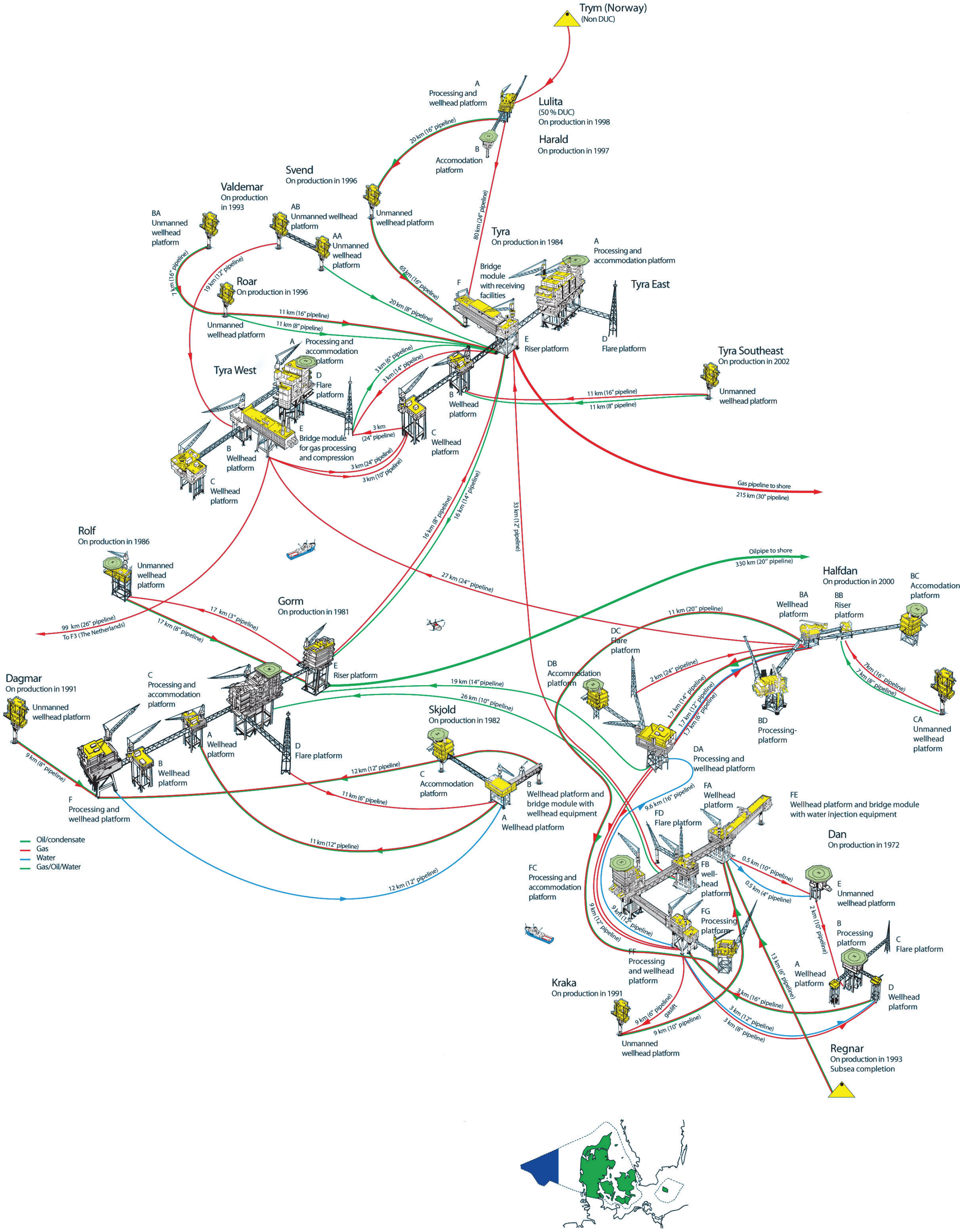

Figure 3.1: DUC in the North Sea [22]

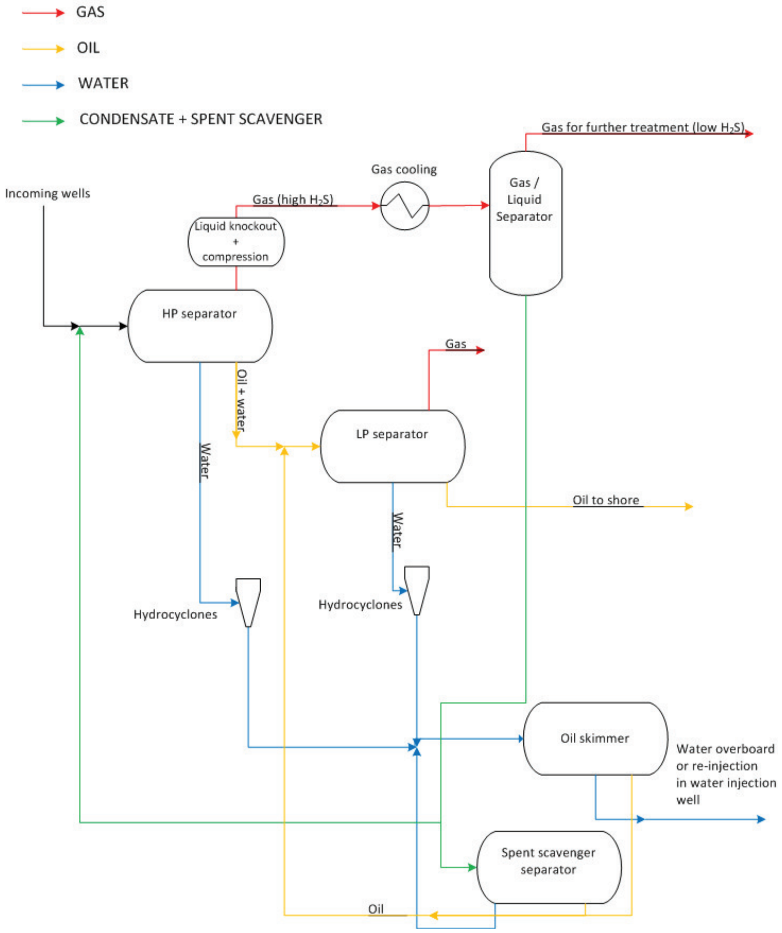

Figure 3.2: Process diagram from Maersk scavenging [2]

a spent scavenger separator. Dan FF does not have a spent scavenger separator, and the liquid from the gas/liquid separator at Dan FF is therefore sent to the spent scavenger separator at Dan FC. It is also possible to re-route the spent scavenger solution back into the raw oil, prior to entering the HP separator. This may be done at Dan FF and Dan FC, while at Dan FG, the spent scavenger may be re-routed to the oil phase coming from the HP separator. The re-routing is not the primary way of handling the spent scavenger solution, but may be used when the spent scavenger separator needs inspection or is otherwise unavailable. In the spent scavenger separator the liquid separates into an oil and an aqueous phase, with the spent scavenger being primarily in the aqueous phase. The oil phase is sent back to the oil from the HP separator, while the aqueous phase is discharged with produced water. Prior to discharging, the aqueous phase is sent through another separator in which gas is bubbled through the solution to create a film of oil particles on top of the water phase, which may then be skimmed away. This is done to comply with the threshold limit for oil in the discharged water. Going into the separator, the water has an approximate oil concentration of 15-40 ppm, and after the separator the concentration has been lowered to around 5 ppm. The skimmed oil is led back to the oil phase coming from the spent scavenger separator, and because of difficulties with separating oil and water completely in the skimming process, some water will also be led back into the oil stream this way. However, the oil flow coming from the skimming separator is very low compared to the oil flow from the spent scavenger separator. At times it is necessary to close the water outlet from the spent scavenger separator, in which case the entire spent scavenger solution is led back into the oil phase prior to entering the LP separator [2]. In table 3.1 the average content of the crude oil sent to Shell is given.

Table 3.1: DUC crude oil content [2]

Content			Properties		
Water	< 0.025	vol%	Density at 15 ℃	0.8573	kg/L
Sulphur	0.261	mass%	Viscosity at 20 ℃	9.163	mm^2/s
Nitrogen	1368	mg/kg	Viscosity at 40 ℃	5.138	mm^2/s
Asphaltenes*	< 0.05	mass%	Viscosity at 50 ℃	4.177	mm^2/s
Benzene	0.11	mass%	Pourpoint (max)	-51	℃
Salt	6-9	mg/kg	Pourpoint (min)	< -60	℃
Sediment by extraction	0.03	mass%			
Hydrogen sulfide	< 1	mg/kg			
Mercury	< 0.01	mg/kg			
Wax content at -30 ℃	4.2	mass%			

3.2 Problems at Shell's refining facility

In figure 3.3 a sketch of the process diagram of the refining process at Shell in Fredericia is shown. The data for temperature, pressure and pH are measured the 23/2-2011. The facility has a maximum capacity of 10,000 tons raw oil per day, which roughly contains 25 tons of water. To desalt the oil, it is mixed with additional 400 t/day water and fed to a desalter. Before entering the desalter, the mixture is heated to around 133 ℃ with a number of heat exchangers. After the desalter, the mixture is further heated to around 169 ℃; at this point the pressure is 9.2 bar. The mixture is then flashed down to 5.4 bar, and fed to a distillation column. The distillate taken out in the top is cooled down to 63 ℃ by passing a heat exchanger and an air cooler. The air cooler is the first place where fouling occurs at the refinery. An interesting observation is that the fouling has only recently started to occur in the air cooler; whereas, it has been occurring for a longer period of time in the rest of the water treatment system. The cooled distillate ends up in a water trap, where water, gasoline and gas are separated, and from here on problems are associated with the treatment of the water. The water has a pH around 8.78 after the water trap, but at optimal conditions the pH should be considerably more acidic, close to 6 [9]. The reason for the higher pH could be amine residues from the scavenger. From the water trap, the water is transferred to a three phase separator that separates oil, gas and water. Also in this separator does fouling occur. At this point, the solution has become concentrated with 4,000 ppm H_2S and 500 ppm NH_3. It is possible that these high concentrations influence the formation of fouling. The aqueous solution is then heated from 48 ℃ to 86 ℃, and fed to a sour water stripper. The top out take from the stripper contains H_2S, and is transferred to a Claus plant, where H_2S is converted to elemental sulphur. During the transfer to the Claus plant, the fluid passes a heat exchanger where fouling is also found. In the top of the stripper, fouling occurs, and also in the bottom of the stripper, where water is recirculated through a reboiler that removes H_2S and NH_3. The clean water from the bottom of the boiler is cooled down, and part of this water, is the water initially mixed with the crude oil before the desalter. In this way the circuit is closed, but the recirculation could also be speculated to be part of the fouling problem since it could possibly send fouling residues or initiators back into the system. However, if this was problematic, then fouling might also be expected to occur in the first part of the refinery.

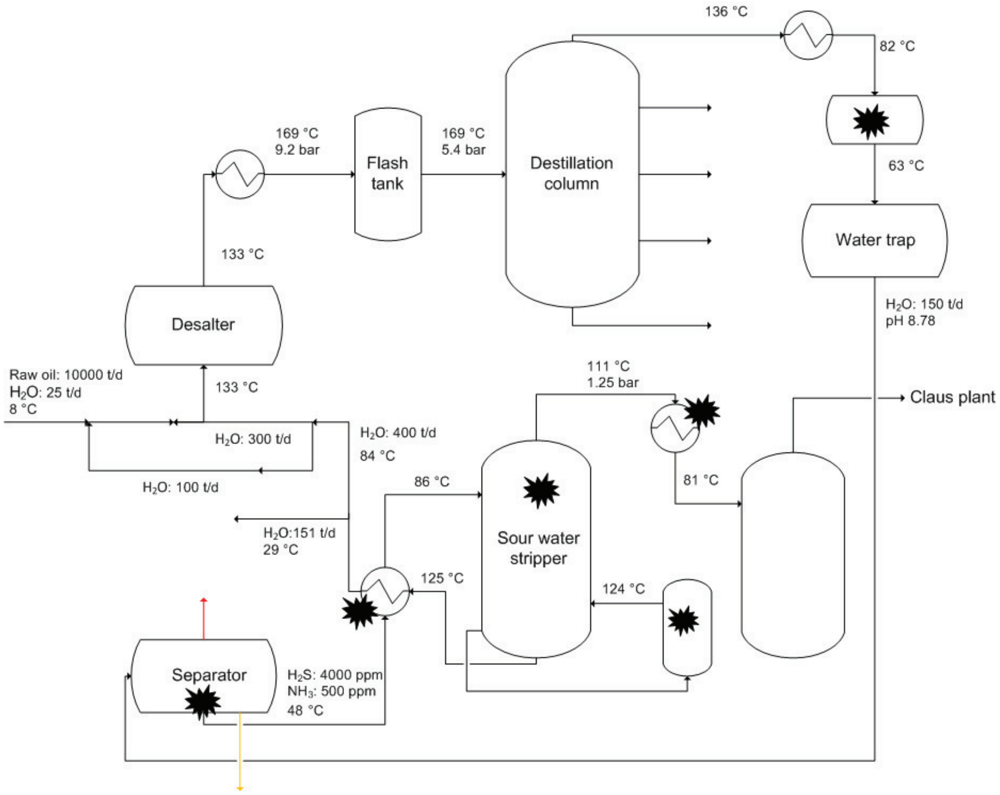

Figure 3.3: Process diagram from Shell refining facility [9]

The black ”splashes” in figure 3.3 are the places in the system where fouling is a problem. What strikes one immediately is that the fouling problem does not occur in the entire process, but only at selected unit operations. Before the raw oil enters the desalter, it passes through a number of heat exchangers, where there is no problem with fouling. It is first after the distillation that the problems begin to occur, and especially the part of the plant where the treatment of water takes place is badly affected. This could indicate that it is first at the refinery that the problem arises. If the fouling precursor was already present in the crude oil, one would expect problems to occur from the beginning of the refining process. However, it is also possible that if the fouling precursor is non-polar, then in the first part of the process, it will be dissolved in the oil and therefore not deposited in the system. Still, if the problems were related to a non-polar compound, then it is to be expected that this compound would be dissolved in the gasoline in the water trap, and the problems should therefore not be associated with the water phase.

That fouling first occurs after the distillation column could also indicate that the distillation process is involved in the formation of fouling. Effects could be increased temperature and H_2S concentration. Indeed it is seen that after the water trap, the concentration of H_2S is very high (4,000 ppm), creating a large driving gradient, which could cause the fouling. It is not only at the distillation column that the temperature is changing. The temperature varies from the inlet temperature (in this case 8 ℃) to 169 ℃. The pressure also varies; some places in the process it reaches values up to 25 bar, and at other points there is almost no gauge pressure. Together, the changing temperature and pressure influence the phase of fluid, and might create conditions suitable for formation of fouling. Fouling may also be affected by changing chemical conditions, like pH. The pH for this refinery is relatively high, and this heightened pH might also influence the formation of fouling, especially if the reactions are either acid or base catalysed.

Chapter 4

Reaction system

This chapter concerns the molecules involved in the scavenging process, and the chemical theory behind the reactions. Furthermore, a model for the reaction mechanism is put forward, and is used as a basis for the construction of a kinetic model for the system.

In figure 4.1 the chemical reactions involved in the scavenging process, as presented by Buhaug and Bakke [5], are shown. General for all three reactions is that H_2S will react with a nitrogen atom in the ring structure in a substitution reaction in which MEA is the leaving group.

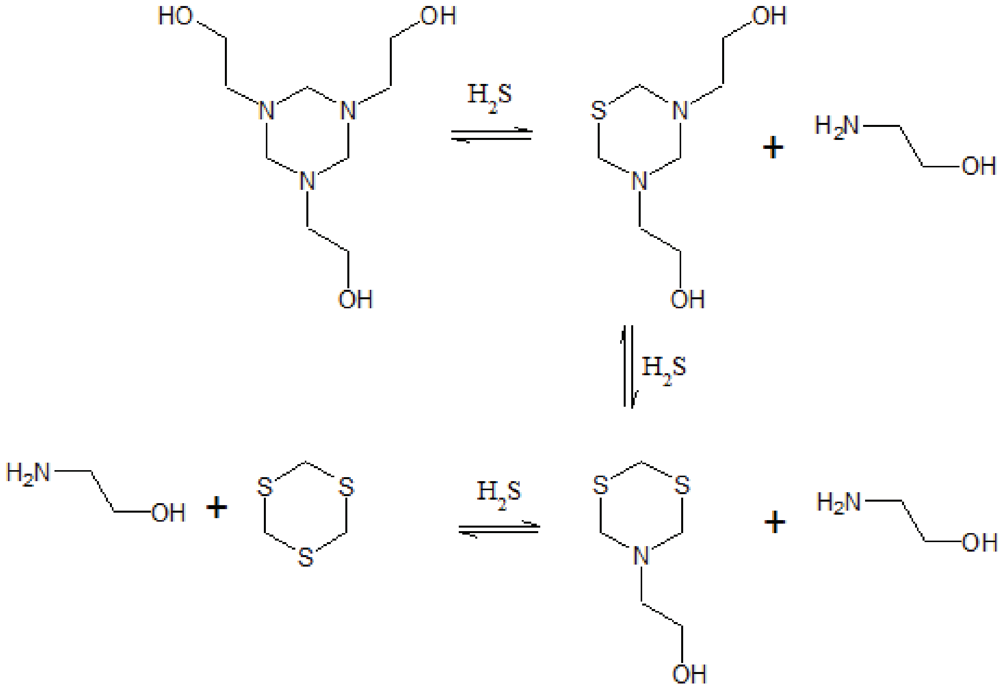

Figure 4.1: Reaction system [5]

4.1 H_2S

Hydrogen sulphide consists of one sulphur atom bonded to two hydrogen atoms. The molecule has a total of eight valence electrons; four are used in sigma bonds between the sulphur atom and the hydrogen atoms, and the remaining four form two lone pairs on the sulphur atom. Because of the four electron pairs situated around the sulphur atom, VSEPR theory*can be used to predict the shape of the molecule to be a tetrahedral. H_2S will not be a pure tetrahedral, but a V-shape since the two lone pairs will be situated closer to the sulphur atom, and therefore decrease the bond angle between the two hydrogen atoms. Molecules with four electron pairs are often described as being sp^3 hybridised*; however, H_2S has a bond angle of 92.5 degrees, and the degree of hybridisation of the s- and p-orbitals may therefore be discussed [23]. With a V-shape structure, H_2S may form a dipole with a negative charge at the sulphur atom and a positive charge at the hydrogen atoms; however, the strength of this dipole will depend on the difference in electronegativity between sulphur and hydrogen, and because sulphur is only marginally more electronegative than hydrogen, the molecule will only be a weak dipole. H_2S has a dipole moment of 0.98 debye*[33]. This, together with the fact that the sulphur atom will not form hydrogen bonds, explains why H_2S is a gas at SATP conditions. The intermediate dipole moment also means that H_2S is only scarcely soluble in both water and nonpolar solvents. A higher solubility is achieved in polar solvents such as aldehydes, ketons, and ethers [32].

The solubility parameters of H_2S affects the distribution between the gas, oil and water phase during the extraction process. In figure 4.2 the simulated distribution between the three phases for an oil well in the Campos Basin of Brazil is shown. The simulation made by Rajagopal et al, has been made to model the removal of H_2S from petroleum production lines with chemical scavengers, including triazine. The H_2S distribution was obtained with available and measured data for the system used with the Sour Peng Robinson equation. The simulation shows that in the reservoir the oil is above bubble point pressure, and no gas phase is present. Therefore, H_2S is distributed between the oil and water phase, with the largest fraction being in the oil phase. In the three phase separator, the pressure has dropped below the bubble point pressure, and the gas phase will contain most of the H_2S [19].

Because of its slight polarisation and lone pairs, H_2S will be attracted to positively charged sites, making it possible for it to participate in S_N1 and S_N2 reactions as a nucleophile. Sulphur's size and polarisability make sulphur containing compounds, like H_2S/HS^- stronger nucleophiles compared to smaller and less polarisable compounds, like H_2O/OH^- [26]. If the reaction takes place in a protic* environment, the larger sulphur atom is less efficiently dissolved because of its inability to form strong hydrogen bonds, and it will therefore be more willingly to react, and because the sulphur atom is more polarisable, it will be better at donating electrons to the electrophilic centre, hereby forming the new bond. Examples of nucleophile substitution reactions with H_2S include formation of thiols and reactions with ethers where the oxygen atom is substituted with a sulphur atom [33].

$$H_2S + ROH \rightleftharpoons RSH + H_2O \tag{4.1}$$

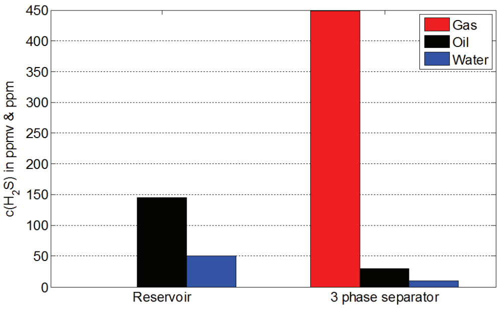

Figure 4.2: Distribution of hydrogen sulphide among the three phases phases in an offshore oil well in the Campos Basin of Brazil [19]

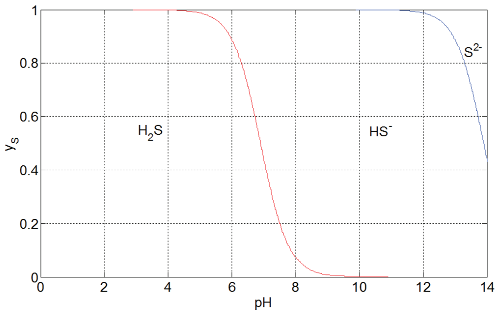

Figure 4.3: Bjerrum diagram for H_2S

In the presence of a proper catalyst, H_2S may also participate in addition reactions, and may react with aldehydes and ketones to form dithiols or cyclic products like trithiane [33].

H_2S is a weak acid with two dissociation constants [13].

$$H_2S + H_2O \rightleftharpoons H_3O^+ + HS^- \qquad pK_a = 6.9 \tag{4.2}$$

$$HS^- + H_2O \rightleftharpoons H_3O^+ + S^{2-} \qquad pK_a = 13.9 \tag{4.3}$$

In figure 4.3 the Bjerrum diagram for H_2S can be seen. This shows that above pH 9, H_2S is completely converted to HS^-. It is the acidic ability that is utilised in regenerative amine systems, where H_2S dissolved in the aqueous amine solution quickly will transfer a proton to an amine. Aqueous amine solutions typically have a pH value between 10 and 12 depending on the concentration and type of amine, and HS^- will dominate. HS^- is a very weak acid with a pK_a value of 13.9, and the S^{2-} ions are therefore only present at very high pH values. Upon heating, the H_2S dissolved as gas in the solution will be driven from the solution, and the equilibrium will then shift to replace the lost H_2S, ultimately regenerating the amine solution.

4.2 Triazines and reaction products

Triazines are six membered heterocyclic compounds consisting of three carbon and three nitrogen atoms. The triazines used in scavenging of H_2S are most often hexahydro-1,3,5-s-triazines, where the structure is symmetrical with alternating nitrogen and carbon atoms, and with the six hydrogen atoms bonded to the carbon atoms. The side group attached to the nitrogen atoms can then be chosen to influence the physical and chemical properties such as the solubility of the triazine. The triazine currently used by Maersk is 1,3,5-tri-(2-hydroxyethyl)-hexahydro-s-triazine (hydroxyethyl-triazine), see figure 4.1.

Triazines can be formed in a condensation reaction between a carbonyl and an amine compound, where the alkyl groups on the carbonyl and nitrogen atom will end up as side groups on the final triazine. Hydroxyethyl-triazine is formed from formaldehyde and MEA in the reaction shown in figure 4.4. The reverse hydrolysis reaction is found to dependent on pH, with the reaction rate increasing with increasing oxonium concentration [6]. Therefore, this reaction should be considered in the evaluation of the total reaction scheme.

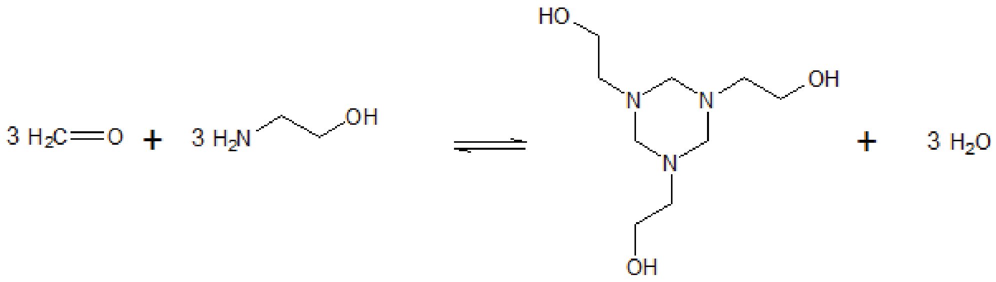

Figure 4.4: Formation of hydroxyethyl-triazine

Both the nitrogen atoms and the carbon atoms are sp^3 hybridised; however, where the carbon atoms have tetrahedral structure, the nitrogen atoms have a trigonal pyramidal structure. This is due to a lone pair on the nitrogen atoms, which also makes them Lewis bases. The nitrogen atoms in triazines are tertiary, meaning that they can only function as hydrogen bond acceptors, not donors. It is also the tertiary structure that makes triazines selective towards H_2S. The water solubility is increased by the presence of the hydroxy groups, which can form active hydrogen bonds to water molecules. No pKa value is reported for hydroxyethyl-triazine [5], but an approximate value can be estimated.

A tertiary structure makes the triazine better at dispersing a positive charge compared to ammonia because the side groups can release electrons, which will help stabilise the protonated triazine. However, because its hydrogen bonding is less effective than primary and secondary amines, a tertiary amine will be a weaker base than these in an aqueous solution, where the solvation shell of water molecules can stabilise the primary and secondary amines to a greater extent. Finally, non-aromatic heterocyclic amines have basicities that are approximately the same as those of acyclic amines. The hydroxy group might withdraw electrons from the nitrogen atom, reducing its basicity. In equation 4.4, the acid equilibrium is shown along with the acid constant.

$$\mathrm{TH^+} \rightleftharpoons \mathrm{T} + \mathrm{H^+} \quad , \quad K_a = \frac{[\mathrm{T}][\mathrm{H^+}]}{[\mathrm{TH^+}]} \tag{4.4}$$

Although hydroxyethyl-triazine has three nitrogen atoms, it seems likely that only one nitrogen atom will be protonated at a time, since several positive charges could destabilise the molecule. With this assumption, a reasonable approximation might be di-methyl-ethanol-amine (DMEA) (pK$_a$ = 8.88 [15]). The acid/base properties of hydroxyethyl-triazine are important because it has been found that it is the protonated species that participate in the reaction with H_2S [6].

The two first reaction products, thiadiazine and dithiazine, may be expected to show similar properties as the triazine because they still contain two and one hydroxy/amino group(s) respectively. However, the presence of sulphur atoms in the molecular structure, and the loss of the MEA group(s) will alter the properties. Especially the solubility parameters can be expected to change, since an electronegative atom, nitrogen, is replaced with a less electronegative atom, sulphur, and because hydroxy group(s) will be lost during the reaction. In practice it is found though that thiadiazine and dithiazine will show an increasing solubility in water. Table 4.1 shows experimentally found values from an investigation made by Maersk, where radioactive ^{14}C isotopes were used to measure the distribution of hydroxyethyl-triazine and its reaction products in an oil mixture with 50 vol% water. The investigation did not distinguish between thiadiazine and dithiazine, and they are simply referred to as reaction products.

Table 4.1: Oil/water distribution for hydroxyethyl-triazine and reactionproducts [2].

		Distribution	
Component	$K_{O/W}$	Oil phase (%)	Water phase (%)
Hydroxyethyl-triazine	0.022	2.15	97.85
Reaction products	0.010	0.99	99.01

The reason for this high solubility in water, in spite of the loss of MEA, could be that sulphur atoms are more easily polarised and that the remaining nitrogen and hydroxy group will be sufficient to polarise the entire molecule, making it a dipole.

4.3 Trithiane

1,3,5-trithiane, s-trithiane, is the compound suspected for causing the fouling. Compared to triazine, all three nitrogen atoms have been substituted with sulphur atoms, and the ring consists of single sigma bonds between the sulphur and carbon atoms, leaving the sulphur atoms sp^3 hybridised with two lone pairs. At SATP s-trithiane is a stable crystalline solid compound with white colour, and its melting point is 216 ℃ [8]. The s-trithiane itself is odourless; however, odours are often reported to be present after formation, due to the presence of impurities or an equilibrium with a trace of monomeric thioketone [8].

Sulphur atoms do not have the same ability to attract electrons as the nitrogen atoms, and s-trithiane is therefore considerably less polarised and is insoluble in water [8].

Although s-trithiane is a stable compound, it may participate in numerous reactions. Certain heavy metals are known to form crystalline complexes with s-trithiane, some of which are found in table 4.2. If the fouling is indeed s-trithiane, then an explanation of why a deposition occurs must be found, and the presence of these heavy metals in the system could be a possibility. Another possibility is that the fouling is linked to the varying temperature and pressure conditions during the refining process. The stability of trithianes towards thermal decomposition varies with the compounds the trithiane was derived from. Trithianes derived from aliphatic aldehydes are reported

Table 4.2: Complexes with heavy metal salts [8]

Formula of complex	Crystal form
$C_3H_6S_3 \cdot AgNO_3 \cdot H_2O$	Leaflets
$C_3H_6S_3 \cdot 2AgNO_3$	Needles
$C_3H_6S_3 \cdot HgCl_2$	Needles
$2C_3H_6S_3 \cdot PtCl_4$	Golden yellow needles
$3C_3H_6S_3 \cdot 2PtCl_2$	Golden yellow needles

to be very stable, and distillation at temperatures up to 245 ℃ is possible without decomposition. Trithianes derived from aromatic aldehydes and ketones are less stable [8]. The thermal stability of s-trithiane derived from hydroxyethyl-triazine is unknown, but since hydroxyethyl-triazine is derived from formaldehyde reactions, similar stability as aliphatic aldehydes may be expected. If this is the case, s-trithiane would be expected to be a thermal stable compound.

When exposed to oxidising compounds, such as H_2O_2 or $KMnO_4$, s-trithiane is oxidised first to a sulphoxide, and then further on to a sulphone. This may be important because the oxygen atoms alter the reactivity of s-trithiane. It has been found that s-trithiane trisulphone will react with formaldehyde in the presence of a base. Under heating the reaction product sets to an insoluble film, which is reported to be tough, flexible and alkali resistant [8]. When hydroxyethyl-triazine is present, it is possible that it will decompose to formaldehyde and MEA, and with heating the reaction conditions for the formation of such a film could be present. Whether the environment in the refining process is sufficiently oxidising is however doubtful. Trithianes can also participate in halogenation and alkylation reactions, which may make it difficult to identify the fouling as pure crystalline s-trithiane [8].

4.4 Reaction system

4.4.1 Hydrolysis of triazine

As mentioned earlier during the discussion of hydroxyethyl-triazine, the hydrolysis to MEA and formaldehyde is strongly dependent on pH. To avoid destruction of the triazine before it has had time to react in the scavenging process, it is necessary to be able to control this reaction.

Experiments which investigated the rate of reaction as a function of pH and temperature have been made, see table 4.3 for results [6]. For constant pH a first order dependency of the triazine concentration has been found.

$$\frac{dT}{dt} = k_{obs} \cdot [T] \tag{4.5}$$

Here T is an abbreviation of hydroxyethyl-triazine.

The observed rate constants clearly show a dependency on pH, and this indicates that the rate constant for the hydrolysis is not a simple first order rate constant, but

Table 4.3: Observed first order rate constants for the hydrolysis of hydroxyethyl-triazine [6]

	k_{obs} (s^{-1})	
pH	22 °C	60 °C
10.9	$(5.6 \pm 0.2) \cdot 10^{-5}$	$(3.7 \pm 0.1) \cdot 10^{-3}$
9.5	$(7.2 \pm 0.5) \cdot 10^{-4}$	0.11 ± 0.01
8.0	$(2.2 \pm 0.2) \cdot 10^{-2}$	–

rather made up of two rate constants, where one is dependent on pH. The following rate law has been found as a best fit to the experimental data [6].

$$\frac{dT}{dt} = k_1 \cdot [T] + k_2 \cdot [T][H^+] \tag{4.6}$$

Where $k_{obs} = k_1 + k_2[H^+]$

Using the data from table 4.3 and the rate law from equation 4.6, k_1 and k_2 can be determined for 22 °C and 60 °C.

$$k_1^{22°C} = 2.6 \cdot 10^{-5} s^{-1} \quad k_2^{22°C} = 2.2 \cdot 10^{6} s^{-1} M^{-1} \tag{4.7}$$

$$k_1^{60°C} = 4.8 \cdot 10^{-4} s^{-1} \quad k_2^{60°C} = 3.5 \cdot 10^{8} s^{-1} M^{-1} \tag{4.8}$$

Even though k_1 and k_2 have different units and therefore cannot be compared directly, it is obvious that the size of k_2 makes the pH very important for the observed rate of hydrolysis. To visualise the influence of pH equation 4.6 can be used to estimate half lives at various pH values, see figure 4.5.

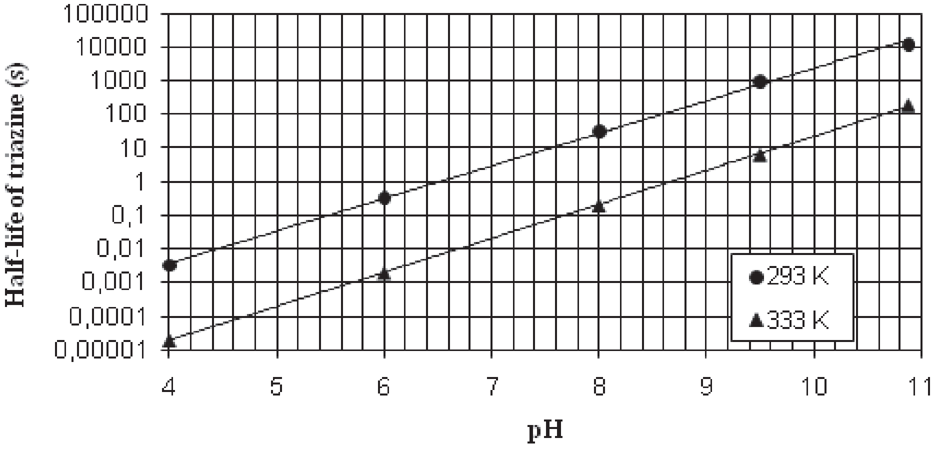

Figure 4.5: Half life of hydroxyethyl-triazine as a function of pH and temperature [6]

It is clear that if the scavenging process is not affected to the same extent by lowering the pH, an effective scavenging must take place at elevated pH values to ensure that the triazine is not decomposed. A fact that may be very important if the gas from which H_2S is to be removed contains high concentrations of CO_2 as well. At the same time, it also shows that hydroxyethyl-triazine is very susceptible to acid catalysed reactions [6].

Experiments have also demonstrated that the hydrolysis of hydroxyethyl-triazine is faster than the hydrolysis of thiadiazine, where the sulphur atom seems to have a stabilising effect on the molecule. The second reaction product, dithiazine, has not been found to hydrolysis even at pH 2 [6]

4.4.2 Reaction mechanisme

According to Bakke and Buhaug [5], it is the protonated triazine that participates in the reaction. Based on their results it seems that the reaction between the triazine/thiadiazine/dithiazine and H_2S can be described with the following reaction mechanism, see figure 4.6.

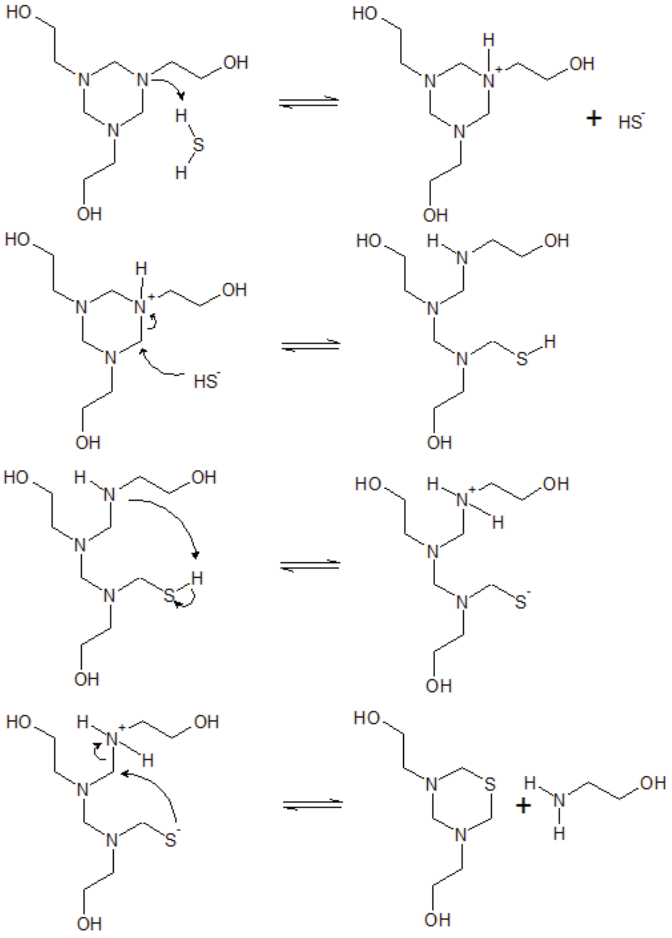

Figure 4.6: Potential reaction mechanism

In the first step, H_2S and the triazine react in an acid/base reaction, where the triazine becomes protonated. The positive charge on the nitrogen atom makes the molecule more electrophilic and the two neighbouring carbon atoms will as such become slightly positively charged making them vulnerable for an attack from the HS^- ion.

This is the next step in the mechanism. The HS^- reacts with one of the carbon atoms in a S_N2 reaction where the nitrogen atom acts as a leaving group. In this reaction the ring structure opens, and a neutral molecule is produced.

Then a proton shift may take place. The lone pair on the nitrogen atom forms a bond to the hydrogen atom from the thiol group, giving the sulphur atom a negative charge. Again the positive charge on the nitrogen atom attracts electrons from the neighbouring carbon atoms, which becomes positively charged.

In the final step, the sulphur atom may form a bond to the third carbon atom through a S_N2 reaction. MEA will be the leaving group, and a closed ring structure is obtained again. The formation of a six-membered ring is energetically favourable, since a ring structure with six members is especially stable. These rings have the lowest strain because of the angles between the bonds, and in a ring the atoms will furthermore be able to share their electrons more efficiently. A sulphur atom with two lone pairs have more electrons to contribute to the ring than a nitrogen atom, and it may do so more easily since the electrons are situated further from the nucleus, making the substitution favourable since it gives a more stable molecule.

4.4.3 Kinetics

Because the reaction is a substitution reaction, where the probable rate limiting step is an S_N2 reaction, it seems reasonable to assume that the rate law will be second order. At the same time, the influence of pH on the rate indicates that it is the concentration of the protonated triazine, which must be used in the rate law. In an aqueous environment the scavenging process may therefore be assumed to be described with the following rate law [5].

$$-\frac{d[T]}{dt} = k[TH^+][HS^-] \tag{4.9}$$

To estimate the concentration of the protonated species, the acid/base equilibrium from equation 4.4 can be used.

$$[TH^+] = K_a^{-1}[T][H^+] \tag{4.10}$$

This can then be inserted into the rate law, so that it only contains known properties[1].

$$-\frac{d[T]}{dt} = k_3'[T][H^+][HS^-] \quad , \quad k_3' = k \cdot K_a^{-1} \tag{4.11}$$

The rate law is simplified with k_3' in the case that the acid constant is unknown, since k_3' then will be the observed rate constant.

---

[1] Here it is assumed that the pK_a value for the protonated species is known

If the kinetic experiments are performed in a buffered solution, where the pH can be kept constant, the concentration of protons will be constant and become part of the rate constant.

$$-\frac{d[T]}{dt} = k_2'[T][HS^-] \quad , \quad k_2' = k_3'[H^+] \tag{4.12}$$

A final simplification can be made if the experiments are run at high HS^- concentration. Then the HS^- concentration will be practically constant, and the reaction may be considered pseudo first order.

$$-\frac{d[T]}{dt} = k_1'[T] \quad , \quad k_1' = k_2'[HS^-] \tag{4.13}$$

Experiments have been made to study the reaction kinetics, with 10[T] = $[HS^-]$ and pH 10.5, which confirmed the first order dependency on the hydroxyethyl-triazine concentration. However, the acid constant for hydroxyethyl-triazine was unknown, and only k_3' could be determined. This was found to be $5.6 \cdot 10^7$ $M^{-2}min^{-1}$ at room temperature [5].

Additional experiments are necessary to confirm the assumption that the reaction is first order in $[HS^-]$, and also to determine the acid constant to allow the final rate constant, k, to be found.

A further comment on these experiments is that they have only considered the rate constant for the conversion of triazine to thiadaizine. It is reasonable to assume that this will be the fastest of the three steps, since the stability of the scavenging molecules increases from hydroxyethyl-triazine to trithiane. To optimise and understand the reaction system, the remaining rate constants must also be determined. They could be especially useful since the fouling problem is suspected to be related to terminal reactions products and not thiadiazine. Knowledge about the total kinetics may then be used to optimise the use of the scavenging chemicals, and possibly achieve a kinetic inhibition of the fouling precursor. By applying reasonable assumptions, a kinetic model may be constructed, which for now may be used to investigate the effect of different rate constants and to compare the hydrolysis with the scavenging reaction.

Kinetic model for scavenging

The model concerns the three nucleofile substitution reactions leading to trithiane, and also includes the hydrolysis of triazine, since this will affect the overall effectiveness of the scavenging. First a number of assumptions are made.

- HS^- is in excess, and the concentration may be considered constant
- The reactions all follow pseudo first order kinetics
- The reactions are considered irreversible
- The pH is constant
- Only triazine is subject to hydrolysis

- The pipeline where scavenging takes place is viewed as a plug flow reactor (PFR)

Since the order of reaction for HS^- is unknown, the concentration of HS^- in the model is considered to be so high that any change is insignificant; therefore, the reactions can be thought to be pseudo first order. No values for the equilibrium constants are known, and as a result the reversible reactions have been neglected, and the equilibrium is assumed to be found far to the right with the products. Because pH influences the reaction rate, both of the scavenging reaction and the hydrolysis, the model is constructed to describe environments with constant pH since this simplifies the equations. The assumption, that only triazine is subject to the acid catalysed hydrolysis, is made since no value is reported for the hydrolysis of thiadazine, other than it is slower than the hydrolyis of triazine. To simplify the model, it is set to zero. The addition of sulphur atoms to the molecular structure alters the reactivity and stability of the molecule, and this forms the basis of the assumption. When Maersk injects the scavenger into the natural gas, it is done in a pipeline, and the pipes may be viewed as a PFR if plug flow is assumed [11]. In figure 4.7 the reactions are illustrated.

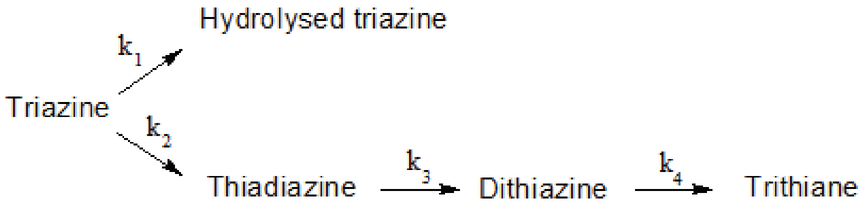

Figure 4.7: Kinetic model

To simplify the notation from here on, we rewrite the reactions as seen in figure 4.8.

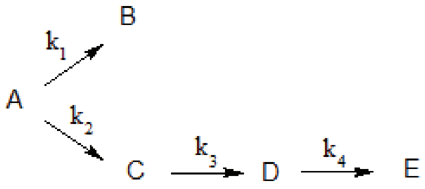

Figure 4.8: Kinetic model simplified notation

As seen, the system consists of a series reaction from triazine to trithiane and the hydrolysis reaction parallel to this system.

Looking first at A where the mole balance is:

$$\frac{dF_A}{dV} = r_A \tag{4.14}$$

Where F_A is the molar flow of A.

(a) Rate law

$$-r_A = k_1 C_A + k_2 C_A \Updownarrow \tag{4.15}$$

$$-r_A = (k_1 + k_2) C_A \tag{4.16}$$

(b) Stoichiometry ($v = v_0$ (volumetric flow))

$$F_A = C_A v_0 \tag{4.17}$$

(c) Combining

$$v_0 \frac{dC_A}{dV} = -(k_1 + k_2) C_A \tag{4.18}$$

$$\frac{dC_A}{d\tau} = -(k_1 + k_2) C_A \tag{4.19}$$

Here we have used that space time, $\tau = \frac{V}{v_0}$.

(d) Integrating we get

$$\int_{C_{A0}}^{C_A} \frac{1}{C_A} dC_A = -(k_1 + k_2) \int_0^{\tau} d\tau \Updownarrow \tag{4.20}$$

$$\ln \left| \frac{C_A}{C_{A0}} \right| = -(k_1 + k_2)\tau \Updownarrow \tag{4.21}$$

$$\boxed{C_A = C_{A0} e^{-(k_1+k_2)\tau}} \tag{4.22}$$

A similar procedure may be used to construct an expression for B.

$$\frac{dF_B}{dV} = r_B \tag{4.23}$$

1. Rate law

$$-r_B = -k_1 C_A \tag{4.24}$$

2. Stoichiometry ($v = v_0$)

$$F_B = C_B v_0 \tag{4.25}$$

3. Combining

$$v_0 \frac{dC_B}{dV} = k_1 C_A \Updownarrow \tag{4.26}$$

Again substituting v_0 and V with τ, and inserting C$_A$ we get

$$\frac{dC_B}{d\tau} = k_1 C_{A0} e^{-(k_1+k_2)\tau} \tag{4.27}$$

4. Integrating, where it is used that $C_{B0} = 0$, we get

$$\int_0^{C_B} dC_B = k_1 C_{A0} \int_0^{\tau} e^{-(k_1+k_2)\tau} d\tau \Updownarrow \tag{4.28}$$

$$C_B = k_1 C_{A0} \left[\frac{-1}{k_2+k_1} e^{-(k_1+k_2)\tau} \right]_0^{\tau} \tag{4.29}$$

$$\boxed{C_B = \frac{k_1}{k_1+k_2} C_{A0} \left(1 - e^{-(k_1+k_2)\tau}\right)} \tag{4.30}$$

For thiadiazine there will both a producing and consuming reaction that needs to be taken into account.

$$\frac{dF_C}{dV} = r_C \tag{4.31}$$

1. Rate law

$$-r_C = k_3 C_C - k_2 C_A \tag{4.32}$$

2. Stoichiometry ($v = v_0$)

$$F_C = C_C v_0 \tag{4.33}$$

3. Combining

$$v_0 \frac{dC_C}{dV} = k_2 C_A - k_3 C_C \Updownarrow \tag{4.34}$$

   We perform the same substitution as with the hydrolysed triazine, substitute v_0 and V with τ, and insert C_A. However, because C_A is also a function of τ, the equation is an inhomogeneous ODE, and to solve it the integrating factor method is used.

$$\frac{dC_C}{d\tau} + k_3 C_C = k_2 C_{A0} e^{-(k_1+k_2)\tau} \tag{4.35}$$

   The integrating factor becomes

$$i.f. = e^{\int k_3 d\tau} = e^{k_3 \tau} \tag{4.36}$$

   When using the integrating factor method, C_C can be found in the following way:

$$C_C = e^{-k_3\tau} \left(\int k_2 C_{A0} e^{-(k_2+k_1)\tau} \cdot e^{k_3\tau} d\tau \right) \Updownarrow \tag{4.37}$$

$$= C_{A0} k_2 e^{-k_3\tau} \int e^{(k_3-k_2-k_1)\tau} d\tau \Updownarrow \tag{4.38}$$

$$= C_{A0} k_2 e^{-k_3\tau} \left(\frac{1}{k_3-k_2-k_1} e^{(k_3-k_2-k_1)\tau} + K \right) \tag{4.39}$$

To determine K, we use the boundary condition $C_C = 0$ at $\tau = 0$

$$0 = C_{A0}k_2\left(\frac{1}{k_3 - k_2 - k_1} + K\right) \tag{4.40}$$

$$K = \frac{-1}{k_3 - k_2 - k_1} \tag{4.41}$$

Inserting K, we get an expression for the thiadiazine concentration

$$\boxed{C_C = \frac{k_2}{(k_2 + k_1) - k_3}C_{A0}\left(e^{-k_3\tau} - e^{-(k_1+k_2)\tau}\right)} \tag{4.42}$$

As with thiadiazine, there are two reactions affecting the concentration of dithiazine.

$$\frac{dF_D}{dV} = r_D \tag{4.43}$$

1. Rate law

$$-r_D = k_4C_D - k_3C_C \tag{4.44}$$

2. Stoichiometry (v = v_0)

$$F_D = C_Dv_0 \tag{4.45}$$

3. Combining

$$v_0\frac{dC_C}{dV} = k_3C_C - k_4C_D \Updownarrow \tag{4.46}$$

We perform the same substitution as in the previous calculations, and again we use the integrating factor method to find an expression for C_D.

$$\frac{dC_D}{d\tau} + k_4C_D = k_3\frac{k_2}{(k_2 + k_1) - k_3}C_{A0}\left(e^{-k_3\tau} - e^{-(k_1+k_2)\tau}\right) \tag{4.47}$$

The integrating factor becomes

$$i.f. = e^{\int k_4 d\tau} = e^{k_4\tau} \tag{4.48}$$

$$C_D = e^{-k_4\tau}\left(\frac{k_3k_2}{(k_2 + k_1) - k_3}C_{A0}\int\left(e^{-k_3\tau} - e^{-(k_1+k_2)\tau}\right)e^{k_4\tau}d\tau\right) \Updownarrow \tag{4.49}$$

$$= e^{-k_4\tau}\frac{k_3k_2}{(k_2 + k_1) - k_3}C_{A0}\int\left(e^{(k_4-k_3)\tau} - e^{(k_4-(k_1+k_2))\tau}\right)d\tau \Updownarrow \tag{4.50}$$

$$= e^{-k_4\tau}\frac{k_3k_2}{(k_2 + k_1) - k_3}C_{A0}\left(\frac{e^{(k_4-k_3)\tau}}{k_4 - k_3} - \frac{e^{(k_4-(k_1+k_2))\tau}}{k_4 - (k_1 + k_2)} + K\right) \Updownarrow \tag{4.51}$$

$$K = \frac{1}{k_4 - (k_1 + k_2)} - \frac{1}{k_4 - k_3} \tag{4.52}$$

Inserting K, we get an expression for the dithiazine concentration.

$$\boxed{C_D = \frac{k_3 k_2}{(k_2+k_1)-k_3} C_{A0} \left(\frac{e^{-k_3\tau} - e^{-k_4\tau}}{k_4 - k_3} + \frac{e^{-(k_1+k_2)\tau} - e^{-k_4\tau}}{(k_2+k_1)-k_4} \right)} \tag{4.53}$$

For the trithiane, the concentration can be calculated by subtracting the other concentrations from the total.

$$C_E = C_{A0} - C_A - C_B - C_C - C_D \tag{4.54}$$

With these five equations the concentrations of each species as a function of time may be found.

To investigate the influence of the secondary rate constants, the model has been used to produce a kinetic scenario. If we assume that the K_a value for triazine might be approximated with the pK_a value for DMEA, the rate constant for the conversion of triazine to thiadiazine at pH 10.5, k_2, can be calculated from the data of Buhaug and Bakke.

$$k_2 = k'_{3,BB} \cdot 10^{-pK_{a,DMEA}} \tag{4.55}$$

$$= 5.6 \cdot 10^7 \cdot 10^{-8.88} \tag{4.56}$$

$$= 7.4 \cdot 10^{-2} M^{-1} s^{-1} \tag{4.57}$$

The rate constant for the hydrolysis at pH 10.5 may be estimated by making linear regression on the natural logarithmic values of the hydrolysis rate constants from table 4.3 as function of pH. The best linear fit is:

$$\ln(k_{hydrolysis}) = -2.1 \cdot pH + 12.6 \tag{4.58}$$

With this fit $k_1 = 1.1 \cdot 10^{-4}$ s^{-1} at pH 10.5.

Since k_2 is a second order rate constant, and the model is build on the assumption of pseudo first order kinetics, it is necessary to choose a HS^- concentration. In alignment with the experiments of Buhaug and Bakke, a concentration of $10[T] = [HS^-]$ is choosen, which results in a $k_2 = 6.9 \cdot 10^{-1}$ s^{-1} for $[T] = 1$ M. By comparing the two first order rate constants, it is seen that k_2 is 6500 times larger than k_1.

There does not exist information about the size of k_3 and k_4 relative to k_2, therefore it is necessary to choose some approximate values. Because thiadiazine is much like triazine, it seems reasonable to assume that the reaction rate for the conversion of thiadiazine to dithiazine will be comparable to the reaction rate of the conversion of triazine to thiadiazine. Still, thiadiazine is a more stable compound than triazine, so the rate constant will be expected to be somewhat lower. With these considerations in mind, the value for k_3 in this model is set to a tenth of k_2. Because dithiazine is even more stable than thiadiazine, and because trithiane was not detected in the experiments by Buhaug and Bakke, k_4 is given a value one thousandth of k_2. In reality these rate constants may be very different though.

The scenario shows that at pH 10.5, 22 ℃ and $[HS^-] = 10[T]$, the hydrolysis reaction is not influential on the scavenging process. However, in very diluted solutions, collisions

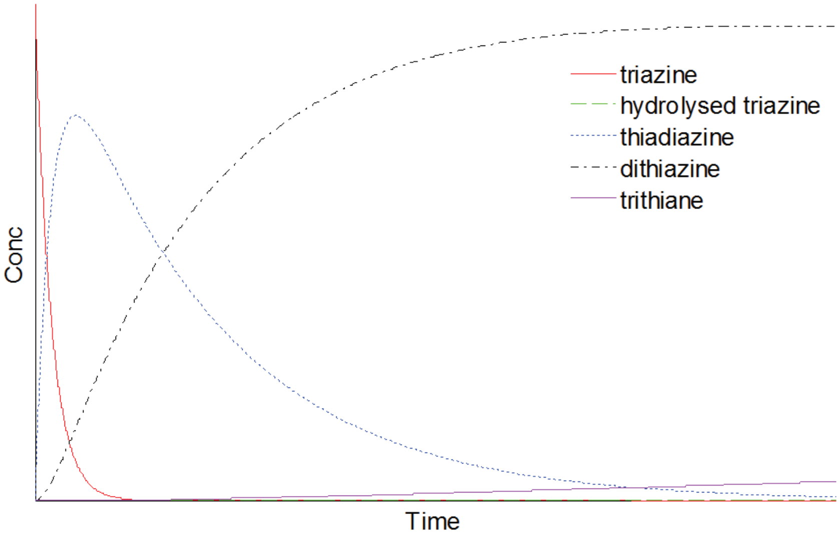

Figure 4.9: Kinetic scenario

between triazine and HS^- will be less likely to occur and the hydrolysis may become important for the total effectiveness of the scavenger. It is also seen that at the chosen rate constants, the triazine is spent relatively fast, giving rise to a rapid build-up of thiadiazine. The thiadiazine concentration peaks when the concentration of triazine is depleted, after which it decreases slowly following an approximated first order reaction. This is due to the relative size of k_2, k_3 and k_4. Initially, k_2 and k_3 ensures that the two exponential terms in the parenthesis in equation 4.42 will be of the same magnitude. As time goes on, the second exponential term, where k_2 is present, becomes much smaller than the first because k_2 is ten times larger than k_3, and the degradation term $(e^{-k_3\tau})$ dominates. Because the conversion from dithiazine to trithiane is much slower compared to the reaction from thiadiazine to dithiazine, the thiadiazine concentration end up decreasing according to the approximate first order degradation. Because the final conversion from dithiazine to trithiane is very slow, dithiazine tends to build-up in the system, but given enough time, appreciable amounts of trithiane could be formed, depending on the size of k_4. This highlights the importance of the transport time for the crude oil from after scavenging until it arrives at the refinery. Prolonged holding times may lead to trithiane being formed in the crude oil if H_2S and dithiazine is present.

Because of difference in size between the rate constants, it is reasonable to assume that the activation energy will be increasing from triazine/thiadiazine to dithiazine/trithiane, and the rate constants therefore most likely will not be affected proportionally by temperature changes. It is therefore possible that by controlling the temperature, a scavenging process that kinetically inhibits the formation of fouling compounds may be carried out. However, in reality it may prove difficult to change to temperature much without significant costs. Another possibility could be to introduce another reaction that removes the precursor for the fouling compound. If it is assumed that the fouling compound is trithiane, then a way of avoiding trithiane formation could be to let dithiazine react in a parallel reaction. Since the reaction rate for trithiane formation is slow compared to the other steps in the scavenging process, there is not much scavenging potential in dithiazine, and a removal of it would not decrease the overall effectiveness of the scavenging process.

In general this discussion highlights the importance of controlling the kinetics of the system, for which reason it is important to know which factors influence the rate of reaction.

Factors influencing rate of reaction

Besides pH, temperature and H_2S concentration there are other factors, which may influence the rate of reaction.

A factor, which will be important for the reaction rate, is the type of triazine. As mentioned during the discussion of triazines, they can have different side groups attached to the nitrogen atoms. In our case the most interesting triazine is hydroxyethyl-triazine, because this is the one currently being used by Maersk, but if another treatment procedure was sought other triazines could become interesting. One of the effects of differing side groups, is a change in solubility parameters. The hydroxy-group makes the triazine water soluble, which is preferable to avoid mixing with the oil. However, if it is decided to remove H_2S at an earlier state in the process, where most H_2S is dissolved in the oil, then a more non-polar triazine could be chosen. Two other triazines have been investigated: ethyl-triazine and methyl-triazine. They were tested in similar manners as the hydroxyethyl-triazine, and were found to have k_3' values of 3.0 and 0.17 [5], which are lower than hydroxyethyl-triazine. However, this is not too surprising since the reactions were carried out in aqueous solutions. It shows that the type of triazine influences the reaction rate, and it is also worth noticing that there is a large difference between the two alternative triazines, although they have comparable miscibility with water.

Another factor that may influence therate of reaction, is the use of a catalyst. For triazines it has been found that quaternary ammonium compounds, see figure 4.10, may act as catalysts in the scavenging process [29, 16]. Just as the triazines, quaternary ammonium compounds can be tailored to be either water or oil soluble, by varying the side groups. Referring to figure 4.10, R_1 and R_2 will be independent alkyl groups or hydroxyalkyl groups having from 1 to 8 carbon atoms. R_3 will be an alkyl or aryl group having from 1 to 20 carbon atoms, and R_4 will be an alkyl or aryl group having

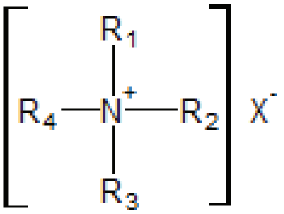

Figure 4.10: Quaternary ammonium

from 7 to 20 carbon atoms. X is an anion, which most often will be either chloride or methylsulphate [29]. If an water soluble ammonium compound is desired, then hydroxyalkyl groups and short chained alkyl/aryl groups should be chosen. However, the ammonium compound should be chosen so that it is sufficiently lipophilic, because the enhancement of the reaction rate is achieved through phase transfer catalysis. Often the nucleofile will be an anion, as in our case where we assumed the H_2S to react as the anion HS^-. Ionic species will be present in the aqueous phase, but often the substrate to take part in the substitution reaction will be in an organic phase. A quaternary ammonium compound can then bring the nucleofile over into the non-polar phase by forming an ion pair; the quaternary compound will be soluble in the non-polar phase because of its alkyl and aryl side groups. In this way, quaternary ammonium compound might catalyse the reaction; furthermore, nucleophiles react faster in polar aprotic*and non-polar aprotic environments, because they are not stabilised here [26].

When triazine reactions are intentionally catalysed with quaternary ammonium, the weight ratio between triazine and quaternary ammonium will commonly vary from 10:0.05 to 10:1. By using benzyl-cocoalkyl-dimethyl-quaternary ammonium chloride together with a mixture of 1,3,5-tri-methoxypropyl-hexahydro-1,3,5-triazine it has been found that the rate of removal of H_2S from a solution of kerosene saturated with H_2S could be significantly improved compared to the use of pure triazine [29]; however no results with the use of hydroxyethyl-triazine was given. It is also questionable how much Maersk's scavenging process will be affected since this is carried out in a gas mixture.

4.4.4 Reversing trithiane formation

A method of preventing and/or remediating trithiane deposition from H_2S scavenging has been reported by Horton et al. [14]. They state that in cases with very high concentrations of H_2S compared to the amount of triazine scavenger, trithiane may be formed. The reactions leading to dithiazine are fast compared to the substitution of the final nitrogen atom, but where the reaction to form thiadiazine and dithiazine can be considered almost complete with the equilibrium being situated far towards the products, this may not be the case for trithiane formation. This reaction may be reversed.

When using hydroxyethyl-triazine, MEA is one of the reaction products for each reaction step. By adding extra MEA or another primary amine or ammonia [14], the reactions may be removed from equilibrium and for the final reaction to return to equilibrium, trithiane will react with MEA to form dithiazine as seen in figure 4.11. Thiadiazine and dithiazine will not be converted to the same degree as trithiane if the equilibrium for these reactions is positioned much farther towards the products. The addition of extra MEA will also help to keep the pH sufficiently high to avoid hydrolysis of triazine.

4.4.5 Alternative reaction products

Bakke and Buhaug did not find trithiane to be formed [5], which might question the idea that the fouling is caused by trithiane deposition. Instead they found that the reaction

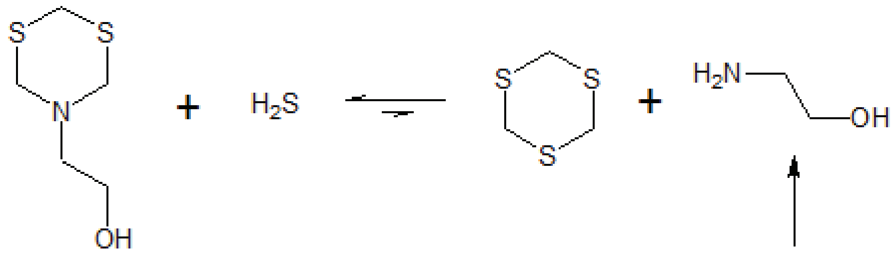

Figure 4.11: Reversal of trithiane formation

terminated with the formation of dithiazine; even when the solution was saturated with H_2S bubbling through the triazine solution, only dithiazine was found, and this was with the triazine and thiadiazine being completely spent. Another possibility is therefore that the fouling is caused by dithiazine.

In a recent study by Taylor and Matherly [30], an attempt has been made to elucidate the structure of the solid by-product from the use of hydroxyethyl-triazine in H_2S scavenging. In their experiments, a solution of 30 w% hydroxyethyl-triazine was put in a glass gas tower, and spent with pure H_2S. This resulted in two phases with the lower being identified as dithiazine. After one hour, very heavy white solids were deposited in the fluid, and the lower phase solidified into a fine white powder [30]. It was these solids that were investigated, with the initial assumption that they were amorphous dithiazine. The crystals were investigated with X-ray diffraction, elemental analysis, NMR and IR.

In figure 4.12 two X-ray diffraction spectra of the "amorphous dithiazine" crystals are shown; one sample obtained by Taylor and Matherly in the laboratory, and one field sample obtained from an unspecified oil field production plant. It is seen that these two samples are very similar, but very different from the X-ray spectrum of crystalline dithiazine crystals seen in figure 4.13. An elemental analysis was performed on all three types of crystals. If the two amorphous dithiazine samples were indeed a physical form of crystalline dithiazine, then similar empirical formulas should be found. In table 4.4 the found empirical formulas are shown. What is immediately clear is that both samples of what was thought to be amorphous dithiazine contain significantly more carbon, hydrogen and sulphur than the crystalline dithiazine, with the laboratory

Table 4.4: Empirical formulas for three dithiazine crystals [30]

Element	Crystalline	Laboratory	Field
Carbon	5.0	9.8	7.2
Hydrogen	11.0	21.5	15.1
Nitrogen	1.0	1.0	1.0
Sulphur	2.0	7.8	4.6
Oxygen	1.0	1.0	1.2

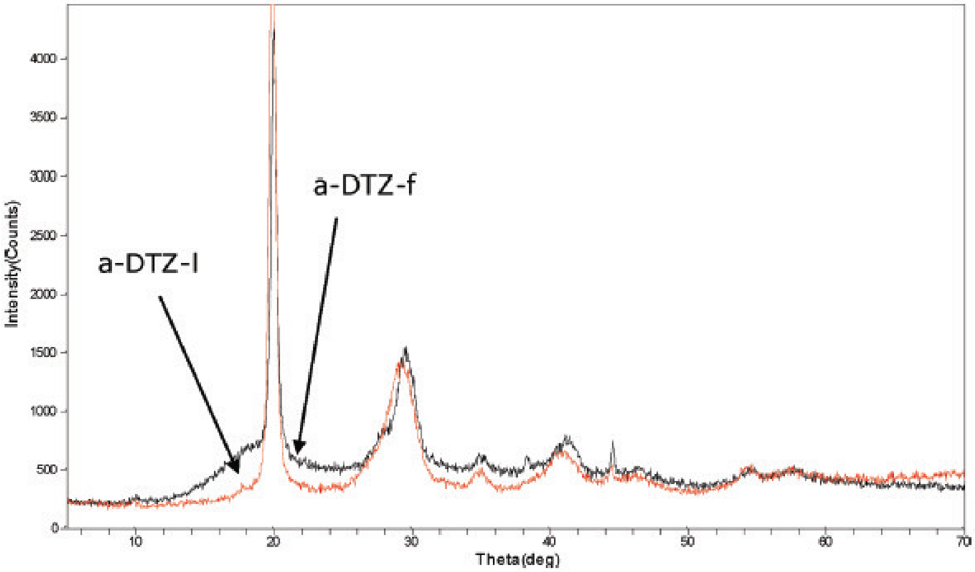

Figure 4.12: X-ray diffraction of amorphous dithiazine crystals obtained in laboratory and field [30]

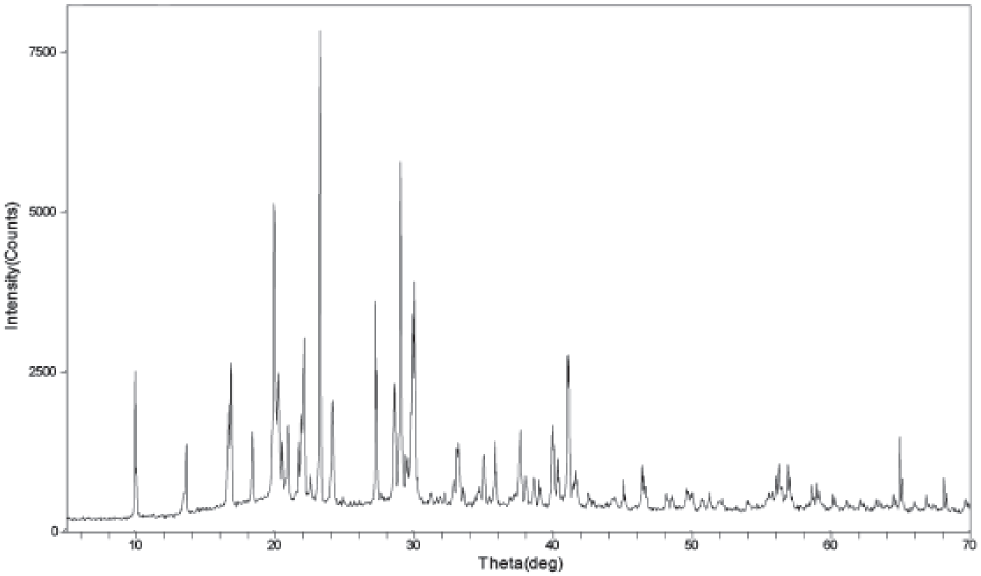

Figure 4.13: X-ray diffraction of crystalline dithiazine crystals [30]

sample representing the most extreme deviation. The NMR analysis did also show multiple resonances in the region 3.8 to 4.4 ppm, which is where methylene adjacent to sulphur is expected to resonate, and was taken as evidence for additional CH_2-S groups. The IR scans performed showed similar spectra for the laboratory and field samples, both of which were very different from the crystalline spectrum, indicating that these represented two different materials [30].

The hypothesis put forward by Taylor and Matherly to explain this difference is that the dithiazine molecules polymerise with long chains of CH_2-S between each dithiazine molecule. By using different triazines it was shown that a terminal hydroxy group was necessary for the formation of the precipitate. When 1,3,5-tris(methyl)-hexahydro-s-triazine and 1,3,5-tris(methoxypropyl)-hexahydro-s-triazine was used instead of hydroxyethyl-triazine, pure dithiazines crystals were obtained. The proposed mechanism is that the triazine is hydrolysed back to MEA and formaldehyde. Formaldehyde then reacts with H_2S to form thioformaldehyde, which may react with the hydroxyl group on a dithiazine molecule and initiate the polymerisation. The proposed scheme is illustrated in figure 4.14. It is therefore possible that the fouling encountered at Shell is in fact polymerised dithiazine, and not trithiane. In Shell's own elemental analysis traces of nitrogen were detected, which could indicate that the fouling is indeed polymerised dithiazine.

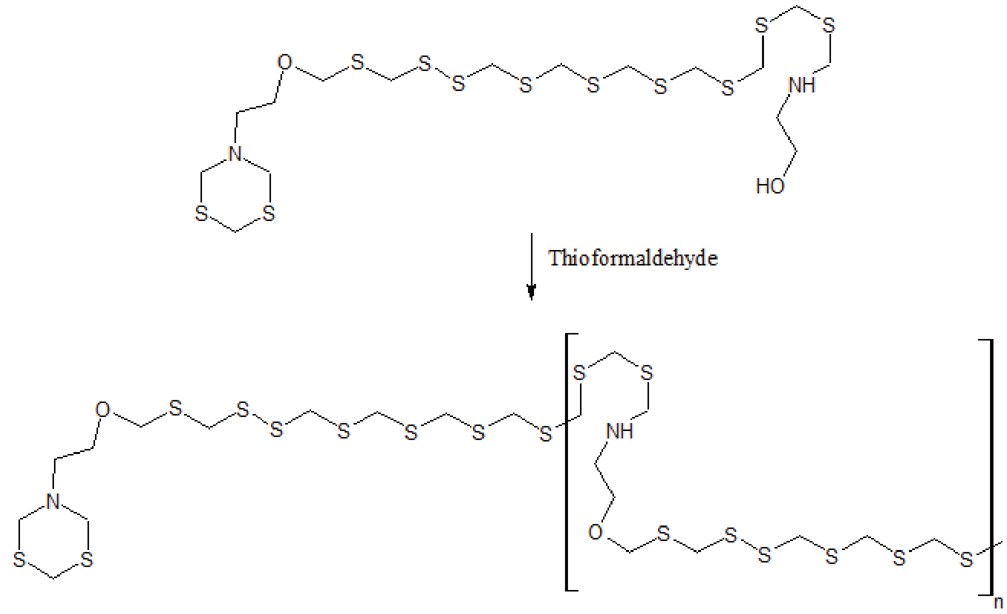

Figure 4.14: Proposed polymerisation scheme [30]

Chapter 5

Mass balance for scavenging process

To estimate the amount of scavenger products being exported to Shell, a mass balance is made on the system. In this mass balance it is assumed that only the oil phase from the spent scavenger separator is recirculated back. Possible overflow of the aqueous phase back into the raw oil is therefore not considered, and the oil stream from the skimmer separator is neglected. For determination of the amount of scavenger products being fed back into the raw oil, it is necessary to consider the equilibrium distribution of the scavenger products between the aqueous and the oil phase. To calculate the concentration in the aqueous phase, C_W, and in the oil phase, C_O, an equilibrium equation is set up. Here it is assumed that all of T is present in the aqueous phase at the beginning. T_i is a random component.

	T_{H_2O}	$\rightleftharpoons$	T_{oil}
Start	$n_{i,total}$		0
Equilibrium	$n_{i,total}$ - x		x

From this the equilibrium concentrations become:

$$C_{W,i} = \frac{n_{i,total} - x}{V_W} \tag{5.1}$$

$$C_{O,i} = \frac{x}{V_O} \tag{5.2}$$

The equilibrium constant for component "i" is defined as, $K_i = \frac{C_{O,i}}{C_{W,i}}$, and we may therefore insert the equilibrium concentrations in this expression, and use the equation for isolation. Here it may be noticed that since no T was present in the oil phase at the beginning, $x = n_{O,i}$.

$$K_i = \frac{\frac{n_{O,i}}{V_O}}{\frac{n_{i,total}-n_{O,i}}{V_W}} \tag{5.3}$$

$$= \frac{n_{O,i} \cdot V_W}{V_O(n_{i,total} - n_{O,i})} \Updownarrow \tag{5.4}$$

$$n_{O,i} = \frac{K_i \cdot V_O \cdot n_{i,total}}{V_W + K_i V_O} \Updownarrow \tag{5.5}$$

$$C_{O,i} = K_i \frac{n_{i,total}}{V_W + K_i V_O} \tag{5.6}$$

Similarly for C_W where $n_{o,i}$ is inserted

$$C_W = \frac{n_{i,total}}{V_W} - \frac{K_i V_O n_{i,total}}{(V_W + K_i V_O)V_W} \tag{5.7}$$

$$= \frac{n_{i,total}}{V_W + K_i V_O} \tag{5.8}$$

To determine how much of each component is transferred to Shell, it is also necessary to know the relative distribution of reaction products and triazine in the spent scavenger solution. Here we may refer to an analysis made by Maersk, where the average composition of the spent scavenger from all scavenging processes was determined to be 44.6 % triazine, 28.4 % thiadiazine and 27.0 % dithiazine [2]. The numbers are taken from a 10 year old report, and the up to date validity may therefore be questioned, but they may still be used to give an overview of the amount of exported scavenging products.

It is also necessary to know the flow of the different mass streams. Accurate numbers are not available, but approximate values exist for the Dan field, which is also the largest consumer of scavenger. The flow values for the different streams used in the calculations are given in table 5.1.

Table 5.1: Data for flows for use in mass balance [2]

	Unit	Dan FF	Dan FC	Dan FG
Injected scavenger	l/hr	250	250	150
Water from g/l[†]sep.	m^3/day	12	12	7.2
Oil from g/l sep.	m^3/day	12	12	7.2
Water from spent scav. sep.	m^3/day	0	24	7.2
Oil from spent scav. sep.	m^3/day	0	24	7.2
Water from LP sep.	m^3/hr	150	13	0
Oil from LP sep.	m^3/hr	250	57	0

[†] The gas liquid separator after scavenger injection.

The calculations are performed for each of the three platforms (DFF, DFC and DFG), but in figure 5.1, which gives an overview of the mass balance, only the sum of the individual streams is shown.

To find the molar amount of scavenger it is used that the concentration of triazine in the scavenging product is 51 wt/wt %, and that the density is 1.1072 kg/L, see appendix E. Below the calculation for the total molar amount of injected scavenger on Dan is shown.

$$\begin{aligned} n_{triazine} &= \frac{F_{inj.scav.} \cdot \rho_{scav.} \cdot c_{scav.} \cdot 24\frac{hr}{day}}{M_{triazine}} \\ &= \frac{650\frac{l}{hr} \cdot 1.1072\frac{kg}{l} \cdot 0.51 \cdot 24\frac{hr}{day}}{219.28\frac{kg}{kmol}} \\ &= 40.17\frac{kmol}{day} \end{aligned} \tag{5.9}$$

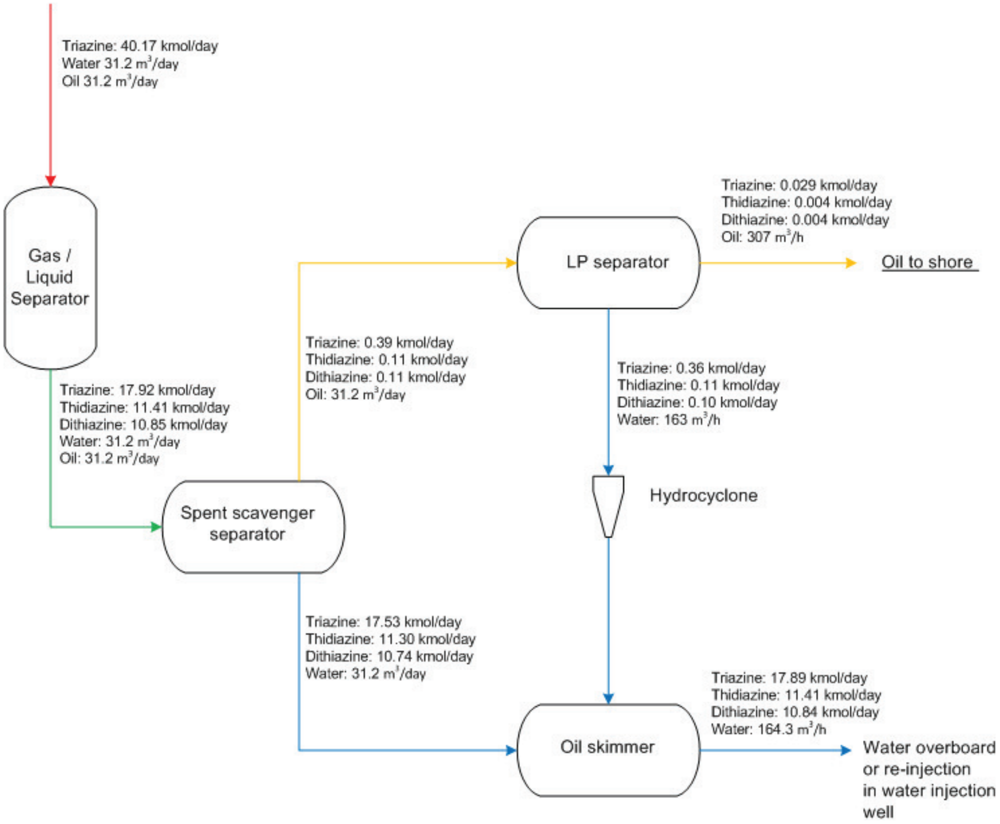

Figure 5.1: Mass balance

To calculate the concentration in each oil and water outlet of the separators, it is assumed that the equilibrium distribution will have time to be established, and that the streams are pure oil and pure water. In reality some water will be present in the oil phase and some oil will be present in the water phase. Especially the amount of water dissolved in oil may influence the mass balance because of the high aqueous solubility of the scavenger compounds. Concentration values for water in oil and oil in water does not exist, and therefore the concentrations are assumed to be zero. When calculating the concentration of scavenger products in the streams after a separator, equation 5.8 is first applied for each species to find the concentration in the aqueous phase, and the result is then inserted into equation 5.6 to find the concentration in the oil phase. For the total amount of mole for each species in the spent scavenger solution, the distribution values are multiplied with the result of equation 5.9.

Shell reports that the fouling occurs very fast at times, and seems to be linked to specific batches of crude oil. A possibility is that this is due to the water from the spent scavenger separator being sent back with the oil to the LP separator because of necessary maintenance of the scavenger system. To investigate the effect of such a procedure, a new mass balance is made, in which the water flow from the spent scavenger is redirected directly to the LP separator. The mass balance is shown in figure 5.2

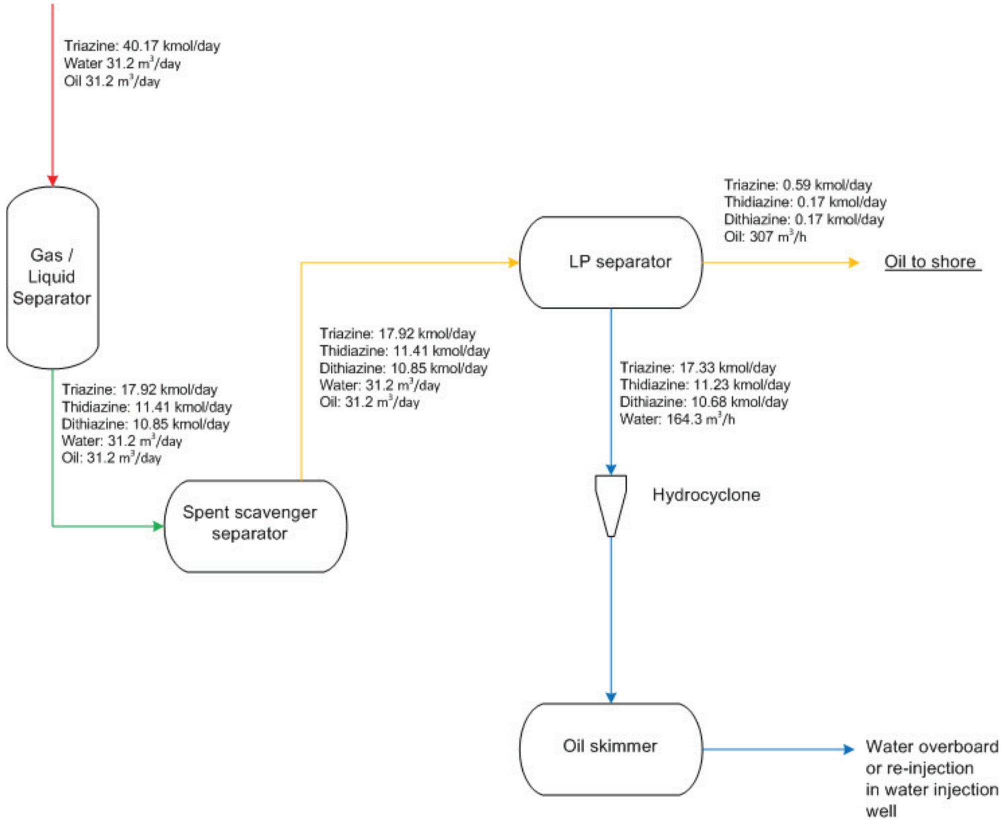

Figure 5.2: Mass balance without spent scavenger separator

In table 5.2 the estimated daily amounts of exported scavenger from the Dan field are shown.

The mass balances show that at standard operation conditions, a relative small amount of scavenger is exported to Shell. Whether this is sufficient to cause fouling is not known, but over a long period of time, a significant amount of fouling could be produced if the scavenger products somehow accumulate at the refinery. It is also clear that batches of oil produced during maintenance of the spent scavenger separator

Table 5.2: Exported amounts of scavenger from Dan

Compound	Standard operation (kg/day)	During maintenance (kg/day)	Factor
Triazine	6.41	129.7	20.2
Thiadiazine	0.78	33.52	43.0
Dithiazine	0.64	27.40	42.8

may contain a significant amount of scavenger, which could explain why the fouling problem seemingly is linked to specific batches of oil. It is plausible that during standard operation, the fouling will only build-up slowly or not at all, and when at batch rich in scavenger arrives, it may accelerated the fouling process, leading to a fast clogging of the system.

It is also worth noticing how the setup of the process affects the final amount of spent scavenger in the exported crude oil. In the LP separator at Dan FC, the oil to water ratio is relatively high, 4.38, compared to the LP separator at Dan FF, 1.67. This means that the spent scavenger products are extracted less efficiently to the water phase, and results in an increased amount of spent scavenger in the crude oil. This is further worsened by the fact that it is the separator at Dan FC that handles the largest amount of spent scavenger; Dan FF handles the spent scavenger from Dan FG. Because of these two effects, the oil from Dan FC will contain 89.5 % of the exported spent scavenger. If the whole Dan field is considered as one, the oil to water ratio in this hypothetical LP separator would be 1.88, resulting in only 3.36 kg/day triazine, 0.40 kg/day thiadiazine and 0.33 kg/day dithiazine being exported. In this way the amount of exported spent scavenger can be halved by having a more optimal oil to water ratio in the LP separator.

CHAPTER 6

Evaluation of problem analysis

In the previous chapters, the fouling problems experienced by Maersk and Shell, and the scavenging process have been analysed.

1,3,5-tri-(2-hydroxyethyl)-hexahydro-s-triazine and its reactions products are all only sparingly soluble in oil, and most will therefore be discharged with the produced water. However, because of the significant production flow, even small amounts of spent scavenger in the oil may result in a considerable amount if allowed to build-up at Shell. Furthermore, several sources report that H_2S scavenging with triazines may lead to precipitation, making the scavenging process a likely source for the fouling found at Shell.

Based on the the problem analysis three hypotheses capable of explaining the nature of fouling problem is put forward.

Hypothesis A The fouling is created by trithiane formation

Hypothesis B The fouling is created by polymerisation of dithiazine

Hypothesis C The fouling is created by a third unknown process

Hypothesis A is the one currently believed to be correct since mass analyses made by Shell, have indicated a composition of the fouling, which could match the empirical formula of trithiane. Some sources do also talk about trithiane formation, but the results of Buhaug and Bakke seems to contradict this. They indicate that the scavenging process terminates with the formation of dithiazine. Hypothesis B, which explains the fouling with the formation of a polymeric material made up by dithiazine molecules linked by long -C-S- chains, could then offer an alternative explanation for the fouling since it would allow for a suitable empirical formula. Should neither A or B be true, a third process has to be responsible for the fouling.

With these considerations in mind, the primary goal of the experiments is to investigate if the fouling can be linked to the H_2S scavenging process, as well as investigate the true nature of the fouling. The specific cause for the fouling and solutions to the problem will also be considered.

Chapter 7

Experiments - The scavenging process

This chapter contains experiments performed to investigate if controlled scavenging experiments from the laboratory will be representative to the actual process. This is done by first making experiments with HS^- ions as described in literature by Buhaug and Bakke [5], and then with H_2S gas as described by Taylor and Matherly [30]. Finally, the spent scavenger solution produced by Maersk, and which is suspected of being the source for the fouling, is used in an experiment, which will investigate the effect of a large H_2S concentration gradient on this specific spent scavenger solution. The reactions are monitored with ESI-MS, which makes it possible to investigate the composition of the reaction mixture during the course of the reaction, by identification of peaks and their relative intensity in the mass spectra. Since no chromatograph is available in connection with the ESI-MS, only qualitative statements can be made. In appendix C a description of the ESI-MS technique is found.

Prior to the investigation of the reaction system, mass spectra of some of the basis chemicals used the experiments were recorded to be used as a reference for identification of peaks in the mass spectra recorded during the investigation of the reaction system.

7.1 MS spectra of basis chemicals

To analyse the hydroxyethyl-triazine and the spent scavenger solution, a mass spectrum was recorded for each. The MS was set to positive ion mode during all experiments, and therefore only positive ions were detected. With most experiments being carried out in alkaline environments due to the presence of amines, the degree of protonation in the solution prior to entering the MS was low. Therefore other positive ions might compete with H^+ protonation, which would influence the m/z value of the peaks in the mass spectra. To investigate the effect of Na^+ ions, a spent scavenger solution was spiked with 1 M NaCl and analysed. Also pure MEA and MEA with 1 M NaCl was analysed.

Before analysis on the MS, the samples had to be diluted. This was done by extracting 1 ml sample and diluting it 1:100 with demineralised water in a 100 ml volumetric flask. A further dilution to 1:10000 was made, and then a sample was collected with a syringe that was placed in the syringe pump attached to the MS, after which the sample was analysed. Between measurements the MS was cleaned by filling the syringe with a 1:1:1 mixture of demineralised water, iso-propanol, and methanol.

7.1.1 Results

The mass spectra for hydroxyethyl-triazine and the spent scavenger are shown in figure 7.1. In appendix F the respective mass lists are found.

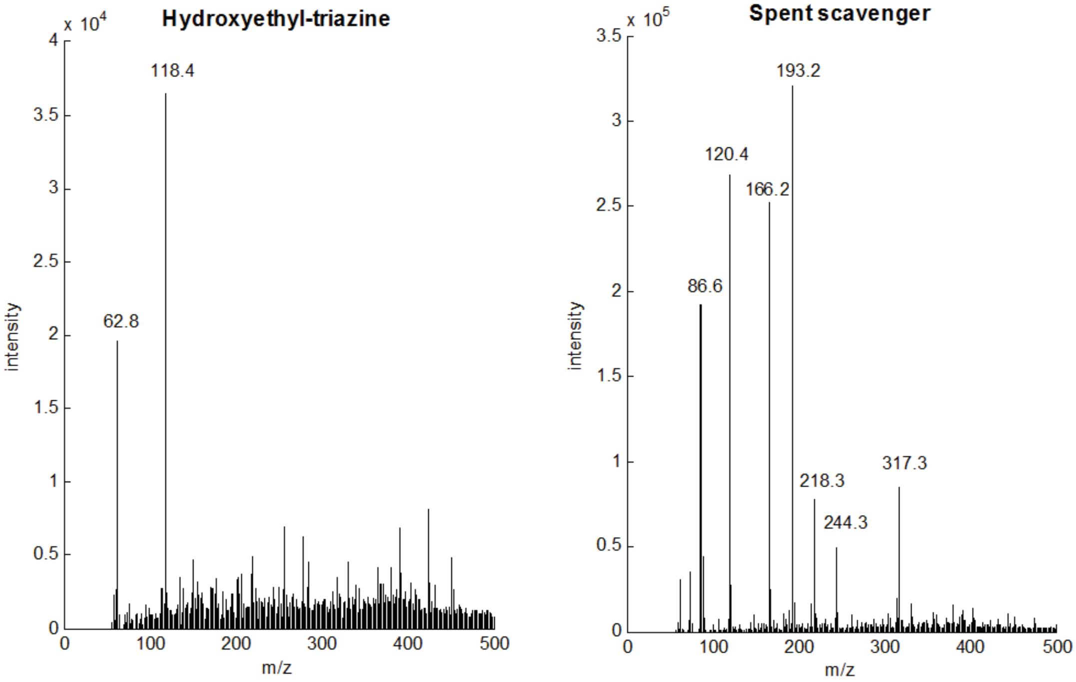

Figure 7.1: Mass spectra of triazine and spent scavenger solution

To indentify the peaks, the nominal mass*of compounds expected to be present in the mixture is calculated; the nominal masses is found in table 7.1. Because the MS set

Table 7.1: Mass list for spent scavenger

Compound	Nominal mass
MEA	61
Hydroxyethyl-triazine	219
Thiadiazine	192
Dithiazine	165
Trithiane	138

to positive ion mode, we expect the neutral compounds to be protonated, giving them a m/z ratio in the spectra equal to their nominal mass +1. Bearing this in mind, the 193 and 166 peaks in the mass spectrum for the spent scavenger are identified as thiadiazine and dithiazine. The M+1 and M+2 peaks may be used to inspect the correctness of the guess. In appendix C a table showing the percentage of the heavier isotopes for each element can be found. For thiadiazine the expected percentage of the M+1 and M+2 peaks compared to the molecular ion peak of are:

$$\begin{aligned} \mathrm{I}_{+1} &= 7 \cdot 1.08\% + 17 \cdot 0.012\% + 2 \cdot 0.038\% + 2 \cdot 0.369\% + 1 \cdot 0.76\% \qquad (7.1) \\ &= 9.34\% \\ \mathrm{I}_{+2} &= 2 \cdot 0.205\% + 1 \cdot 4.29\% \qquad (7.2) \\ &= 4.7\% \end{aligned}$$

Because thiadiazine is the base peak in the spectrum, we can directly see what percentage the intensity of the 194 and 195 peaks are of the 193 peak (9.4 % and 5.1 %). Both measured values are within 10 % of theoretical value, which confirms the theory of 193 being thiadiazine. For dithiazine the expected percentage compared to the molecular ion peak of the M+1 and M+2 peaks are:

$$\begin{aligned} \mathrm{I}_{+1} &= 5 \cdot 1.08\% + 12 \cdot 0.012\% + 1 \cdot 0.038\% + 1 \cdot 0.369\% + 2 \cdot 0.76\% \qquad (7.3) \\ &= 7.47\% \\ \mathrm{I}_{+2} &= 1 \cdot 0.205\% + 2 \cdot 4.29\% \qquad (7.4) \\ &= 8.79\% \end{aligned}$$

By using the data in table F.1 we find the measured percentages to be 7.42 % and 9.37 %. Again both measured values are within 10 % of the theoretical values, and it seems very plausible that 166 indeed is protonated dithiazine.

The triazine is expected to be found at a m/z ratio of 220, but no peak is seen here in either spectrum. This is especially surprising for the triazine solution since it should consist of almost pure hydroxyethyl-triazine (51 wt/wt %) and a small amount of MEA (1 wt/wt %). Inspecting the mass spectrum for the triazine, it is seen that the amount of noise is significantly higher compared to the spectrum of the spent scavenger, which indicates that the degree of ionisation of the triazine solution is low. If the triazine is not ionised in the ESI-MS, then it would explain why it does not show up in any of the spectra. Also interesting, there is no peak at 139 in the spectrum for the spent scavenger, where mono-protonated trithiane is expected to be. Furthermore, MEA (62) is not detected either, although it is formed 1:1 with thiadiazine and 2:1 with dithiazine.

In figure 7.2, the mass spectrum for the spent scavenger spiked with 1 M NaCl can be seen.

The spectrum of the spiked spent scavenger solution shows that 215 has become the base peak, and that 188 has gone from having an intensity of 3.8 % of the base peak in the pure spent scavenger, to 33.6 % in the spiked solution. We also see that 242 has appeared in the spectrum. The peaks 188, 215 and 242, all correspond to a difference of one Na^+ ion from the nominal mass of dithiazine, thiadiazine and triazine. The fact that addition of Na^+ ions enhances the signals of the 188, 215 and 242 peaks, relative

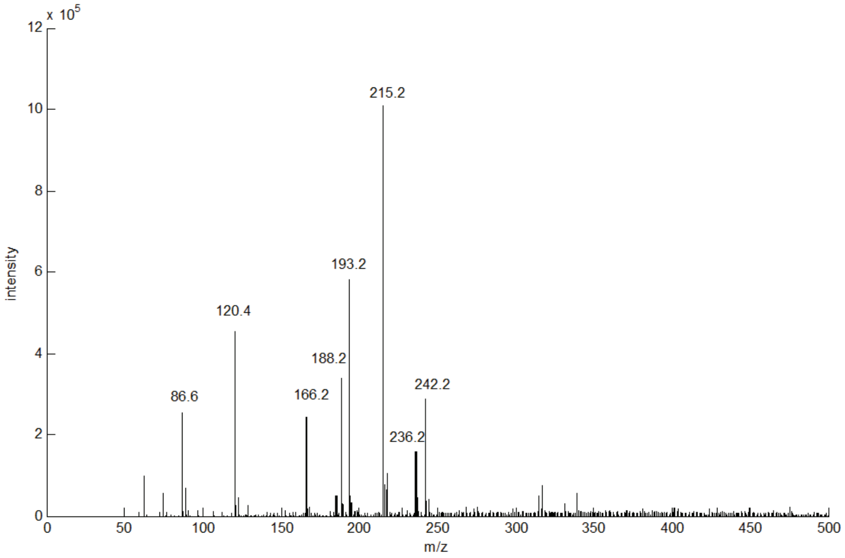

Figure 7.2: Mass spectrum spent scavenger spiked with 1 M NaCl

to the 166, 193 and 219 peaks, confirms the theory. Therefore, 188 is a dithiazine/Na^+ complex, 215 is a thiadiazine/Na^+ complex and 242 is a triazine/Na^+ complex. An interesting observation from this is that by adding Na^+ ions, triazine appears in the mass spectrum. This supports the theory that triazine is not easily protonated by the ESI-MS. A possibility is that the protonation leads to a rapid hydrolysis of the molecule, which therefore does not show up in the spectrum. Also, even with the addition of Na^+ ions, no signal for trithiane (peak at 161) is observed. The spent scavenger solution does therefore not seem to contain any trithiane.

To investigate whether MEA could be responsible for some of the peaks in the spectra, MS spectra for pure MEA and for MEA in a solution spiked with 1 M NaCl are made, see figure 7.3. To the left in figure 7.3 the spectrum for pure MEA is seen. The only peak present here, which is also present in the spectra for the spent scavenger is 62.8. This is also present in the triazine solution. Protonated MEA is expected to be found at 62, which therefore does not match with a peak at 62.8. However, in none of the previous spectra is a peak at 62 found. Both solutions solution should contain a relative significant amount of MEA, and the peak at 62.8 might therefore be associated with MEA. The remaining peaks in the spectrum are not multiples of the mole weight of MEA, and in general it seems that the background noise is quite significant.

The solution spiked with 1 M NaCl is displayed to the right in figure 7.3. Here the spectrum is very ordered, with the peaks lying at equal intervals. This is because NaCl completely dominates the spectrum, since the peaks can be described as being multiples multiple of NaCl molecules associated with a Na^+ ion, m/z = $(NaCl)_z$+Na^+.

This leaves the two peaks at 86.6 and 120.4, and some other peaks, unidentified although they have a relative high intensity in the spectrum for the spent scavenger. A possibility is that they are impurities from the natural gas. Water soluble compounds

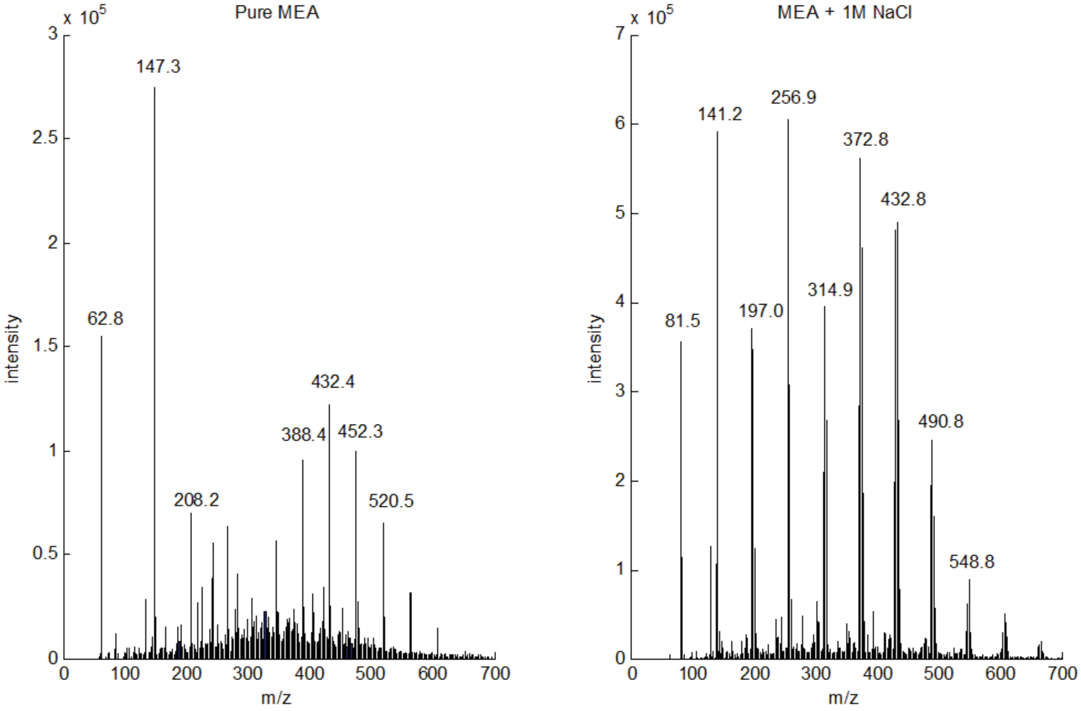

Figure 7.3: Mass spectra for pure MEA and MEA spiked with 1 M NaCl

from the gas phase might become dissolved and transferred to the spent scavenger separator.

7.2 MS analysis of reaction system, HS^- ions

A major part of the literature on the subject of H_2S scavenging with triazines is based on a reaction between HS^- ions and the triazine, which is also a convenient method to use since it allows for easy control of the amount of reactants as well as physical and chemical parameters such as temperature and pH; requirements necessary for kinetic investigations. The purpose of this experiment is to identify the reaction pathway(s) and the terminal reaction product(s) for this reaction system, by analysing how the composition of the reaction mixture changes during the reaction.

7.2.1 Chemicals and apparatus

Chemicals: 0.100 M / 0.100 M Na_2HPO_4 / Na_3PO_4 buffer, $NaHS_{(s)}$, hydroxyethyl-triazine (51 wt/wt%).
Apparatus: Water bath (25 ℃), 100 ml round bottom flask, magnet, magnet stirrer, thermometer, parafilm, scale, pH meter.

7.2.2 Method

The experiment was based on the experiments performed by Buhaug and Bakke, where an aqueous solution of HS^- and triazine was prepared and analysed at different times during the reaction. 4.2140 g NaHS was weighed out, and dissolved in 40 ml phosphate buffer, while 10.7855 g hydroxyethyl-triazine solution was weighed out in an 100 ml round bottom flask. Prior to the experiment, the density of the triazine solution had been determined to 1.1072 g/ml, see appendix E, giving a volume of 9.74 ml triazine. The pH was adjusted to 10 with 4 M HCl. A magnet was added to the round bottom flask, and while stirring, the HS^- solution was poured in. The final concentrations were 0.5 M triazine and 1.5 M HS^-, which ensured that a theoretical complete use of the scavenger was possible. The solution was placed in a temperature controlled water bath set to 25 ℃, and the top of the round bottom flask was closed with a plug to avoid evaporation. The temperature was measured with a thermometer during the course of the reaction, but with the current setup it was possible to keep a constant temperature. In figure 7.4, the setup for the experiment can be seen.

The reaction was studied by extracting samples and measuring them on an ESI-MS. The samples were extracted at the following times: 0, 1, 2, 3, 4 and 5 hours. There was only little change from 4 to 5 hours, and after this the reaction rate had decreased to a level where only one sample per day was deemed necessary. Further samples were collected at the following times: 24, 48, 72, 96, 168, and 192 hours.

As seen in figures 7.4 and 7.5 the solution had a yellow colour, which it attained from the HS^- ion. As the reaction progressed, and HS^- was consumed, the intensity of the colour diminished, and at the end of the experiment, the colour was only very weak, and the solution only had a faint odour of H_2S. Together this indicated an almost complete scavenging of the HS^- ion.

After three days a white precipitate was seen. At the end of the experiment, it was isolated via filtration through a Büchner funnel, dried in a desiccator, and an IR

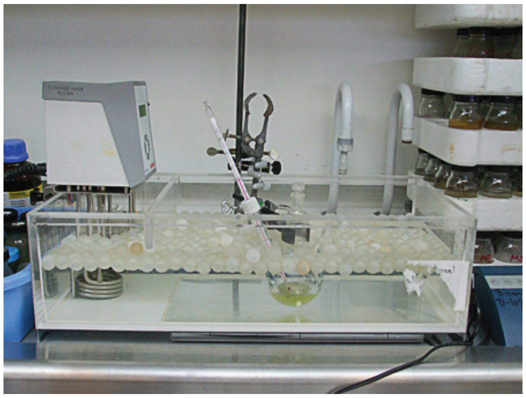

Figure 7.4: Setup for scavenging reaction

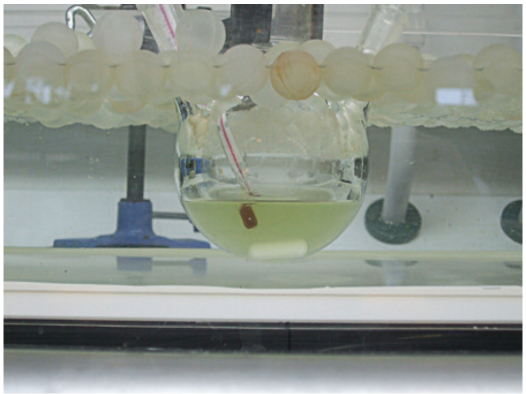

Figure 7.5: Close up of scavenging reaction

spectrum was recorded with a FTIR-ATR spectrometer. See appendix B for theory about IR spectroscopy and the FTIR-ATR method.

7.2.3 Results

In figures 7.6 and 7.7 the mass spectra for start, 1, 2, 3, 4, 24, 72, and 192 hours are shown. In appendix F tables F.4 and F.5 give the mass lists, where the intensity of the most significant peaks can be found.

To a start, the reaction mixture is dominated by the triazine, which is also to be expected. The presence of the 215 peak shows that some scavenging has already taken place. After 1 hour, the mixture is mainly composed of thiadiazine, with only very little dithiazine and no triazine detected. After 2 hours, dithiazine has become the base peak, and it continues to be this for the remainder of the reaction. In general, this means that the reaction proceeds as expected, with triazine forming thiadiazine, and then dithiazine. Most interestingly we see no peak at 139 or 161, which is where we would expect to see trithiane. Not even after 192 hours. This indicates that during an experiment conducted according to the conditions of Bakke and Buhaug, trithiane is not formed.

Also interesting are the peaks, which have not yet been identified: 86.6, 120.4 and 204.1. The peaks at 86.6 and 120.4 were also seen in the spectrum for the spent scavenger and are therefore products of the scavenging reaction. Of the three peaks, 86.6 and 120.4 are formed first, seemingly in connection with the first step in the scavenging process from triazine to thiadiazine. 204.1 seems to be related to the dithiazine formation, and is first present in appreciable amounts after two hours. But where dithiazine is persistent in all spectra when first formed, 204.1 is consumed more easily and has after 72 hours almost disappeared from the mixture. To try to identify the peaks, we look at the molecular ion peaks, and their isotope peaks.

If we assume that the three compounds are mono-protonated with H^+, and round up, the nominal masses for the unprotonated molecules become 86, 119, and 203. This shows that 86 has no or an even number of N-atoms, and 119 and 203 an odd number of N-atoms according to the N-rule, see appendix C. Looking at the mass lists in tables

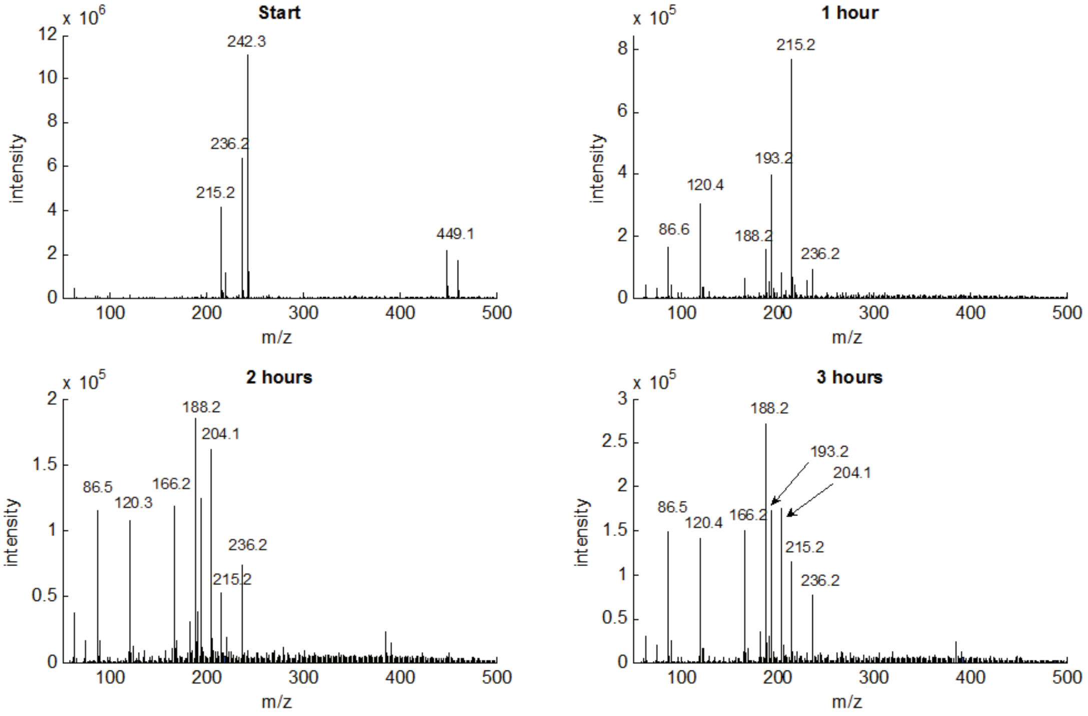

Figure 7.6: Mass spectra for first three hours of the scavenging reaction

F.4 and F.5, we see that for all three peaks, there are smaller peaks at m/z values +1 and +2 relative to the molecular ion peaks, and that the M+2 peaks are larger than the +1 peaks. For 86.6 there is actually not detected a M+1 peak. Of the atoms present in our mixture, only O and S have isotopes that give M+2 peaks. However, the abundance of ^{18}O is very low compared to ^{13}C, which means that for the M+2 peak to be larger than the M+1 peak, the compound has to consist of much more oxygen than carbon. Instead, the relative size of the peaks indicates that the structure of 86.6, 120.4 and 204.1 contains one or more sulphur atoms. If we calculate the relative intensity of the M+2 peaks compared to the molecular ion peak, we may estimate the number of sulphur atoms. In table 7.2 the calculated values are shown. The large variation of the relative intensity of the 86.6 and 88.6 peaks indicates that the 88.6 is in fact not the M+2 peak of 86.6. For the 120.4 and 204.1 peaks, the values for the relative intensity between the peaks and their M+2 peaks are more consistent, and it seems reasonable to assume that 122.4 is the M+2 peak of 120.4 and 206.1 the M+2 peak of 204.1. Since the only significant contributor to a M+2 peak in our mixture is sulphur, we make a first guess based on sulphur as the sole contributor in the molecule to the M+2 peak.

$$120.4: \quad \text{Number of S atoms} = \frac{10.03\%}{4.29\%} = 2.34 \tag{7.5}$$

$$204.1: \quad \text{Number of S atoms} = \frac{10.83\%}{4.29\%} = 2.52 \tag{7.6}$$

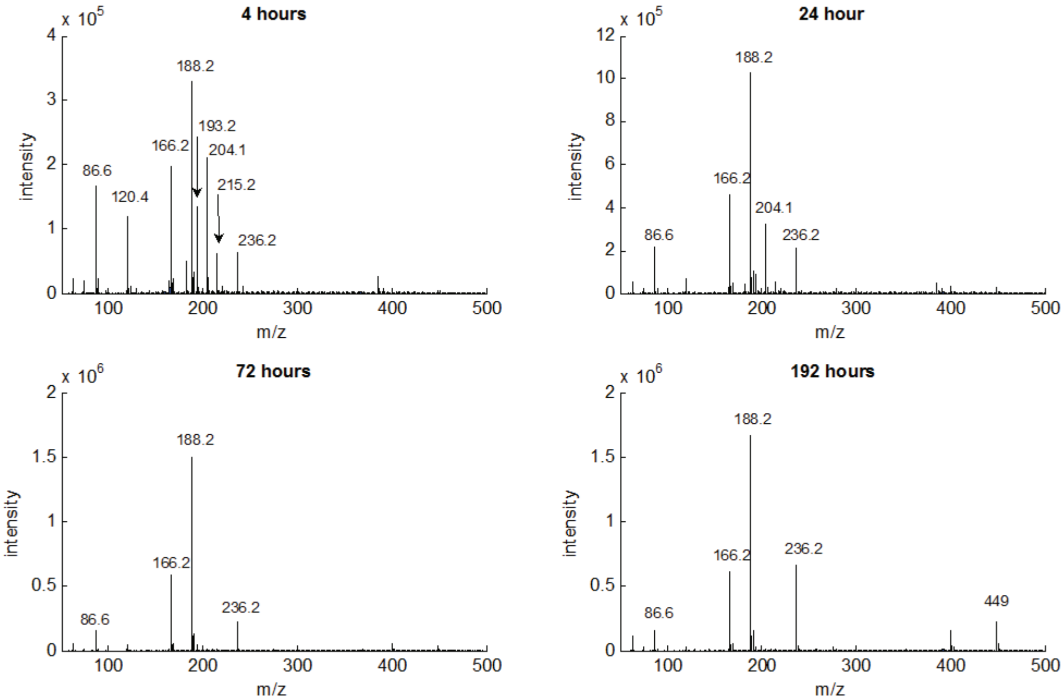

Figure 7.7: Mass spectra for final hours of scavenging reaction

Table 7.2: Relative intensity for M+2 peaks for 86.6, 120.4 and 204.

Time (hours)	86.6/88.6 (%)	120.4/122.4 (%)	204.4/206.6 (%)
1	27.06	10.33	-
2	15.24	10.83	11.15
3	17.34	9.97	11.37
4	12.76	9.21	12.04
5	14.07	9.82	10.09
24	9.83	-	9.48
48	8.04	-	10.84
Average	14.91	10.03	10.83

These values indicate that two sulphur atoms might be present in the molecules; however, if this is so, then there must be other M+2 contributors present as well to bring the theoretical intensity within 10 % of the measured intensities. As mentioned before, the only other significant M+2 contributor we can expect to find in the mixture is ^{18}O, but with a contribution of 0.205 per atom, many more oxygen atoms would be necessary than what seems reasonable. These values therefore indicate that 122.4 and 206.1 are in fact not M+2 isotope peaks for 120.4 and 204.1.

We do know that 86.6, 120.4 and 204.1 somehow take part in the reaction as intermediate compounds, since they are all created and consumed during the reaction. 120.4 has almost completely disappeared after 24 hours, while 86.6 is more persistent, and is present even after 192 hours. One possible explanation could be that the compounds are not protonated, but instead associated with Na$^+$ ions. If we assume that more than one Na$^+$ ion can associate with a molecule at a time, then we can come very close to the m/z ratios seen in the spectra. 86.6 and 120.4 seem to be created alongside with thiadiazine. The m/z ratio for a thiadiazine with two and three Na$^+$ ions are:

$$m/z_{\text{thiadiazine+2Na}^+} = \frac{192+23+23}{2} = 119 \tag{7.7}$$

$$m/z_{\text{thiadiazine+3Na}^+} = \frac{192+23+23+23}{3} = 87 \tag{7.8}$$

204.1 cannot be linked to a dithiazine and two sodium ions, but if we find the m/z ratio for a protonated thiadiazine and a non-protonated thiadiazine associated with a Na$^+$ ion we get:

$$m/z = \frac{192+193+23}{2} = 204 \tag{7.9}$$

In this way we may imagine compounds that explain the peaks. Because these peaks are expected to have multiple charges (+2 and +3), their M+1 isotope peaks would not be situated at their m/z value +1 along the x-axis, but rather 1/2 and 1/3 along the x-axis. The MS does not pick up peaks at 120.9 and 86.9, but this may be due to the resolution of the MS. For the compounds with a +2 charge, the M+2 isotope should be found at an m/z ratio one higher. No peak is found at 121, but for a single thiadiazine molecule the M+2 isotope peak might be too weak to show up in the spectra. We do see a peak at 205 though, and if we assume this to consist of two thiadiazine molecules, then the expected percentage becomes:

$$I = 2 \cdot (2 \cdot 0.205\% + 4.29\%) = 9.4\% \tag{7.10}$$

The average measured intensity of the 205 peak relative to the 204 peak is 9.66 %, which fits well within 10 % of the expected value. On the other hand, none of the three peaks seems to respond to the addition of NaCl, which would be expected if they caused by Na$^+$ association. This therefore counts against the theory.

For a final comment on the spectra, we may look at the last four spectra in figure 7.7. Here it is seen that the 188 peak becomes increasingly dominating over time. The other peaks either decrease in size relative to the 188 peak or disappear completely.

Even the 166 peak decreases relative to the 188 peak, although they represent the same compound. The only compound, which seems to increase relative to the 188 peak, is the 236 peak. If we consider the 236 peak as part of a constant background signal, then this would indicate that the concentration of dithiazine in the solution is decreasing. If we further assume that the Na^+ ions bind to a specific number of dithiazine molecules, this would explain why the 166 peak decrease relative to the 188 peak. That the concentration of dithiazine should be decreasing fits well with the observation of precipitate in the solution. This might be either crystalline dithiazine or another compound formed from dithiazine. Somehow, this precipitate must also include the other peaks that have disappeared from the spectrum, including 86, 120 and 204.

In figure 7.8 the IR spectrum for the precipitate is shown. The precipitate absorbes at: 3400, 2954, 2922, 2852, 1655, 1459, 1365, 1174, 1022, 871, 754, 734 and 707 cm^{-1}.

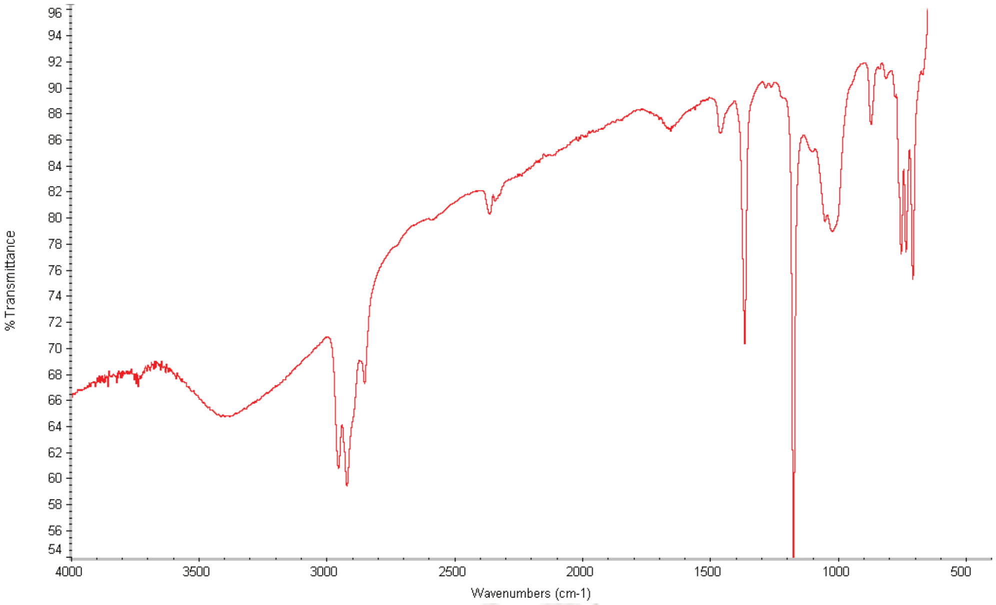

Figure 7.8: IR spectrum of precipitate from reaction

7.3 Actual scavenging - triazine and H_2S

The purpose of the experiment is to investigate if the process investigated by Buhaug and Bakke is representative for the actual scavenging system. Therefore, H_2S is bubbled through a non-buffered triazine solution where no extra ions have been added, and samples are taken out and analysed on ESI-MS during the experiment.

7.3.1 Chemicals and apparatus

Chemicals: $NaHS_{(s)}$, hydroxyethyl-triazine (51 wt/wt%), 37 % HCl.
Apparatus: 250 ml flask with tubes for leading bubbles through liquid, magnet and magnet stirrer, seven 50 ml boiling flask with double neck, plastic tube, adaptor for rubber tube, 25 ml dripping funnel.

7.3.2 Method

Six batches of 1.8048 g NaHS (0.0322 mole) and one extra of 3.6096 g (0.0644 mole) were weighed off and transferred to the boiling flasks, which were then closed with plugs. The first boiling flask was attached to the dripping funnel, which was filled with concentrated HCl. An adaptor was attached to the boiling flask, which was used to connect the boiling flask to the 250 ml flask with a rubber tube. Finally, the 250 ml flask was filled with 25 ml hydroxyethyl-triazine (0.0644 mole), and a magnet was added. HCl was slowly dripped down on the NaHS, where the two chemicals reacted to form gaseous H_2S.

$$NaHS_{(s)} + HCl_{(aq)} \rightarrow NaCl_{(s)} + H_2S_{(g)} \tag{7.11}$$

The H_2S then bubbled through the triazine solution, from where a sample of 0.1 ml was taken out after each batch of H_2S. In figure 7.9 the setup for the experiment is shown.

Figure 7.9: Experimental setup for experiment

Figure 7.10: Precipitate from reaction

A complete use of the H_2S was not achieved, which was visible from the fact the grease used to lubricate the glassware became yellow when unreacted H_2S was dissolved in it.

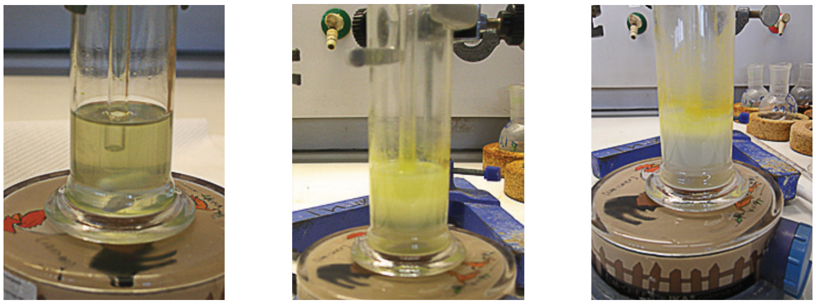

Figure 7.11: Scavenging solution: start, 4:1 (1 day) and 4:1 (2 days)

After H_2S had been bubbled through in a ratio of 4:1, the solution became blurred, and after standing the night over, a second phase was seen. By stirring the two phases, they could be completely mixed and would only separate very slowly. After another 24 hours, the solution had become completely opaque, with the second phase having a white colour. The lower phase was very viscous, and made mixing with the magnet difficult. In figure 7.11, pictures of the solution prior to reaction, one day after the final batch of H_2S and two days after the final are shown. These clearly show how the solution changes during the reaction. To investigate the nature of the second phase, the solution was filtrated with a Büchner funnel, and the retentate was dried in a desiccator. The precipitate can be seen in figure 7.10.

7.3.3 Results

In figure 7.12, mass spectra of the solution after reaction with the first four batches of H_2S can be seen. The first spectrum shows the composition of the scavenger solution prior to reaction with H_2S. The 242 peak is identified as a triazine/Na^+ complex. This is even though no sodium has been added to the mixture. It must therefore either originate from the triazine solution, which could happen if the triazine was not dissolved in demineralised water, or be present because of a contamination somewhere in the reaction/sampling process, e.g. insufficient cleaning of the glassware. The base peak in the spectrum is 461, which is a positive difference of 219 relative to the 242 peak; exactly the nominal mass of a hydroxyethyl-triazine molecule. This peak therefore seems to be the result of two triazine molecules associated with a single Na^+ ion. We verify this by calculating the theoretical intensity of the M+1 isotope peak in percent of the molecular ion peak. In the experiment it is measured to be 22.62 %.

$$I = 2 \cdot (9 \cdot 1.08\% + 3 \cdot 0.368\% + 3 \cdot 0.038\% + 21 \cdot 0.012) = 22.38\% \tag{7.12}$$

The measured value is thus within 10 % of the expected value, and our theory seems to be correct.

In the spectrum in the top right corner of figure 7.12, an amount of H_2S equal to half the number of moles of triazine has been bubbled through the scavenger solution. Theoretically, half the triazine should therefore be converted to thiadiazine. It is also

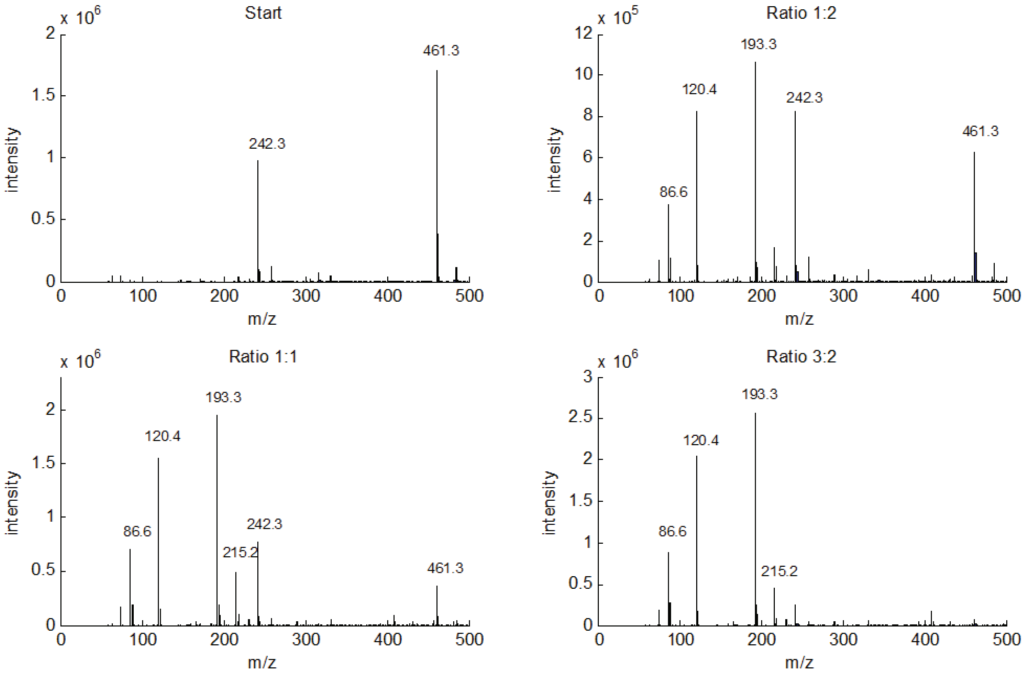

Figure 7.12: Mass spectra for scavenger solution after reaction with H_2S in the ratios H_2S to scavenger: start, 1:2, 1:1 and 3:2

evident from the spectrum that a significant amount of thiadiazine (193) has been formed. Furthermore, we see the 86.6 and 120.4 peaks.

In the third spectrum equal amounts of H_2S and triazine has been used. The triazine should therefore be completely converted to thiadiazine at this point in the reaction. It is seen that the amounts of triazine has decreased from the second spectrum relative to the amount of thiadiazine, but there is still significant amounts left. Also, no dithiazine is seen at this point.

After using an amount of H_2S 1.5 times the amount of triazine dithiazine is expected to have been formed to some extent. However, when inspecting the fourth spectrum, no peak is seen at 166. The triazine peaks have almost disappeared though.

In figure 7.13 spectra for the final batches of H_2S can be seen. At a H_2S:triazine ratio of 2:1, dithiazine is detected, but only in small amounts relative to the thiadiazine. However, at a ratio of 3:1 dithiazine has become the base peak in the spectrum, and at a ratio of 4:1 the solution is almost exclusively consisting of dithiazine. The spectrum for the ratio 5:2 is dominated by the 215 peak; also, the 242 peak is very intense together with the 188 peak. This indicates that the spectrum is heavily influenced by Na^+ ions, and its use in the comparison with the remaining spectra is therefore limited.

The peak at 204.1 is not detected when using gaseous H_2S, and since it was not found in the spent scavenger solution either, it may be a by-product from the use of HS^- ions. Also very interesting, no trithiane is detected indicating that the reaction

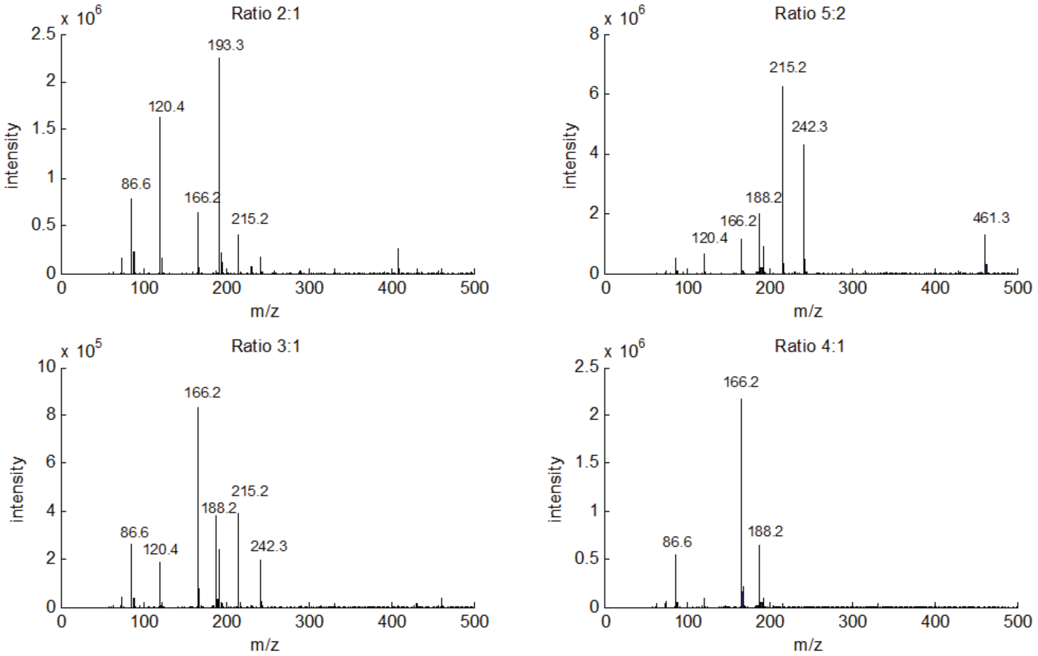

Figure 7.13: Mass spectra for scavenger solution after reaction with H_2S in the ratios H_2S to scavenger: 2:1, 5:2, 3:1 and 4:1

stops at dithiazine.

In figure 7.14, the IR spectrum of the precipitate from the reaction can be seen. As seen in the figure, the peak at 3400 cm^{-1} completely dominates the spectrum. A possibility is that the amount of MEA in the precipitate is high, since the amine and hydroxy group would significantly contribute to absorption around 3400 cm^{-1}. Because the precipitate is dried in a desiccator, MEA might not evaporate. To clean the precipitate, a small amount is dissolved in 100 ml demineralised water and then re-filtrated with a Büchner funnel. The new spectrum for the cleaned precipitate is shown in figure 7.15.

It is clear that the water has decreased the intensity of the peak at 3400 cm^{-1} relative to the rest of the peaks. The precipitate absorbs at the following peaks: 3405, 2957, 1638, 1367, 1282, 1174, 1051, 879, 746, 733 and 708 cm^{-1}. Comparing these absorption bands with the precipitate from the reaction between HS^- and the triazine, a very high degree of overlap is seen. The two precipitates absorb at the same wavelengths, with the only difference being that the precipitate from the previous experiment absorbs at 2852 and 1459 cm^{-1}. However, we also see that the peak at 3400 cm^{-1} is more intense in the spectrum for the precipitate from this experiment, which may indicate that some MEA is still left even after being washed with water. The presence of MEA might lower the intensity of some of the weaker peak, and upon inspection 2852 and 1459 is found to be very weak peaks. The comparison therefore indicates that the two precipitates are the same compound.

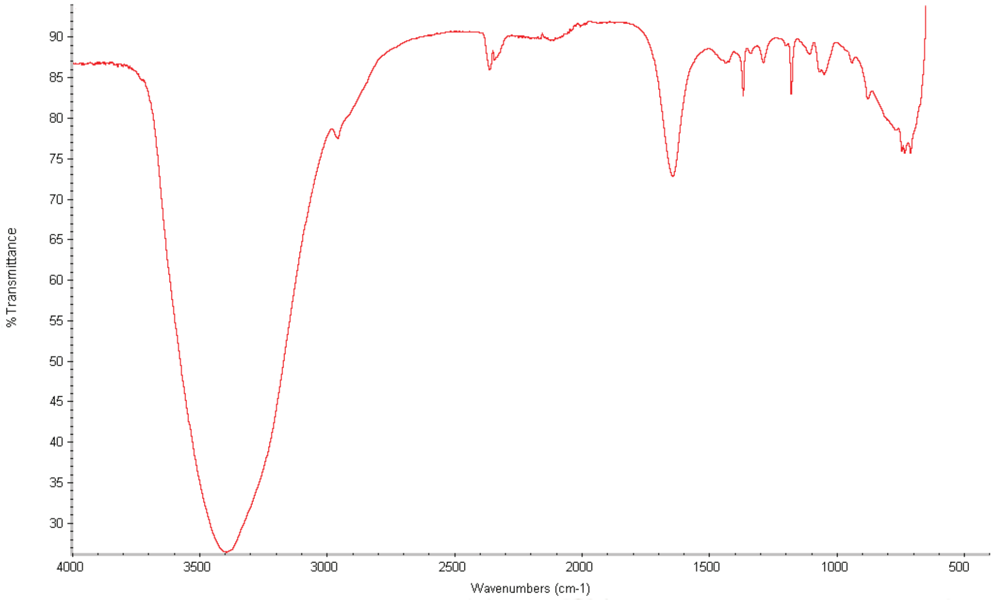

Figure 7.14: IR spectrum of precipitate

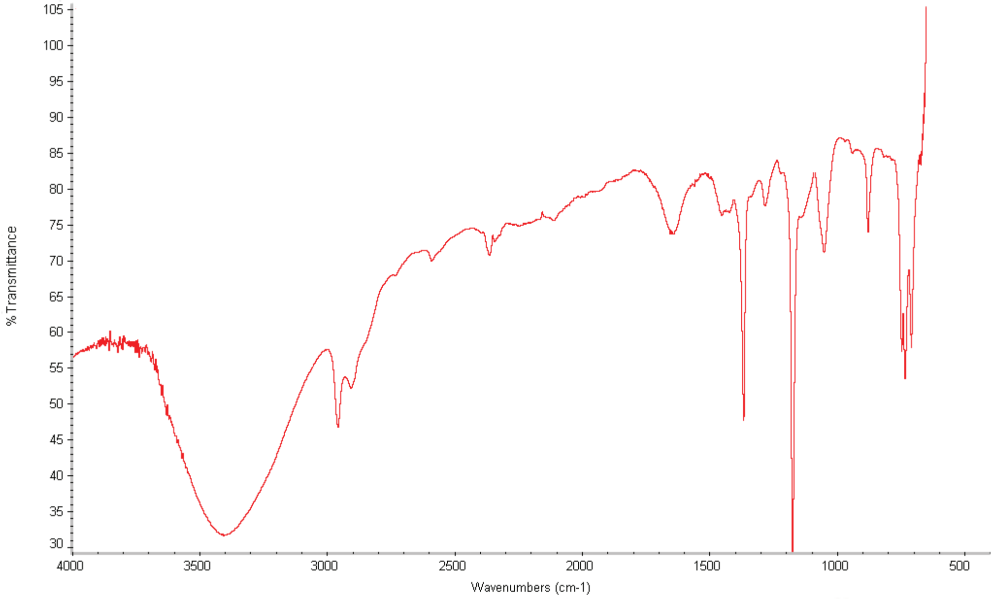

Figure 7.15: IR spectrum of cleaned precipitate

7.4 Spent scavenger reaction with H_2S

The purpose of this experiment is to investigate if the same precipitate that was produced in the two previous experiments may be formed from a reaction between the spent scavenger solution and H_2S. Since the exact mechanism leading to the precipitation is unknown, the difference in matrix between the previous experiments and the spent scavenger solution might have an influence on the precipitation reaction.

7.4.1 Chemicals and apparatus

Chemicals: $NaHS_{(s)}$, aqueous spent scavenger, 37 % HCl.
Apparatus: 250 ml flask with tubes for leading bubbles through liquid, magnet and magnet stirrer, 50 ml boiling flask with double neck, plastic tube, adaptor for rubber tube, 25 ml dripping funnel.

7.4.2 Method

The experiment was setup in the same way as the previous experiment where H_2S was bubbled through triazine, with the only difference being that the triazine is replaced by spent scavenger solution. In figure 7.16 a picture of the setup is shown. 50 ml spent scavenger solution was measured out, and transferred to the 250 ml flask. 11.2146 g of NaHS (0.200 mole) was weighed out and transferred to the 50 ml round bottom flask, to which a dripping funnel with concentrated HCl was attached. The round bottomed flask and the 250 ml flask was connected with a plastic tube, and H_2S from the reaction between NaHS and HCl was bubbled through the solution. After the experiment no

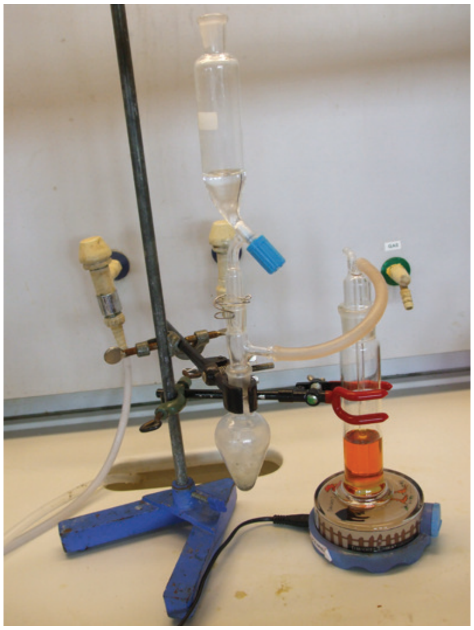

Figure 7.16: Setup for experiment

Figure 7.17: Two phases after reaction

visual change could be seen, and the solution was therefore left over night. The extra reaction time allowed for a precipitate to be formed. The precipitate did not settle completely, but was floating in the bottom of the spent scavenger solution. A picture of the precipitate in the solution can be seen in figure 7.17. To investigate it, the solution was filtrated with a Büchner funnel, and the retentate was dried in a desiccator. Apparently two substances were present on the filter paper; a solid powder and a very viscous liquid. An IR spectrum was recorded of each, and the filtrate was analysed with ESI-MS.

7.4.3 Results

In figure 7.18 the mass spectrum for the spent scavenger solution after reaction with H_2S can be seen. Table F.8 in appendix F gives the mass list for the spectrum. From the spectrum it can be seen that the solution consists almost purely of dithiazine, which is in accordance with the result from the two previous experiments. In figure 7.19, the IR spectrum of the powder from the retentate is shown. The spectrum has the following significant peaks: 3388, 2959, 2911, 1675, 1367, 1282, 1175, 1058, 881, 745, 734 and 708 cm^{-1}, which makes it almost identical to the spectra from the two previous experiments. In figure 7.20, the IR spectrum of the viscous liquid from the retentate is shown. The spectrum has the following significant peaks: 3393, 2915, 1659, 1429, 1391, 1367, 1336, 1283, 1195, 1176, 1104, 1055, 967, 941, 873, 807, 771, 729, 690 and 668 cm^{-1}. It is therefore very different from the powder, and is probably a completely different compound.

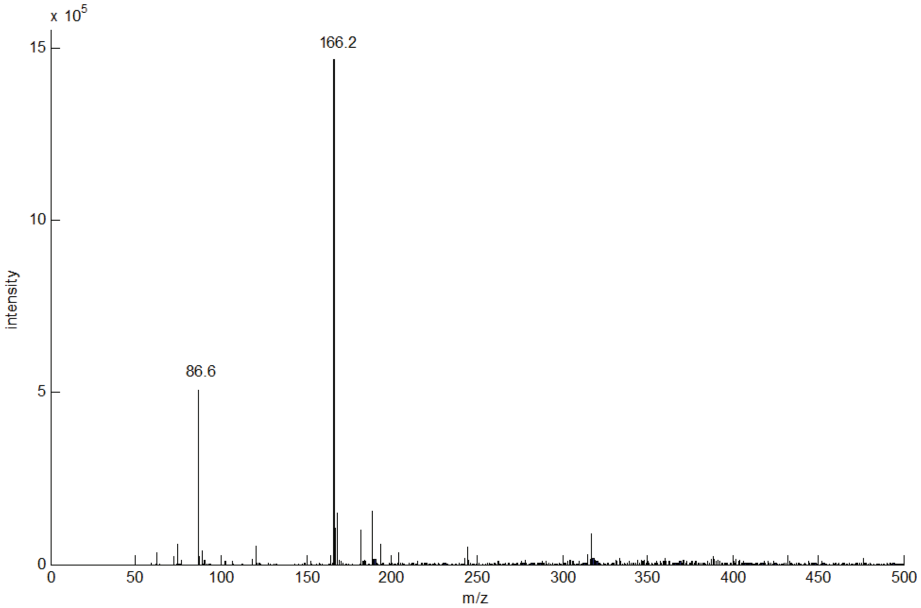

Figure 7.18: Mass spectrum for spent scavenger solution after reaction with H_2S

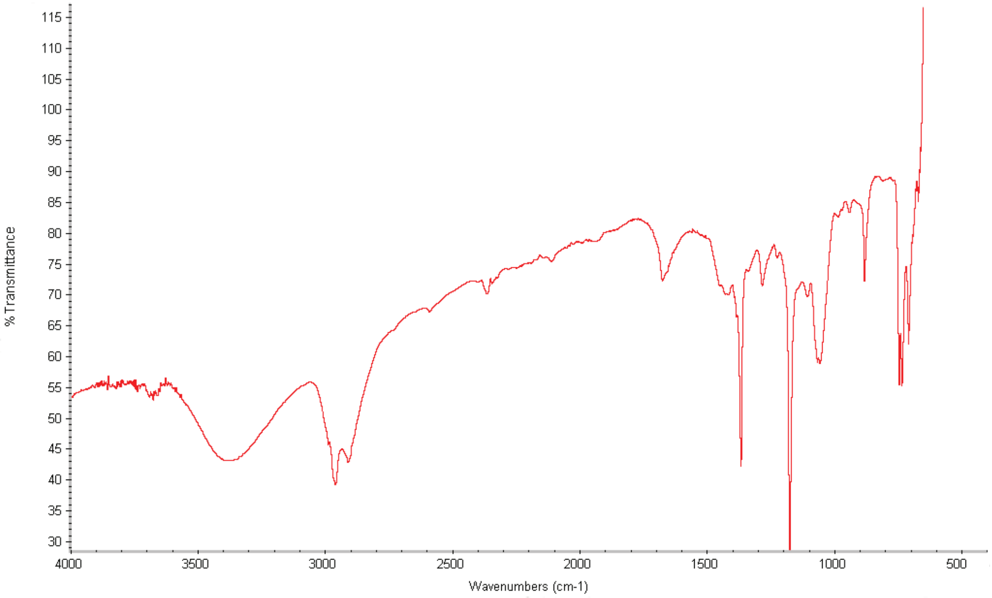

Figure 7.19: IR spectrum of powder from retentate

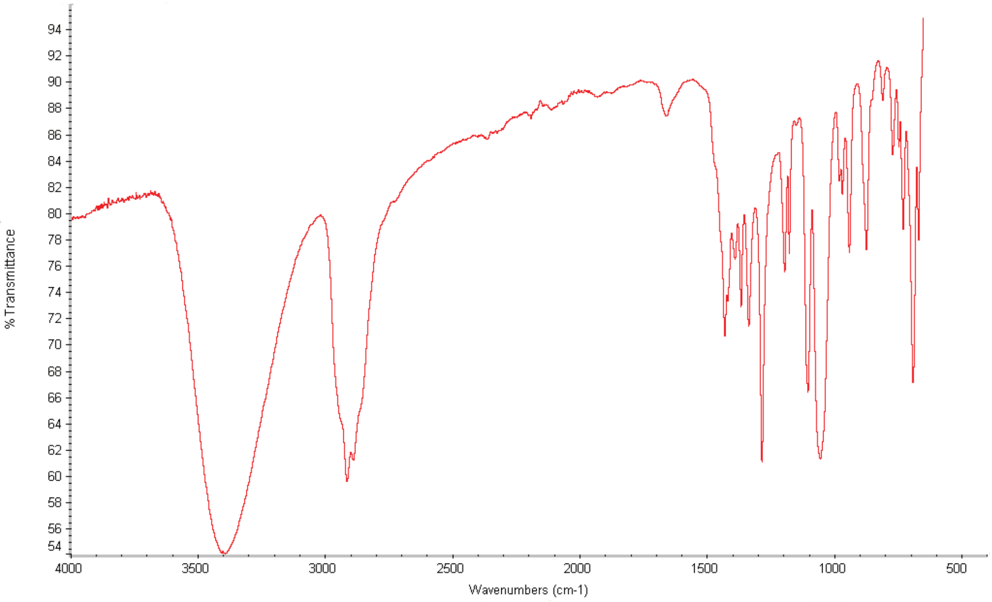

Figure 7.20: IR spectrum of viscous liquid from retentate

7.5 Effects of heating on spent scavenger

Since the first place where the fouling occurs at Shell, is in the air cooler immediately after the distillation column, the distillation process might be related to the formation of the fouling. The purpose of this experiment is therefore to investigate the effect of heating and condensing on the spent scavenger solution, and on the reaction between the spent scavenger and H_2S.

7.5.1 Chemicals and apparatus

Chemicals: Aqueous spent scavenger, NaHS, 37 % HCl.
Apparatus: 250 ml flask with tubes for leading bubbles through liquid, magnet and magnet stirrer, 50 ml boiling flask with double neck, plastic tube, adaptor for rubber tube, 25 ml dripping funnel, oil bath, condenser tube with water cooling, 250 ml boiling flask.

7.5.2 Method

50 ml of aqueous spent scavenger was saturated with H_2S by bubbling 0.200 mole H_2S through the solution. The saturated solution was transferred to a 250 ml boiling flask and brought to the boiling point with an oil bath. A condenser tube with water cooling was attached to the boiling flask to simulate the condensation and to avoid evaporation. After one hour the heating was ended.

Parallel to the experiment with the solution saturated with H_2S, a blind experiment with heating of pure spent scavenger solution was made. The procedure for this experiment was the same as described above. The setup for the experiments can be seen in figure 7.21.

Figure 7.21: Experimental setup for experiment

Figure 7.22: Precipitate from reaction

Already after five minutes the solution saturated with H_2S changed from clear to blurry. After heating, the solution had become light brown and still blurred, but after settling, a small clear top phase appeared, while the lower phase was filled with a beige precipitate. To investigate the nature of this precipitate, 2 ml of the lower phase was taken out with a Pasteur pipette, dissolved in 50 ml demineralised water, filtrated on a Büchner funnel and then an IR spectrum was recorded. In figure 7.23 pictures of the saturated solution during the process can be seen, and in figure 7.22 a picture of the precipitate is shown. To the right in figure 7.23, a picture of the pure spent scavenger solution after heating is shown. Here it is visible that the solution changed to a more deep red colour as a result of the heating. To investigate if the scavenging compounds were degraded during the heating, a MS spectrum was recorded for this solution.

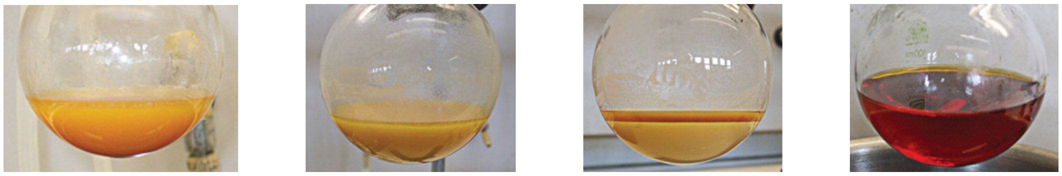

Figure 7.23: From left to right: Heated solution saturated with H_2S after 5 minutes, after one hour, and after settling. Pure spent scavenger after heating.

7.5.3 Results

In figure 7.24 the mass spectrum of the heated spent scavenger solution is shown. Comparing this mass spectrum with the one for the unheated spent scavenger, it is seen that the relative size of the peaks 86.6, 120.4, 166.2 and 193.2 has not been altered, while the peaks with higher m/z values have increased in intensity. From the previous experiments, the first four significant peaks are known to be part of the scavenging system; whereas, the peaks at higher m/z values have not been connected to the scavenging system. No new peaks at m/z values lower than the thiadiazine and dithiazine peaks are seen, which otherwise could have indicated that a degradation took place. The colour change to deep red, seems to be linked to the increase in the intensity of the higher molar mass compounds. These are most likely water soluble components from the natural gas, which are also removed with the liquid phase after the injection of the scavenger.

Figure 7.25 contains the IR spectrum of the precipitate, and in figure 7.26, it is compared to the IR spectrum of the precipitate from the reaction between the pure triazine and H_2S. It is very clear that the two spectra are completely identical, and that the precipitate must have the same chemical structure in both cases.

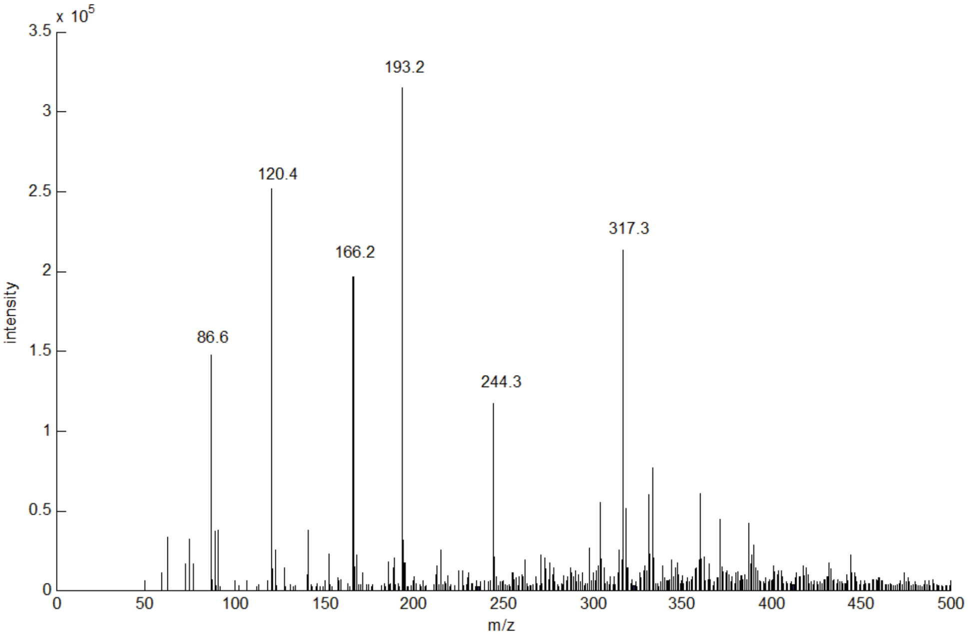

Figure 7.24: Mass spectrum of heated spent scavenger solution

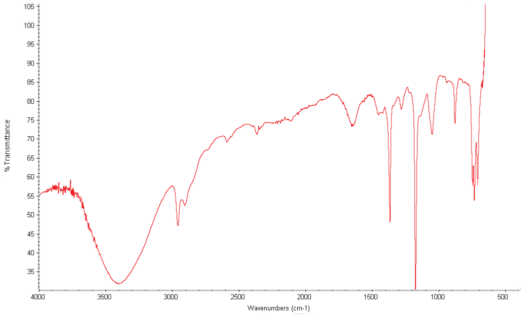

Figure 7.25: IR spectrum for precipitate

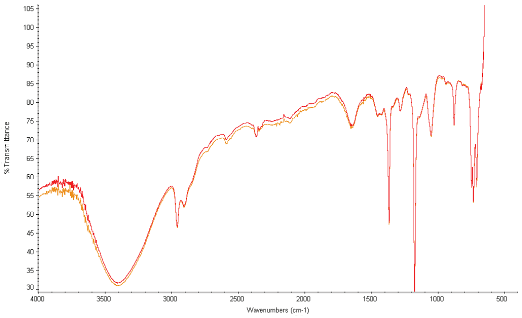

Figure 7.26: Comparision of IR spectra of precipitate from reaction between H_2S and heated spent scavenger (orange) and pure triazine and H_2S (red)

7.6 Evaluation of experimental series

These experiments have demonstrated that the reaction pathway is the same for HS^- ions and gaseous H_2S, which indicates that gaseous H_2S is first dissolved in the scavenger solution via an acid/base reaction, in which it is converted into the HS^- ion. This means that controlled experiments with HS^- ions may be used to study the reaction.

The MS analysis have shown that the reaction follows the expected pathway with triazine being converted to thiadiazine and then to dithiazine. However, in none of the experiments was the reaction found to proceed to trithiane formation. During the reaction, compounds that are not yet accounted for were detected (peaks at 86.6, 120.4 and 204.1). A possibility is that they are thiadiazine/Na^+ complexes, but they may also be intermediate compounds that are important for the final reaction. The 204.1 peak was only found when using HS^- ions, and may be an artefact of this experiment, but both 86.6 and 120.4 were detected in all experiments. In all experiments, the final reaction mixture consisted almost exclusively of dithiazine, and from this solution a precipitate, which was identical for all the experiments, was formed. This shows that a large concentration gradient of H_2S may indeed overspend the scavenger, leading to a precipitation from dithiazine. Besides dithiazine, the final reaction mixture was also found to contain the unidentified compound (86.6). This might be involved in the precipitation reaction. In the reaction between the spent scavenger and H_2S, a second substance was found in the retentate, which might indicate that two types of precipitate may be formed. It is possible to form significant amounts of precipitate from the spent scavenger solution, and this makes it a suitable source for the fouling at Shell.

By applying heat, the rate of reaction was significantly increased, giving a precipitate within minutes. If the precipitates from these reactions are identical to the fouling found at Shell, this may be the key to explain how the fouling is formed. At 20 ℃, the fouling is first formed after one day in a solution saturated with H_2S, which would not be sufficient time for fouling to occur in the refinery system, but with a reaction time of minutes instead of days, fouling may occur quickly in places subjected to high H_2S gradients and heat. Such conditions are found after the distillation column, where fouling is also found to occur for the first time.

The MS analyses did not detect trithiane, which might question if the fouling is indeed trithiane. On the other hand, it is also possible that the MS is not sensitive towards trithiane. It was found difficult to detect MEA and triazine, and it is possible that the same is true for trithiane. Still, the fact that the final reaction mixture seems to consist of dithiazine, is more in line with the hypothesis B, the polymerisation reaction. However, no peaks at higher m/z values were detected, which would otherwise have been a strong indication of a polymerisation. The MS analysis is therefore not conclusive as to which hypothesis about the fouling formation is correct.

Chapter **8**

Experiments - Structural elucidation of fouling

This chapter contains the experiments performed to investigate the fouling encountered at Shell and Maersk. The main purpose of these experiments was to test which of the three hypotheses put forward earlier is correct, and also to see if the precipitate formed in the previous experimental series may be linked to the fouling. It is possible that the fouling is a complex material, which is a combination of several components, of which the precipitate seen in our experiments only is one. The black fouling found at Maersk post scavenger injection was investigated to see if it had any connection to Shell's fouling. The fouling was analysed with a TS/VS analysis, infrared spectroscopy and X-ray diffraction.

8.1 TS/VS analysis of fouling

To determine the amount of organic and inorganic matter, ash, in the fouling, a TS/VS analysis is performed. Both the fouling from Shell, also the fouling from Maersk are analysed. To determine the composition of the inorganic part of the fouling, an ICP AES analysis is performed. Knowledge of the composition may be valuable for the understanding of how the fouling is formed, since it is possible that certain deposition areas are necessary for the fouling to start building up.

8.1.1 Method

TS/VS analysis

The TS/VS analysis was performed with basis in Danish Standard DS 204 [28]. Because the two types of fouling were very heterogeneous, five increment samples were taken, which could then be used to calculate an average. Five crucibles were marked, incinerated for one hour at 550 ℃ to remove any organic residues. and left to cool down in an desiccator. The crucibles were weighed ($m_{crucible}$) before five grams of fouling were added, after which the crucibles were weighed again ($m_{crucible+sample}$). To determine the amount of dry matter, the crucibles were dried at 90 ℃ for 48 hours, put back in the desiccator to cool down, and then weighed ($m_{crucible+TS}$). The dried samples were incinerated at 550 ℃ in a muffle oven for one hour, and left to cool down in the oven over night. Finally, the crucibles were weighed again to determine the amount of non-volatile solids ($m_{crucible+ash}$).

ICP AES

Three samples of each type of fouling were prepared by weighing the fouling into 100 ml autoclave bottles, giving a total of six samples. To check if the results follow the pre-calibrated curve, 0.5 g, 1.0 g and 1.5 g were weighed off. The second sample should then give twice the concentration measured in the first sample, and the third sample should give a concentration three times as high. In this way, the validity of the results could be evaluated. In table 8.1 the amounts of fouling weiged off for the ICP-AES analysis can be seen.

Table 8.1: Weighed off amounts of fouling for ICP analysis

Nr	m(fouling) (g) (Shell)	m(fouling) (g) (Maersk)
1	0.5020	0.5020
2	1.0022	1.0125
3	1.5025	1.5021

To open the structure of the fouling, each sample was mixed with 10 ml of demineralised water and 10 ml concentrated HNO_3 to reach a concentration of 7 M HNO_3. The autoclave bottles were sealed, marked with autoclave tape, and put in an autoclave where they were treated at 200 kPa and 120 ℃ for 30 minutes. They were left to cool down in the autoclave over night. Upon opening the autoclave it was discovered that the bottle with 1 g Shell fouling had exploded, and no further work was done with this sample. The remaining samples were filtrated into 50 ml volumetric flasks, where the filtrate was diluted with demineralised water.

To determine the content of metal atoms, an existing Multi method was used. In this method, the ICP is calibrated to measure As, Cd, Co, Cr, Cu, Fe, Mn, Ni, Pb, Sb, Zn, Mg, Be, Se, Mo, V, Ti, Tl and Ca. The calibration curve of this method was tested before the actual measurements by using a standard solution with a concentration of 10 mg/L for all the metals, and was found to be well calibrated for all metals. After this, a sample list was made in the computer software and the samples measured.

8.1.2 Results

Shell fouling

In table 8.2 the weighed results from the TS/VS analysis can be seen. The amount of

Table 8.2: Weighed amounts in TS/VS analysis of Shell fouling

Crucible	$m_{crucible}$ (g)	$m_{crucible+sample}$ (g)	$m_{crucible+TS}$ (g)	$m_{crucible+ash}$ (g)
120	18.2447	23.3161	22.2093	18.2665
28	17.1797	22.3027	20.8437	17.2289
F9	21.5235	26.7566	25.3559	21.5644
E	22.8960	27.8539	26.5585	22.9154
13	17.6067	23.1150	21.7492	17.6287

dry matter, or total solids (TS), is calculated with formula 8.1.

$$TS = \frac{m_{crucible+TS} - m_{crucible}}{m_{crucible+sample} - m_{crucible}} \cdot 10^3 \frac{g}{kg} \tag{8.1}$$

The amount of ash is calculated with formula 8.2.

$$Ash = \frac{m_{crucible+ash} - m_{crucible}}{m_{crucible+sample} - m_{crucible}} \cdot 10^3 \frac{g}{kg} \tag{8.2}$$

The amount of volatile solids, VS, is calculated with formula 8.3.

$$VS = \frac{m_{crucible+sample} - m_{crucible+TS}}{m_{crucible+sample} - m_{crucible}} \cdot 10^3 \frac{g}{kg} \tag{8.3}$$

In table 8.3 the final calculated results are shown. The mean values are shown with 95 % confidence intervals.

Table 8.3: TS/VS analysis for Shell fouling

Crucible	TS (g/kg)	Ash (g/kg)	VS (g/kg)
120	746.263	4.2986	253.737
28	715.206	9.6037	284.794
F9	732.338	7.8156	267.662
E	738.720	3.9129	261.280
13	752.047	3.9940	247.953
Average	736.915 ± 17.6866	5.9250 ± 3.2569	263.085 ± 17.6866

Table 8.4 shows the concentration of metal ions as determined with the ICP-AES. Only the metals that were detected are shown. The final column is the average of the two samples.

We see that for Cu, Fe and Ti the amounts detected in sample two is close to three times that of sample one, which fits well with the amounts of fouling weighed off. For Mg and Ca the correlation breaks down, indicating some problems in measuring these in this specific matrix. As a result, the content of these two metal atoms will be regarded with some uncertainty.

Table 8.4: ICP-AES analysis for Shell fouling

Sample Metal	1 (mg/l)	2 (mg/l)	Content (mg/kg)
Cu	0.179	0.682	20.26
Fe	4.882	12.92	458.1
Mg	0.820	0.670	51.98
Ti	0.213	0.809	24.07
Ca	2.371	2.501	159.7

Maersk fouling

In table 8.5 the readings from the balance for the TS/VS analysis can be seen.

Table 8.5: Weighed amounts in TS/VS analysis of Maersk fouling

Crucible	$m_{crucible}$ (g)	$m_{crucible+sample}$ (g)	$m_{crucible+TS}$ (g)	$m_{crucible+ash}$ (g)
17	13.6215	18.6732	18.3563	14.0426
7	15.1161	20.1600	19.8595	15.7322
30A	17.1690	22.3781	22.0636	17.8323
3/1	16.1304	21.3160	20.9907	16.6440
22	17.3181	22.2427	21.9429	18.0088

In table 8.6 the final calculated results are shown.

Table 8.6: TS/VS analysis for Maersk fouling

Crucible	TS (g/kg)	Ash (g/kg)	VS (g/kg)
17	937.269	83.358	62.731
7	940.423	122.148	59.577
30A	939.625	127.335	60.375
3/1	937.269	99.044	62.731
22	939.122	140.255	60.878
Average	938.741 ± 1.766	114.428 ± 28.413	61.29 ± 1.766

Table 8.7 shows the concentration of metal ions as determined with the ICP-AES. Only the metals that were detected are shown. The final column is the average of the three samples.

Table 8.7: ICP analysis for Maersk fouling

Metal \ Sample	1 (mg/l)	2 (mg/l)	3 (mg/l)	Content mg/kg
Cu	0.052	0.297	0.392	10.96
Fe	12.84	42.00	49.71	1669
Mn	0.102	0.736	0.827	24.68
Zn	3.113	13.08	11.38	444.9
Mg	5.184	15.16	14.22	579.4
Mo	0.113	0.380	0.410	14.56
Ca	36.31	112.9	123.7	4436

8.1.3 Evaluation

The TS/VS analysis shows that only a small part of the fouling from Shell is ash, making it a mostly organic compound. We also see that the fouling consists of a large portion of volatile matter, which upon evaporation changes the colour of the fouling significantly. These results are a clear indication that the fouling is a heterogeneous compound, which do not solely consist of one molecule. The presence of compounds that evaporate at 90 ℃ is interesting when considering that the fouling often occurs when the material stream encounters a cooling operation. It may be that first when the temperature is sufficiently low, will the smaller molecular weight compounds condense to take part in the formation of the fouling. It could also be that the volatile compounds become absorbed by the fouling, without having a significant role in the formation of the fouling. Another possibility is that the fouling decomposes at elevated temperatures, and that it is this weight loss, which gives the volatile matter.

The fouling from Maersk has a lower content of volatile solids and a higher amount of ash. This is an indication that the two types of fouling are not the same material.

In both cases the inorganic part of the fouling mainly consists of iron and calcium, which could be an indication of iron corrosion and calcium carbonate. These are relatively common compounds, so it is not surprising that they are found. The presence of iron corrosion products could indicate that the fouling is connected to places in the piping vulnerable to corrosion. Such places will have an increased surface roughness where it might be easier for the fouling to deposit or start formation. The calcium could originate from the chalk layers from which the oil is extracted. This would also explain why the concentration is higher in the Maersk fouling. The presence of calcium in the fouling could indicate that the corrosion is taking place around calcium deposits under which the oxygen could rapidly become depleted creating a corroding environment. It could also be that calcium simply deposits on the fouling as this grows. Especially for the Shell fouling do the inorganic compounds seem to be relative insignificant, since only a very small amount is found in the TS/VS analysis.

8.2 IR and X-ray analysis of fouling

The purpose of this experiment was to investigate the nature of the fouling found at Shell. To test hypothesis A that the fouling is s-trithiane, spectra obtained for the fouling were compared with spectra for pure trithiane. This was done because although IR and X-ray diffraction are qualitative techniques, it is difficult to give certain conclusions without comparison with a spectrum of the pure compound.

The three samples (s-trithiane, Shell fouling and Maersk fouling) can be seen in figure 8.1.

Figure 8.1: From left to right: Trithiane, Shell fouling, Maersk fouling

There is an obvious difference in colour between the samples. The pure trithiane is white, the Shell fouling is yellowish and the Maersk fouling is black. This could indicate a difference in composition; however, for the Maersk fouling it may be that the black colour is a result of mixing with oil. Another difference is the smell. The pure trithiane has an acidic smell, while the Shell fouling has a much more pervasive and putrid smell, which necessitates that work with it is carried out in fume hood. The black Maersk fouling is odourless.

As a preparation for both analyses, the samples were grinded to a smaller particle size with a mortar. Especially for the black fouling from Maersk, this was difficult due to the texture of the sample.

8.2.1 Method

IR

For the IR analyses an ATR (attenuated total reflectance) cell was used, see appendix B for background theory of the method. During a measurement, the sample was placed on the crystal, and a tower was lowered onto the sample, and tightened to give a good contact between the sample and crystal. A spectrum was recorded, after which the sample was removed from the crystal, which was cleaned with 70 wt% ethanol.

Because the IR radiation with lower wavenumbers penetrate the sample more efficiently than higher wavenumbers, radiation with lower wavenumbers will spend more time in the sample, and as such an imbalance develops in the absorption of the radiation. To compensate for this, the recorded spectrum is subjected to ATR correction. Finally, transmittance is chosen as the y-variable.

X-ray diffraction

Background theory of X-ray diffraction may be found in appendix A. Before the diffraction spectra could be recorded, it was necessary to prepare the samples by pressing the powder to a solid disc. This was done by taking a sample holder, and separating the top and bottom; the top lid could be used as a mould for the disc. The top lid was placed upside-down on an aluminium block, where it was held in place by three knobs. Then sample powder was filled into the hole, and with an aluminium cylinder it was pressed into a disc. By removing the top lid from the block, and reconnecting it with the bottom of the sample holder, a disc of sample with a smooth surface had been created.

A disc of each sample was prepared, and the sample holders were placed in the autosampler tower from slot number two and down. In slot number one, a standard silicon sample was placed. This is always measured before an experiment, and ensures that the effectiveness of the diffractometer is determined. It was decided to make a complete scan from 5 to 105 degrees for all samples.

8.2.2 Results

IR

In figure 8.2, the IR spectrum obtained for the pure trithiane is shown.

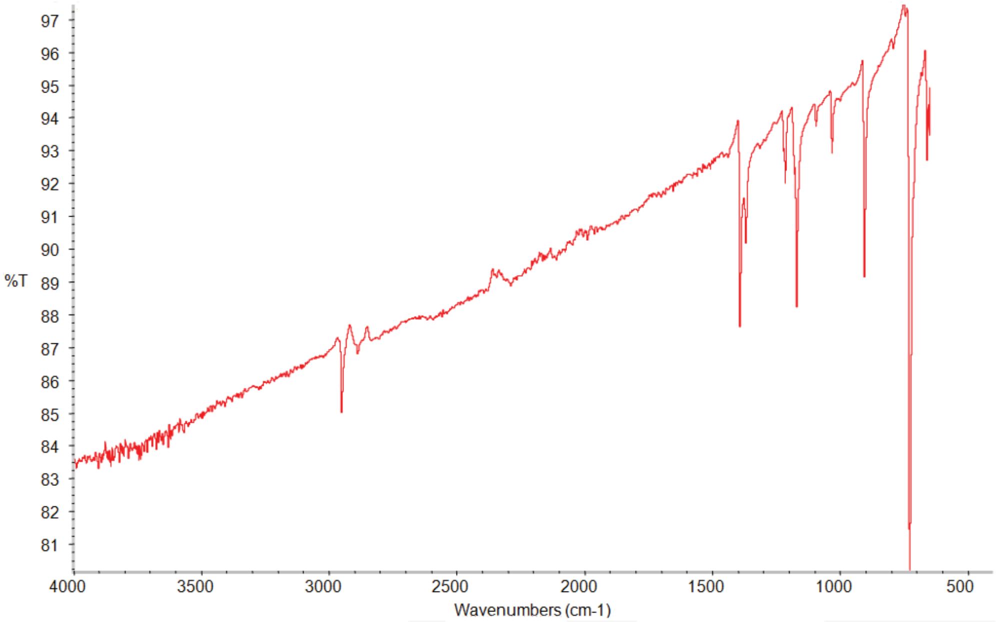

Figure 8.2: IR spectrum for trithiane

It has significant peaks at the following wavenumbers (numbers are in cm^{-1}):

- 2952
- 1392
- 1369
- 1217
- 1171
- 1034
- 907
- 730
- 661

IR absorption due to the sulphur groups occur from around 800 cm^{-1} and down. For $-CH_2$-S-CH_2- functional groups the peak is expected to occur in between 695 - 655 cm^{-1} with a weak to medium intensity [25], and if additional heavier atoms are added to the structure, the absorption band may be blue shifted. This absorption band fits well with the two peaks at 661 and 730 cm^{-1}. For acyclic molecules, there are two stretching modes: symmetrical and asymmetrical. For cyclic molecules the ring structure may give, ring stretch, or a pulsating motion where the point of mass is unaltered, ring breath. The peak at 660 cm^{-1} is probably due to ring breath, and the peak at 730 ring stretch [17].

Because the C-S bonds do not cause absorption above 800 cm^{-1}, the remaining peaks in the fingerprint region must be attributed to motions of the C-H bonds. The peak at 907 cm^{-1} could be CH_2 rocking, the peak at 1171 cm^{-1} could be CH_2 twisting, the peak at 1217 could be wagging, and the peaks at 1369 and 1392 cm^{-1} could be scissoring [17].

The methylene groups in the ring ($-CH_2$-S-) are expected to show stretching motion between 2985-2920 cm^{-1}, which fits well with the peak at 2952 cm^{-1}. However, the peak is very weak compared to what would be expected for trithiane since it carries three methylene groups. Furthermore, a peak between 1435 - 1410 cm^{-1} for the bending motion would have been expected, but no peak is seen here

In figure 8.3, the IR spectrum obtained for the Shell fouling is shown.

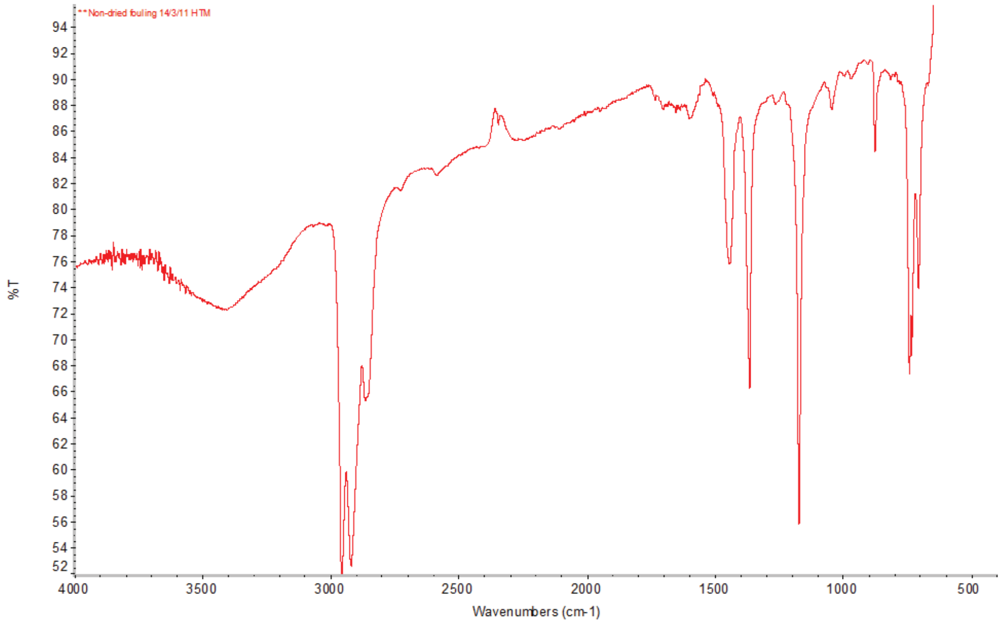

Figure 8.3: IR spectrum for Shell fouling

It has significant peaks at the following wavenumbers (numbers are in cm^{-1}):

- 3400
- 2956
- 2923
- 2867-2855
- 1584
- 1449
- 1366
- 1175
- 1051
- 880
- 745, 734, 707

The peaks around 700 - 750 cm^{-1} are most likely caused by stretching of the C-S bond, since this was responsible for the 730 cm^{-1} peak for trithiane. However, here we see three peaks instead of one, indicating that the C-S bonds in the fouling are different. The peak with highest energy, could be caused by terminal sulphide groups (775 - 675

cm^{-1} [25]), which could be the result of ring opening or branching of a chain structure. Furthermore, the peak at 661 cm^{-1}, which was caused by the ring breath motion of the trithiane ring, is no longer seen. This could indicate that there no longer is a ring structure, and that the remaining C-S peaks are due to stretching of an acyclic structure.

The peaks at 1175 and 1366 cm^{-1} were also found in the trithiane spectrum, and they most likely describe the same vibrational motion in the molecule, which is bending of the methylene groups. The peak at 907 cm^{-1} is no longer present, instead a peak at 881 cm^{-1} occurs. This peak could again be explained by methylene rocking. There are also two new peaks, 1449 and 1584 cm^{-1}, where the peak at 1449 cm^{-1} fits well a methylene bending. It is possible that the peak at 1584 cm^{-1} is caused by bending of the N-H bond in a secondary amine (1580-1490 cm^{-1} [25]); however, if this was the case we would also expect peaks due to C-N stretching, which would occur around (1190 - 1130 cm^{-1} [25]), at least one for symmetric stretching and one for asymmetric stretching. Unless these peaks are masked by the 1175 peak for methylene bending, then they are not present in the spectrum.

Around 2850-2950 cm^{-1} we see a much more pronounced peak compared to the trithiane spectrum, and the main peak consists of three sub-peaks. The peak at 2956 cm^{-1} is probably due to -CH_3 asymmetrical stretching (2975 - 2950 cm^{-1} [25]). Methylene groups have absorption bands that are more red shifted (2940 - 2915 cm^{-1} [25]) for asymmetrical stretching. These can therefore not explain the 2956 cm^{-1} peak, but fit well for the 2923 cm^{-1} peak. The smaller peak at 2867-2855 cm^{-1} are then probably due to symmetrical stretching of both methylene and methyl groups (2870-2840 cm^{-1} and 2885-2865 cm^{-1} [25]). The presence of methyl groups also indicates that the structure is linear and not cyclic. Furthermore, the methyl peak is of same intensity as the methylene peak, which could indicate branching of the chain, or very short chains. Another possibility is that the two main peaks are due to different methylene groups. The presence of sulphur atoms can blue shift the absorption band for methylene stretching (2985 - 2920 cm^{-1} for asymmetrical and 2945 - 2845 cm^{-1} for symmetrical stretching [25]), which brings the absorption into the range of 2956 peak. However, methylene stretching affected by sulphur atoms will only give peaks of medium intensity, whereas ordinary methyl and methylene absorption give peaks of medium to strong intensity. The effect of the sulphur atoms could therefore drown in a methyl signal.

There is also a broad but weak peak from 3100 - 3500 cm^{-1}. Broad peaks in this area are usually an indication of the presence of hydroxy groups and/or amines. If a nitrogen atom is present in the structure, it could very likely be as a tertiary amine (as seen in dithiazine), which will have a peak between 1210-1150 cm^{-1}, but this may be masked by the 1175 cm^{-1} peak. However, a tertiary amine will not have any N-H bonds, which is the bonds that will absorb in the 3100 - 3500 cm^{-1} region. If the broad weak peak is indeed due to the presence of an amine structure, then it will have to be primary or secondary. The polymeric structure proposed by Taylor and Matherly does include secondary nitrogen atoms, which might therefore be the most likely type of amine group. Secondary aliphatic amines absorb between 750 - 710 cm^{-1} and 1580 - 1490 cm^{-1} [25], due to wagging of the N-H bond, and between 1190 - 1170 cm^{-1} due to C-N stretching [25]. These bonds could be explained by the peaks in the spectrum.

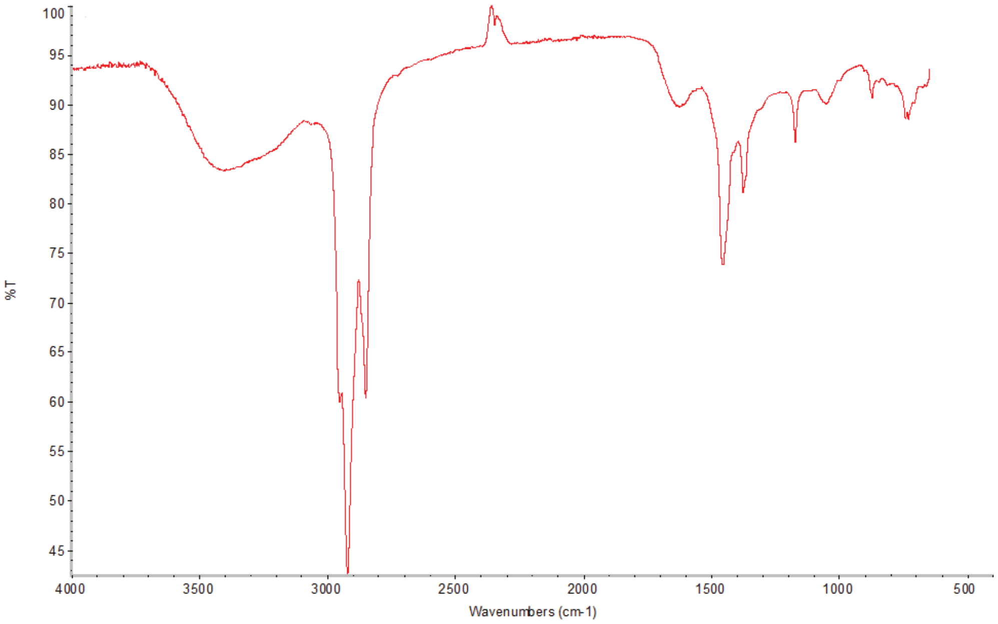

Figure 8.4: IR spectrum for Maersk fouling

In figure 8.4, the IR spectrum obtained for the Maersk fouling is shown. It has significant peaks at the following wavenumbers (numbers are in cm^{-1}):

- 3400
- 2923
- 2853
- 1458
- 1376
- 1175
- 730

The IR spectrum of the Maersk fouling shows some interesting similarities with the spectrum of the Shell fouling. Again the peak at 730 cm^{-1} could be caused by C-S stretching. The peak is weak in intensity, which makes it difficult to assess whether it consists of several peaks, but apparently there is no peak indicating ring breath absorption. As with the Shell fouling peaks due to methylene bending motion is found at 1175, 1376 and 1458 cm^{-1}. However, the absorption in the fingerprint region is much weaker than the peak around 2900 cm^{-1}. We see absorption at 2923 cm^{-1}, which is methylene asymmetrical stretching, and at 2853 cm^{-1} which is probably methylene symmetrical stretching. There is no strong methyl absorption, indicating that the chains are long, giving a high ratio of methylene to methyl groups.

Looking at the sample, it has a black colour, and a very viscous liquid can be pressed from the fouling. This indicates that the fouling consists of a significant portion of oil, which would also explain why the methylene stretching peaks are so dominant.

X-ray diffraction

In figures 8.5, 8.6 and 8.7, the X-ray diffraction spectra for pure trithiane and the fouling found at Shell and Maersk are shown. The spectrum for trithiane shows many distinct peaks, and has a baseline with very low noise level, which indicates a high degree of crystallinity. There are three crystal planes which are responsible for the main part of the diffracted radiation. However, without knowing the crystal system, labels cannot be assigned to the peaks.

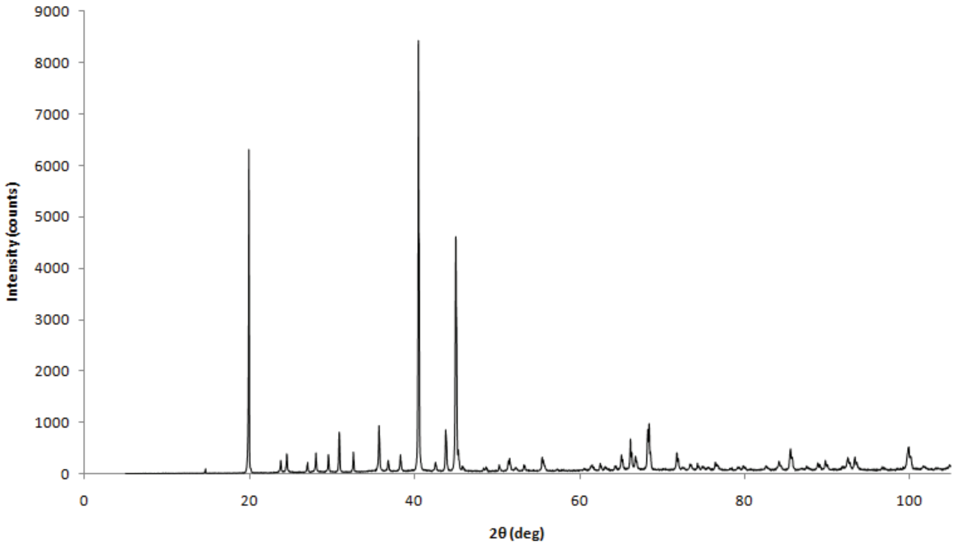

Figure 8.5: X-ray diffraction spectrum of pure trithiane

The Shell fouling shows only three peaks, and it has a higher and more unstable baseline level. This indicates a lower amount of crystallinity in this material.

In the spectrum for the Maersk fouling, no peaks are seen. This material has therefore no crystal planes that can give rise to diffraction and is completely amorphous.

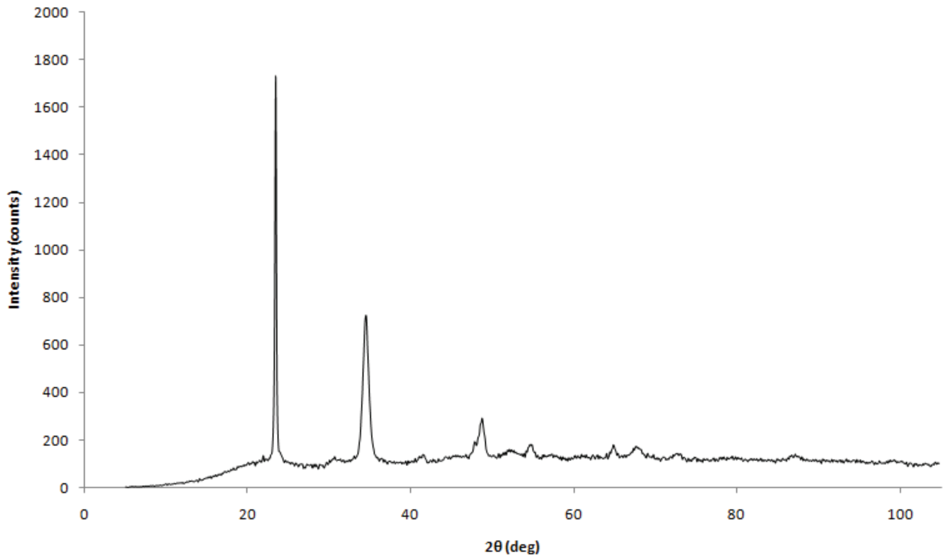

Figure 8.6: X-ray diffraction spectrum fouling

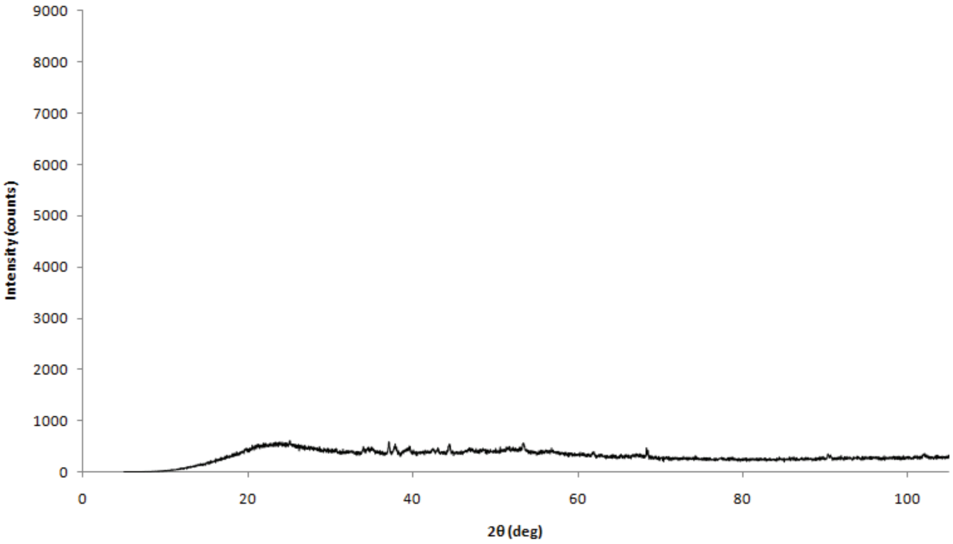

Figure 8.7: X-ray diffraction spectrum Maersk fouling

8.2.3 Evaluation

The IR spectrum for trithiane only has a very weak peak at 2952 cm^{-1}. However, when compared with a spectrum found at the distributor of the chemical, Sigma Aldrich, it is seen that this peak should be much more dominant, see figure 8.8. Furthermore, we should also see a peak at 1450 cm^{-1}. The absence of these two peaks should therefore not be used to distinguish between trithiane and the fouling. One possibility is that the compound purchased at Sigma Aldrich, is actually not trithiane. It is also possible that the compound has decomposed. However, the fingerprint regions are identical, and none of the two explanations seem reasonable, since they would both also be expected to affect the fingerprint region. Instead, it seems more plausible that there has been an insufficient contact between the powder and the crystal, which will affect the absorption peaks at higher wavenumbers most. This would also explain the tilted baseline.

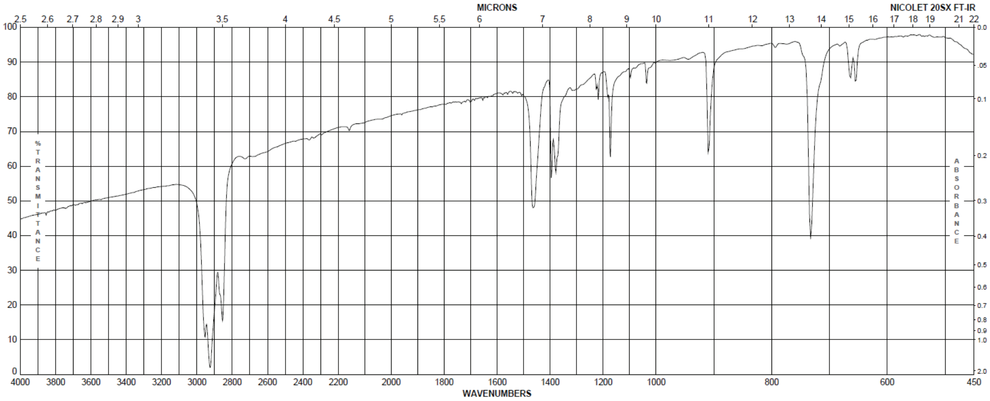

Figure 8.8: IR spectrum for trithiane from Sigma Aldrich [1]

With this in mind the spectra of the fouling from Shell and the pure trithiane are reasonably similar. There are many coinciding peaks, which could indicate that the two materials are identical, especially considering that one is a technically pure chemical and the other a field sample. However, there are also differences, especially the absence of a peak at 660 cm^{-1} for the fouling, which would indicate that the fouling is not a cyclic compound. Also the peaks around 730 cm^{-1} for the fouling indicates that there are either several kinds of C-S bonds in the structure or N-H and C-S bonds, whereas the single peak for the trithiane indicates the all C-S bonds are equal here, as would also be expected for trithiane. Furthermore, the fouling also shows signs of an alcohol/amine peak, which should not be present if the fouling was trithiane. Another possibility could then be that the Shell fouling is crystalline dithiazine; however, as we see in figure 8.9, the IR spectrum for crystalline dithiazine contains more peaks in the fingerprint region than found for the Shell fouling. Especially from 1100 and down many peaks are found. The increased amount of peaks is due to the presence of peaks from N-H, C-N, O-H and C-O vibrations. The fact that peak intensity for a functional group is proportional to the number of times the specific group is present in the molecule could explain why we do not see all these peaks in the fouling spectrum. If the fouling was

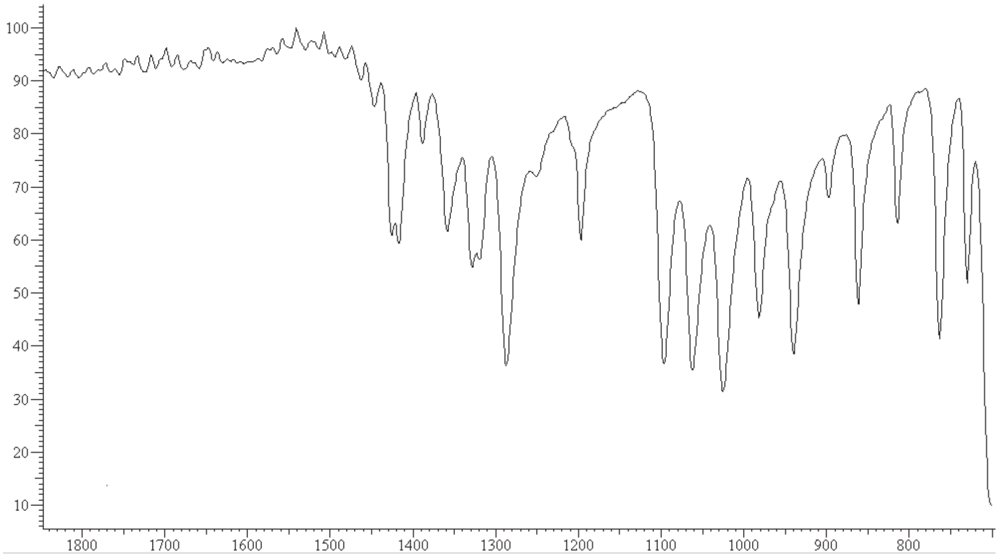

Figure 8.9: IR spectrum for crystalline dithiazine [30]

indeed a polymeric material, the C-S and C-H bonds would take up the main part of the molecular structure, and these peaks would come to dominate the spectrum.

The X-ray analysis indicates that the fouling is different from pure trithiane. It shows fewer peaks, and with a considerably lower intensity than the trithiane peaks. This indicates that the fouling has a structure which is more amorphous in character. However, the fouling is not amorphous trithiane, because if we look in figure 8.10, where the two spectra are compared, it is seen that the peaks of the fouling do not match any of the peaks found for trithiane. This means that the fouling has a completely different crystal structure from trithiane.

A most interesting observation is that the spectrum of the fouling is very equal to the one found by Taylor and Matherly, when they investigated crystals obtained from a reaction between H_2S and hydroxyethyl-triazine [30], see figure 4.12. The peaks found in our X-ray analysis is shifted towards higher diffraction angles, but this could be explained with a difference in the X-ray source between the two experiments. If Taylor and Matherly have used an X-ray source with a wavelength shorter than Co, then from Bragg's law diffraction would be expected to occur at lower angles. Furthermore, it may be noticed that the peaks lie in equal distance relative to each other when the two spectra are compared. The fouling found at Shell may therefore very well be the same as investigated by Taylor and Matherly. They speculated that their compound was a dithiazine polymer with C-S chains in between. This would also fit well with the IR results, since they indicate an acyclic structure composed of different C-S bonds, with a small amount of amine bonds as well.

The IR and X-ray spectra for the fouling found at Maersk indicate that this is not the same compound as the fouling found at Shell. The structure is completely amorphous, but it has some of the some of the same functional groups, especially the peak for C-S stretching. It was also observed that this fouling seemed to be mixed with oil. One

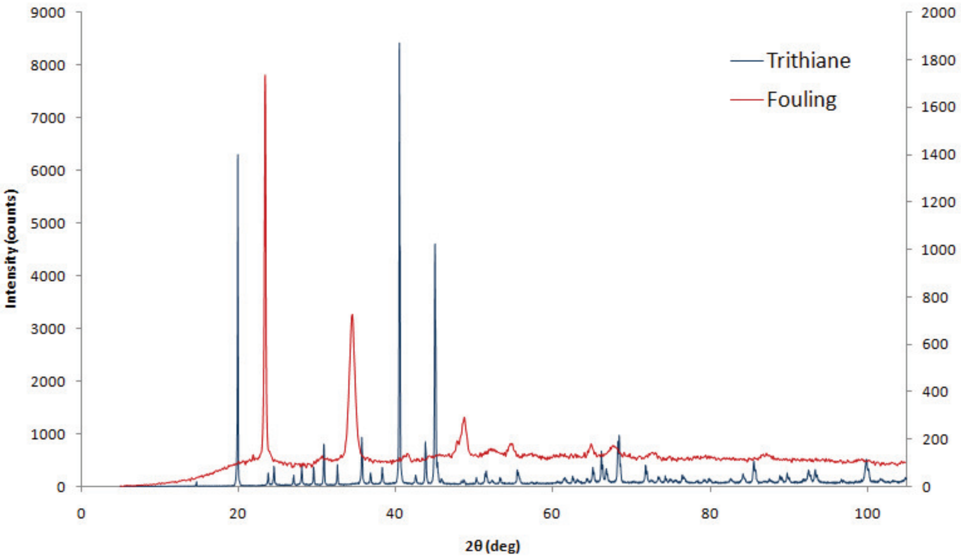

Figure 8.10: Comparison of X-ray diffraction spectrum for fouling and trithiane

possibility is that we have the same fouling found at Shell, or a precursor for it, in an oil matrix. The polymer chains could buttress the oil structure forming a composite like compound. Such a compound would most likely be completely amorphous, explaining both the IR and the X-ray spectra.

If the IR spectra for the precipitates produced in the laboratory are compared with the IR spectrum for the fouling, a high degree of overlap is seen. The two spectra share peaks at 2956, 2923, 1366, 1175, 1051, 880, 745, 734 and 707 cm^{-1}. The precipitate also absorbs at 1282 cm^{-1}, but this is a very weak peak, and at 1638 cm^{-1} where the fouling absorbs at 1584 cm^{-1}. The peak at 3400 cm^{-1} is more intense for the precipitate than for the fouling. This could either be because the precipitate contains a higher concentration of amine/hydroxyl groups compared to the fouling, or that the precipitate is still polluted with possible MEA residues. The methylene peak is also weak for the precipitate, but this might partly be due to overlap from the broad 3400 cm^{-1} peak. All in all, this is a clear indication that the two compounds are the same, and it seems certain that the fouling at Shell is caused by spent scavenger in the crude oil.

Also in the experiment with H_2S being bubbled through the spent scavenger a viscous liquid was found in the retentate. The spectrum contained many more peaks than the solid precipitate, which suggested and entirely different structure. If this spectrum is compared with the spectrum for crystalline dithiazine, a high amount of overlap between the peaks is found. In figure 8.11 it has been attempted to put the two spectra on top of each other via graphical manipulation to ease the comparison. From the figure it can be seen that many of the peaks do overlap or lie very close to each other. Some of the peaks seem to be shifted when comparing the spectra, but considering that the spectra have been made for two different samples and with two different IR spectrometers, the match is very good. The peak at 1055 in the spectrum for the viscous liquid is very strong compared to the other peaks in the spectrum, but this may be because it is composed of two peaks, seen in the spectrum for the crystalline dithiazine, and that these have not been separated due to the resolution of the spectrometer. In total, these two spectra indicate that the viscous liquid is crystalline dithiazine. That crystalline dithiazine may be formed, is a further indication that the scavenging process terminates at dithiazine, and does not react to form trithiane.

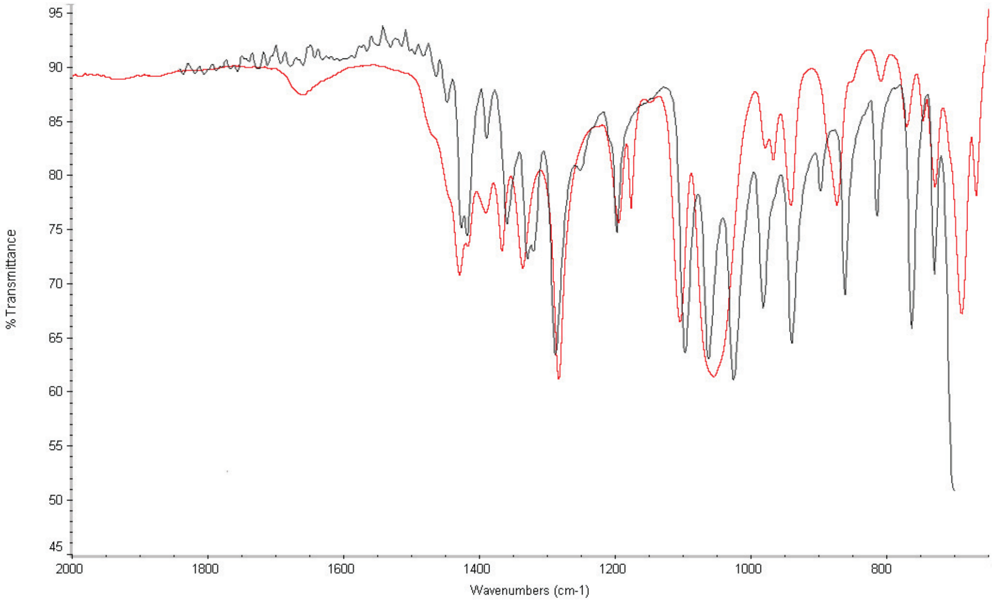

Figure 8.11: Comparison of IR spectra for crystalline dithiazine and the viscous liquid from retentate

From the results, it seems then that the reaction between H_2S and the spent scavenger may either lead to a C-S polymer formed from dithiazine, or crystalline dithiazine. However, the exact mechanism for going from dithiazine to a polymer is unknown.

Chapter 9

Experiments - Polymerisation

It has been proposed that a polymerisation of dithiazine molecules occurs due to the presence of thioformaldehyde in the reaction mixture. Thioformaldehyde may be formed in a reaction between formaldehyde and H_2S, and formaldehyde may be formed in the hydrolysis of triazine. However, since the amount of sulphur and carbon found in the structure is very high, a significant amount of formaldehyde must be formed to be able to explain the elemental composition. Whether enough formaldehyde is formed may be questioned.

The kinetic model made in chapter 4 shows that the scavenging reaction is much faster than the hydrolysis of triazine back to formaldehyde and MEA. Also, a large part of the triazine is spent in the scavenging reaction, and our experiments with ESI-MS, have only found a weak signal for triazine in the spent scavenger, indicating that only a small amount is present. Furthermore, the presence of MEA in the reaction mixture, formed during the scavenging reaction, will affect the equilibrium of the hydrolysis reaction to shift the reaction towards triazine formation. Actually, 1 wt/wt % MEA is added to the initial triazine solution by the manufacturer, to completely avoid formaldehyde formation. MEA is so efficient at suppressing formaldehyde formation that the content of formaldehyde in the triazine is set to nil by the manufacturer. It is possible that at elevated temperatures the rate of hydrolysis relative to the rate of scavenging is increased, but given the fact that an identical precipitation was observed at room temperature as well as during boiling, high temperatures do not seem to affect the reaction system in such a way. Instead an alternative explanation for how a polymerisation may take place is proposed.

The compound present in the highest concentration in the reaction mixture will be MEA. It is formed 1:1 with thiadiazine and 1:2 with dithiazine, and does therefore seem to be a more suitable precursor candidate for a polymerisation. MEA is a known scavenger of H_2S as earlier discussed in chapter 2, but here it is assumed to work because of acid/base reactions with the H_2S. A solution of MEA may because of its acid/base properties dissolve equimolar amounts of H_2S, and it is possible that when the amount of HS^- relative to MEA becomes high, substitution reactions may take place.

$$HOCH_2CH_2NH_2 + H_2S \rightleftharpoons HSCH_2CH_2NH_2 + H_2O \tag{9.1}$$

$$HOCH_2CH_2NH_2 + H_2S \rightleftharpoons HOCH_2CH_2SH + NH_3 \tag{9.2}$$

$$HSCH_2CH_2NH_2 + H_2S \rightleftharpoons HSCH_2CH_2SH + NH_3 \tag{9.3}$$

In this way, compounds with terminal sulphide groups may be formed, and sulphide groups are known to form disulphide bonds in a reduction reaction.

$$H_2NCH_2CH_2SH + HSCH_2CH_2NH_2 \rightleftharpoons H_2NCH_2CH_2S{-}SCH_2CH_2NH_2 \tag{9.4}$$

In these reactions, a formation of ammonia is proposed, and ammonia is actually detected in the water treatment system at Shell, which could support this theory.

The formed sulphide compounds could then react with dithiazine as proposed in figure 9.1. Here a condensation reaction at the hydroxy group links a dithiazine molecule with one of the reaction products from the reaction between MEA and H_2S. This creates a terminal sulphide group, which may then react with further sulphide containing compounds. To link the chain to a second dithiazine, the same ring opening that was proposed in the scavenging reaction mechanism might produce a terminal sulphide group

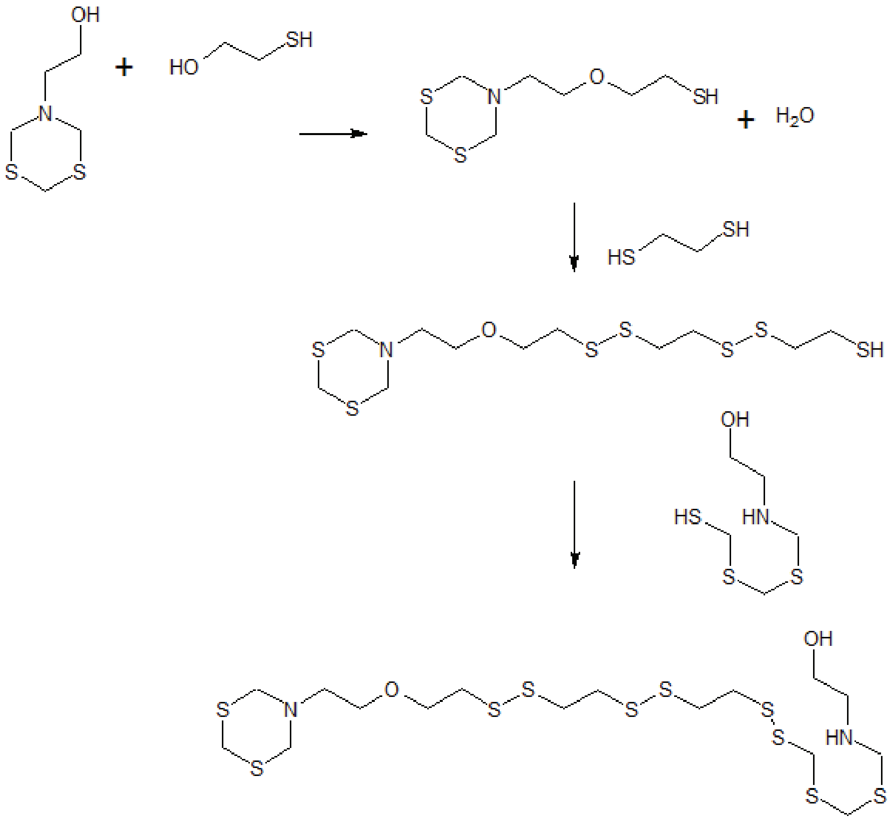

Figure 9.1: Alternative polymerisation process

on the dithiazine. Although the scavenging reaction ends with dithiazine formation, it is still possible that the ring will open and form a terminal sulphide group. The energy needed to dissociate the nitrogen group from the opened ring may simply be too high for this to take place, and the molecule may revert back to dithiazine. We may therefore consider the dithiazine molecule in the mixture in a constant equilibrium between the opened and closed form. The polymer formed in such a process would then be of the type presented in figure 9.2. Here the length of the chain between each dithiazine molecule may vary.

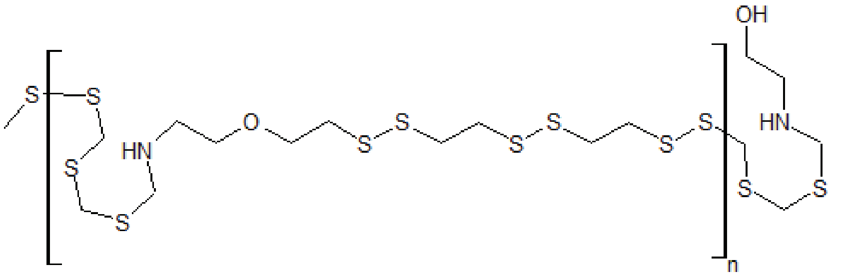

Figure 9.2: Alternative polymer

To investigate if such a process is possible, an experiment where MEA is subjected to a high concentration of H_2S is made, to see if any sulphide compounds may be formed.

9.1 Method

Chemicals: $NaHS_{(s)}$, monoethanolamine, 37 % HCl.
Apparatus: 250 ml flask with tubes for leading bubbles through liquid, magnet and magnet stirrer, 50 ml boiling flask with double neck, plastic tube, adaptor for rubber tube, 25 ml dripping funnel.

The experiment was carried out in the same fashion as the previous experiments where H_2S had been bubbled through a solution. 12.5 ml MEA (0.2 mole) was measured out and transferred to the 250 ml flask, where it was diluted with 12.5 ml demineralised water. This was done to obtain a concentration of MEA in the same range as when using the triazine solution, where the concentration of triazine was 51 wt/wt %. Then HCl was dripped upon the NaHS, and the evolved H_2S gas was led through the MEA solution. During the experiment the temperature rose in the mixture, due to the exothermic acid/base reaction. 0.2 mole H_2S was bubbled through the MEA solution to ensure that all MEA was used. The solution was then left for three days before it was analysed. Due to the unknown solubility parameters of possible products, both ESI-MS and GC-MS was used to analyse the solution. For the ESI-MS analysis, a 1 ml sample was taken and diluted 1:10000 with demineralised water before it was analysed with the MS. For the GC-MS analysis, 1 ml sample was extracted to a test tube, where it was mixed with 1 ml pentane. The pentane phase was transferred to a vial and analysed on the GC-MS.

9.2 Results

In figure 9.3 the mass spectrum from the ESI-MS is shown. The peak at 62.8 is the dominating peak in the mass spectrum, and we recognise this from the spectrum of MEA. The same is true for the peak at 147.3. The spectrum is characterised by a large number of smaller peaks, which may be part of a background signal. This was also seen earlier for pure MEA, and it can therefore not be taken as a result of the reaction with H_2S. In total, the ESI-MS analysis does not indicate that a reaction has taken place, although the 147.3 peak has decreased relative to the 62.3 peak.

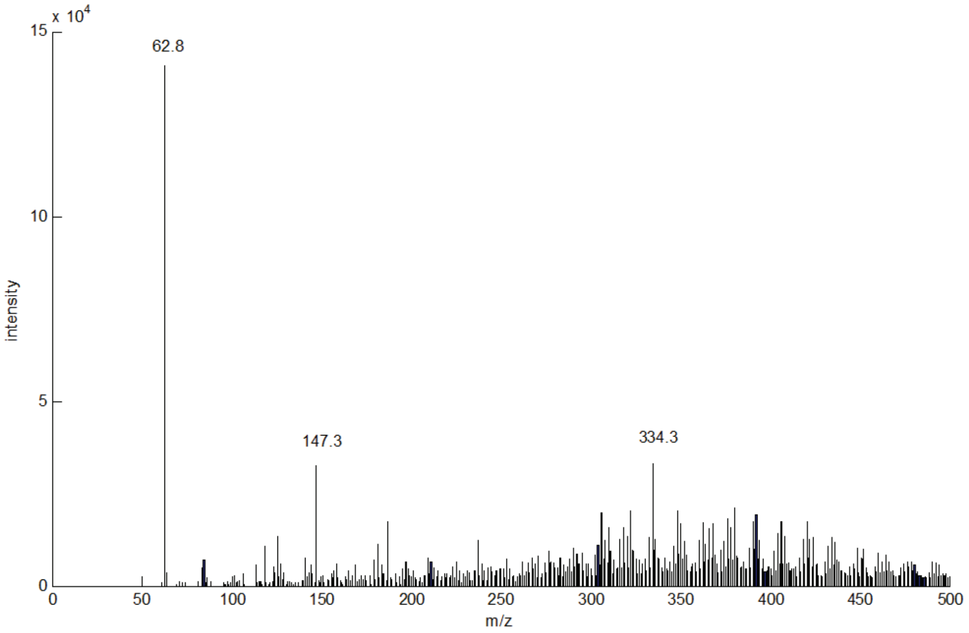

Figure 9.3: ESI-MS spectra of MEA after reaction with H_2S

In figure 9.4 the chromatogram and the mass spectrum of the peak after 3.94 minutes (circled with red) from the GC-MS analysis of the pentane phase are shown. Most of the peaks in the chromatogram are due to pentane, and other hydrocarbons dissolved in the pentane. However, by using the NIST library installed on the computer, the mass spectrum shown in figure 9.4 is identified as bis(1-methylethyl)-disulphide (49.6 %), see figure 9.5. The peak in the chromatogram is very weak, so the concentration of the disulphide is low, but it is very interesting that it is formed. This indicates that some reaction has taken place. Whether the compound truly is bis(1-methylethyl)-disulphide is questionable, since it will depend on the compounds in the NIST library. However, the high percentage indicates that it could very likely be a disulphide.

As long as only one group, of the hydroxy and amino group, is replaced with a thiol group, the compound should still be most soluble in water, which might explain why only a small amount of sulphide compound is found with the GC-MS, and if the ESI-MS is not capable of charging the compounds, they might not be detected at all. Still, with

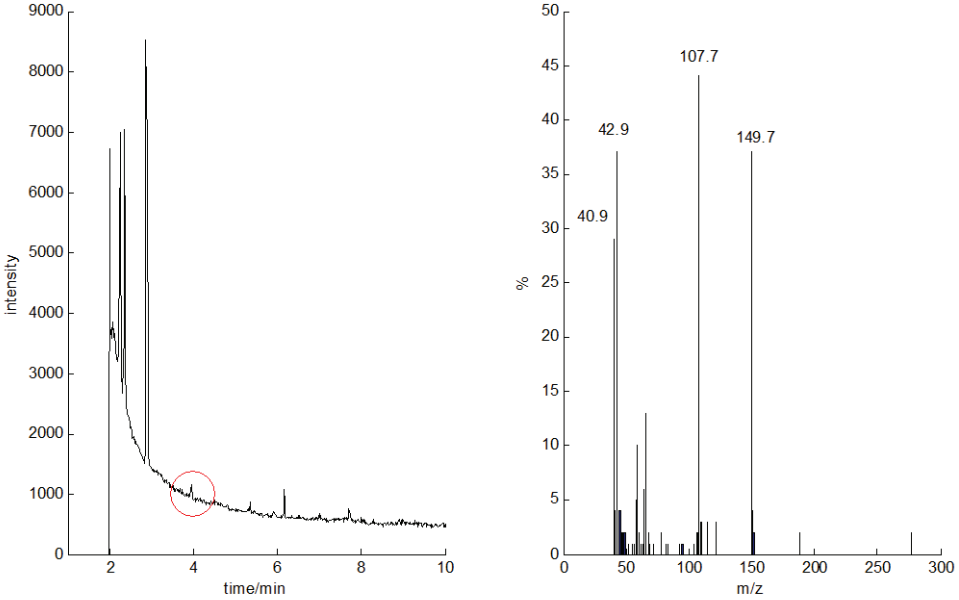

Figure 9.4: Chromatogram of pentane phase and mass spectrum for peak after 3.94 minutes

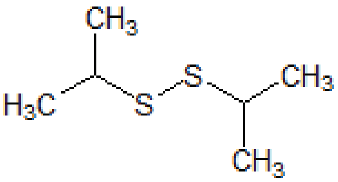

Figure 9.5: Bis(1-methylethyl)-disulphide

the detection of the disulphide, the hypothesis about MEA being the precursor for a polymerisation cannot be rejected.

Chapter **10**

HSP analysis of fouling

To gain additional knowledge regarding the nature of the fouling from Shell, a HSP analysis is conducted. This will potentially also provide useful information about methodes to clean the system after fouling has occurred. Based on the previous experiments, it is assumed that the fouling has a polymeric nature as suggested by Taylor and Matherly [30]. Therefore, the main part of the structure is expected to be S-C segments, and the fouling is therefore expected to be most soluble in non-polar solvents. With this in mind, three additional solvents are chosen to cover the non-polar area sufficiently: trichlorethylene, n-heptane and n-dodecane. Furthermore, these components will also give clues to the solubility of the fouling in oil like substances, which will be important to evaluate whether the fouling will be dissolved in or precipitate from oil.

10.1 Method

The analysis is performed with a total of 35 solvents, listed with their HSP values in table 10.1. 35 test tubes was filled with 0.5 g of fouling. Then 3 ml of solvent was added, a lid was put on the test tubes, and the solutions were mixed for 30 seconds on a whirl mixer. After mixing, each solution was assessed for see if the fouling had dissolved. The solutions were assessed again after two weeks, and these are the final reported values. If the fouling was completely dissolved, it was given a ”2”, for interaction ”1”, and for no interaction ”0”.

10.2 Results

In the sixth column in table 10.1, the solubility results are shown. None of the samples experienced complete dissolution, and as a result, the evaluation of the effect of the different solvents was based on other parameters. In many of the samples, the liquid phase changed colour after being mixed with the fouling. This can be explained by the extraction of a colouring component from the fouling, or the formation of such a compound after reaction between the solvent and the fouling. A distinct colour change was therefore taken as an indication of the fouling becoming dissolved to some degree.

Table 10.1: Solvents used in HSP analysis

Number	Solvent	δ_P	δ_H	δ_D	Solubility
1	Acetone	10.4	7.0	15.5	2
2	Acetophenone	8.6	3.7	19.6	2
3	Butan-1-ol	5.7	15.8	16.0	0
4	Butylacetate	3.7	6.3	15.8	1
5	Water	16.0	42.3	15.5	0
6	Chlorobenzene	4.3	2.0	19.0	1
7	Chloroform	3.1	5.7	17.8	1
8	Cyclohexanol	4.1	13.5	17.4	0
9	Cyclohexanone	6.3	5.1	17.8	2
10	1,1-dichloroethylene	5.2	2.4	16.4	2
11	Dichloromethane	6.3	6.1	18.2	1
12	Diethylether	2.9	5.1	14.5	0
13	N,N-dimethylmethaneamide	13.7	11.3	17.4	0
14	Dimethylsulfoxide	16.4	10.2	18.4	0
15	1,4-dioxane	1.8	7.4	19.0	1
16	Ethanolamine	15.5	21.2	17.0	0
17	Ethylacetate	5.3	7.2	15.8	2
18	Ethyleneglycol	11.0	26.0	17.0	0
19	Ethyleneglycolmonobutylether	5.1	12.3	16.0	0
20	Ethyleneglycolmonomethylether	9.2	16.4	16.2	0
21	Methaneamide	26.2	19.0	17.2	0
22	Hexane	0.0	0.0	14.9	0
23	Isophorone	8.2	7.4	16.6	1
24	Methanol	12.3	22.3	15.1	0
25	4-methyl-pentan-2-one	6.1	4.1	15.3	2
26	Ethylmethylketone	9.0	5.1	16.0	2
27	Morpholine	4.9	9.2	18.8	1
28	Nitrobenzene	8.6	4.1	20	2
29	Propan-1,2-diol	9.4	23.3	16.8	0
30	Tetrahydrofurane	5.7	8.0	16.8	2
31	Toluene	1.4	2.0	18.0	1
32	Trichloroethylene	3.1	5.3	18.0	1
33	Dodecane	0.0	0.0	16.0	0
34	Tetrachloroethylene	5.7	0.0	18.3	1
35	Heptane	0.0	0.0	15.3	0

To further support the conclusion drawn from the colour change of the solvent, the colour change of the fouling itself was also evaluated. In many of the samples, the fouling lost colour to a varying degree, where in the most extreme cases the fouling became white resembling chalk. A final observation used in the evaluation, was that for some solvents, like acetone, part of the fouling was turned into a fine white powder. This was also taken as an indication that the solvent is capable of dissolving the fouling, at least to some extent. To get useful information from these results, they are plotted in a coordinate system with the axes representing the three solubility parameters. This produces a total of four plots that can be seen in figure 10.1.

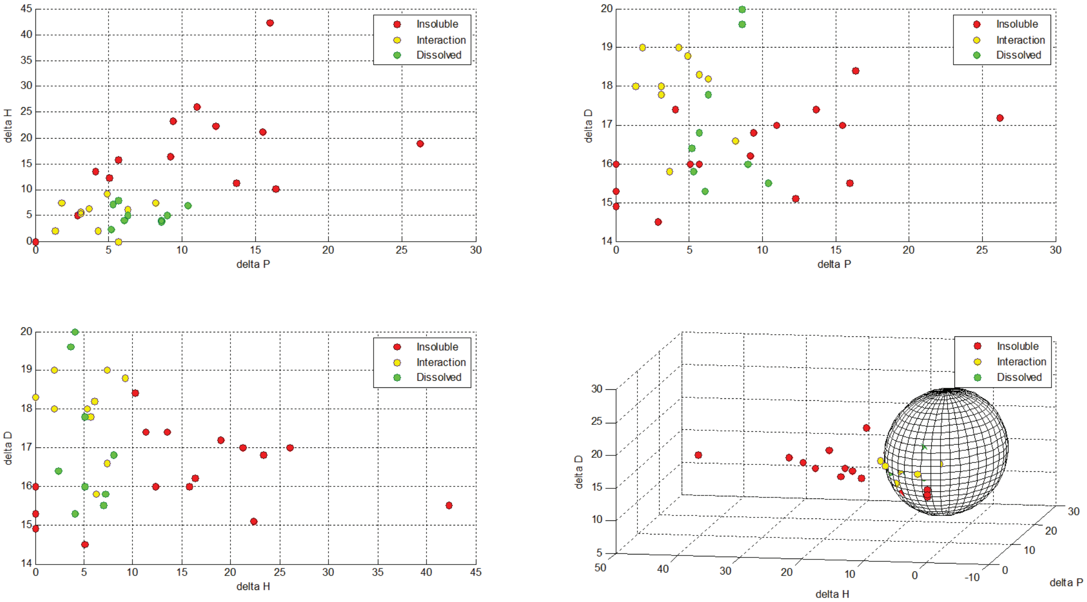

Figure 10.1: HSP plot for Shell fouling

The three 2-D plots make it possible to investigate the influence of each of the three intermolecular forces. The first plot with δH and δP, shows that δH has a very large influence on the solvents ability to dissolve the fouling. At δH values above 10, all solvents are incapable of dissolving the fouling, no matter the size of δP and δD. δH is however not able to give as good a separation between the yellow and green data points; these roughly lie in the same area. The same result is seen in the third graph displaying δH and δD. Also here is there a clear separation along the δH axis. In total the results indicate that a small degree of hydrogen bonding must be present to dissolve the fouling; however, if the hydrogen bonding capability of the solvent becomes too high, the solvent molecules will form bonds between themselves so efficiently that it becomes energetically unfavourable to form bonds to the fouling, since this would require the solvent molecules to break their own ordered structure. Some red data points are also seen below $\delta\text{H} = 10$, and this indicates that δH alone cannot explain the solubility.

Looking at plots one and two, where δP is displayed it is seen that the polar forces are also important for the solubility. It is seen that the green data points all occur at intermediate δP values (5-11). At values below 5, most data points are yellow and above all data points are red. The maximum limit for δP can be explained in the same way as the trend for the hydrogen bonding. As the dipole dipole forces of the solvent increases in strength, the degree of order in the solvent molecular structure also increases. At a certain level it may become energetically unfavourable to break this ordered structured to dissolve the fouling. The lower limit indicates that for the solvent molecules to associate with the fouling, a minimum of polarity is necessary. This could be due to the presence of amine groups and oxygen atoms in the structure of the fouling, but the sulphur atoms may also be part of the explanation. Because the valence electrons are situated farther away from the nucleus, sulphur atoms in the fouling may become polarised by polar solvents, and in this way interact with the solvent. Furthermore, the molar volume of the molecules has not been taken into account here, and it could be the explanation for the overlap between green and yellow data points. It may be that smaller molecules like acetone, can better penetrate and dissolve the fouling than a large molecule with similar polar strength.

Plots two and three show the influence of the dispersion forces. From the plots, it is evident that δD alone cannot explain the solubility, since there is a distinct lack of grouping. It does seem that the amount of red data points decrease with increasing δD, but this may be a coincidence. It is also seen that the data points with high δD also have suitable δH and δP values, and it might be because of these that the data points are not red. A final remark on the δD variation is that compared to δH and δP, the variation in the δD values for the solvents are not as large, which also makes it more difficult to give certain conclusions.

In the final plot, all three forces are plotted simultaneously alongside with the solubility sphere. The centre and radius of this sphere is chosen so that it includes the green data points, preferably in the centre of the sphere, and with the yellow points near the edge and the red data points outside the sphere. Due to the mixing of the green and yellow data points, it is not possible to choose a sphere capable of separating them. Instead, the sphere is chosen so that it includes the solvents that give green data points without worrying about where the solvents only capable of interaction end up. The equation for the sphere is given by formula 10.1.

$$9.365^2 = (\delta P - 11.5)^2 + (\delta H - 1.0)^2 + (\delta D - 18.73)^2 \tag{10.1}$$

10.3 Evaluation

The HSP method can only give approximate results regarding the solubility of a compound. This is because the method is based solely on observations, and it does not include any parameters that can be readily measured. In the experiment only three categories are used to differentiate between the solubility of the fouling in the different solvents; insoluble, interaction and soluble. With these categories we do not account for the amount of fouling that can be dissolved in a given solvent; therefore the experiment will depend on the relative amounts of fouling and solvent. If too small amounts of fouling are used, then solvents where only very small amounts can be dissolved will be put in the same category as solvents with a high solubility capability, and if too large amounts of fouling are used the opposite will be true. In this experiment, none of the solvents were capable of dissolving the fouling completely, indicating that too large amounts of fouling may have been used. It is also possible that the heterogeneity of the fouling ensures that not one solvent alone can dissolve all components.

The degree of solubility has been determined by the colour change in the liquid phase and the solid phase, and also the powderisation of the fouling. This is not an optimal procedure for classification, which is also evident from the mixing of solvents classified as soluble and interaction in the HSP plot. However, we do get some relative information about where the fouling is affected most by the solvents.

An important conclusion from this experiment is that the fouling is not soluble in non-polar solvents, like oil. This means that if the fouling had been formed before the distillation, it would have precipitated from the oil, and fouling in the part of the refinery that handles oil would have been expected. In general the fouling is very difficult to dissolve and none of the solvents used in this experiment can be easily applied to clean the system after fouling has occurred. It may still be possible though to find a better solvent, or a mixture of solvents, capable of dissolving the fouling more efficiently.

Chapter 11

Suggestions for solutions

From the mass balance made in chapter 3, it seems that the fouling may be linked to specific batches of crude oil, where the concentration of spent scavenger is significantly higher compared to the standard crude oil. If this is correct, an online analysis of the crude oil could be made to detect batches rich in spent scavenger. A preliminary study should first be made to investigate if the fouling is indeed linked to such specific batches before any solutions are applied. It has been attempted to detect spent scavenger compounds in the oil with GC-MS, and also to measure the sulphur content of the oil to see if this could be related to the use of scavenger. However, as seen in appendix G, none of the methods seem to be usable. Therefore, another method of analysis must be found. In this study, IR spectroscopy has been used to characterise the fouling, and many process analytical technologies (PAT) are based on the use of infrared radiation, especially near-infrared (NIR). However, IR might not be the best choice for detecting thiadiazine and dithiazine in oil since S-H and C-S give weak/medium peaks, while C-H bonds give a strong peaks. As seen for the Maersk fouling, CH_2 groups can be expected to dominate the spectrum. Instead Raman spectroscopy may be used, since both S-H and C-S will give strong Raman peaks. To find whether Raman spectroscopy can be used to detect changes in spent scavenger concentration, a chemometric study should be made. An alternative to continuous measurement could be to take samples of the oil, and mix them with water. The spent scavenger products will then be extracted into the water phase, and as seen in this project, they may then be detected with ESI-MS. If the ESI-MS is coupled with a LC, the amount of scavenger products may be determined. For this method to work, it will be necessary to construct a sampling procedure in accordance with the theory of sampling (TOS), to ensure representative samples. A variographic analysis could be made to find the optimal sampling rate.

If a method for determining batches of oil with high concentration of spent scavenger is developed, a treatment method for the oil is required. The most obvious method for removing the spent scavenger products is by utilising their high solubility in water. A two phase separator can be installed in parallel with the pipeline going into the desalter, and when a batch of scavenger rich oil is detected, it can be led into this separator. Here the oil can be mixed with water, which will extract the spent scavenger products, and thus removing them from the oil. The oil can then be sent back into the refinery while the water is treated elsewhere. The same method could also be used offshore, where an additional two phase separator could be installed.

Another solution could also be to intentionally provoke the formation of fouling. This could be done by adding H_2S to the top distillate and keep the solution heated. In this way, most dithiazine should hopefully be converted to fouling, and if the solution is then filtrated, the fouling could be removed in a controlled way. To avoid having to stop the process to clean the filter, two filters should be installed in parallel. This will allow cleaning of one filter for fouling, while the other is kept in use.

A last possibility is to choose another method for H_2S scavenging, with an amine solution being a good candidate. This will require large installation costs, but because the amine solution is regenerative, the operation costs will be lower. As more seawater must be injected into the wells to maintain the pressure, the concentration of H_2S will likely increase. As the amounts of H_2S to be removed increase, regenerative methods will become more cost efficient, and an amine solution might therefore be a good investment in the long run.

CHAPTER 12

Discussion

One of main questions in the report has been the nature of the fouling, especially whether it is a polymeric material. From the experiments it has been found that the final solution prior to precipitation consists almost entirely of dithiazine. No triazine or thiadiazine is left and no trithiane is detected either. Dithiazine therefore has to be the precursor for the fouling. If the precipitate was pure dithiazine, it would most likely bare resemblance to crystalline dithiazine. However, the fouling has a low crystallinity and the IR spectrum is very different from crystalline dithiazine. Furthermore, elemental analyses made by Shell and Maersk show that the fouling contains a very high amount of carbon and sulphur and has a low nitrogen and oxygen content, which does not match with the structure for dithiazine. This indicates that the fouling is dithiazine with an increased amount of sulphur and carbon. The results from this project matches very well with the results achieved by Taylor and Matherly. The IR and XRD spectra have a very high agreement, and it is therefore likely that the other results from Taylor and Matherly's investigation can be extrapolated to this project, and these did indicate a polymerisation. On the other hand, if a polymerisation took place, peaks of high molar weight could possibly have been detected in the MS analysis, but no such peaks were seen. Therefore, hypothesis B cannot be said to have been proven correct, but with the available experimental data it seems to offer the best explanation of the nature of the fouling.

The experiments performed in this project has demonstrated that the fouling is formed as a result of an overspending of the scavenger. However, this alone does not explain why the fouling is found at specific places at Shell, and not distributed throughout the entire system. The fouling only occurs in the water treatment process, post distillation. This may be explained by the solubility of the spent scavenger products. Due to the high aqueous solubility, these will be present in the aqueous phase of the crude oil. H_2S is more soluble in oil, and although it may also dissolve in water, most will be present in the oil phase because of the large amount of oil relative to water in the crude oil. Post distillation H_2S will be taken out with the top distillate together with the water and spent scavenger products. This will create a high H_2S concentration gradient, which together with the elevated temperatures may cause rapid fouling formation. The top distillate has a temperature around 136 ℃, and will therefore be on gas form. After passing a heat exchanger, the temperature is lowered to around 80 ℃, making the distillate a liquid. If the proposed reaction mechanism is correct, ionisation is necessary for the reaction, and ions will be stabilised in a liquid aqueous environment. Therefore, it may be that the fouling formation can first initiate after passing through the heat exchanger, and this could explain why the first place fouling is encountered, is in the air cooler after the heat exchanger. From here, the fouling is found in two heat exchangers, a separator, a boiler, and a stripper column. It is likely that most of the fouling is formed quickly after the first heat exchanger and then spreads to the rest of the system from here. To understand why fouling occurs at these specific places, a flow analysis is necessary. It is possible that the deposition is linked to places in the process where the water is either stagnant or where suitable surfaces are available for deposition.

Chapter 13

Conclusion

The fouling encountered at Shell originates from the use of the H_2S scavenger 1,3,5-tri-(2-hydroxyethyl)-hexahydro-s-triazine. Experiments have demonstrated that the precipitate produced in the laboratory from a reaction between the spent scavenger solution from Maersk and H_2S is identical to the fouling found at Shell. The same precipitate has been produced from reactions between the triazine and H_2S/HS^-. During scavenging the triazine is first converted to thiadiazine, and then to dithiazine, where the reaction terminates. The final theoretical compound that may be formed in the scavenging reaction, s-trithiane, is not detected. The rate of precipitation is greatly enhanced by increasing the temperature, and at the boiling point precipitation occurs within minutes.

The fouling is most likely a polymer consisting of dithiazine molecules linked by chains of carbon and sulphur atoms. This is necessary to explain the high carbon and sulphur content, and is also backed by IR analyses, which indicate a ring opening and the presence of different C-S bonds.

The hypothesis of thioformaldehyde being responsible for the polymerisation of the dithiazine molecules does not seem plausible from kinetic considerations. An alternative process may be the formation of thiol compounds from a reaction between MEA and H_2S, which may form disulphide bonds between the molecules. A disulphide compound was detected after reaction between MEA and H_2S, although only in a very low concentration, making this a viable alternative to thioformaldehyde.

By closing the water outlet from the spent scavenger separator during maintenance, and sending both the water and oil phase back to the oil prior to the LP separator, the amount of thiadiazine and dithiazine in the oil will increase with a factor 43, and with a factor 20 for triazine. This will give periodic high concentrations of spent scavenger in the oil, and may result in the fouling problem being linked to specific batches of oil. If the oil to water ratio is optimised in the LP separator at Dan FC, the amount of exported spent scavenger may be halved.

The fouling is very difficult to dissolve, which ensures a rapid precipitation when it is formed. This will also complicate removal of the fouling, since no suitable solvent capable of completely dissolving the fouling has been found. The solvents with the greatest effect on the fouling has HSP values $\delta H = 0\text{-}9$ and $\delta P = 5\text{-}11$. δD was not found to influence the solubility.

Chapter 14

Further work

The experiments made in this project have strongly indicated that the Shell fouling is a polymer, but the exact mechanism leading to the formation of fouling is yet unknown. So far two compounds are suspected of being responsible for the polymerisation: formaldehyde and MEA. To investigate if any of these two compounds may create the fouling, a first approach could be to produce thioformaldehyde and some of the proposed MEA/thiol compounds, and let them react with dithiazine to see if the fouling may be produced from either pathway. In the MS experiments, peaks at 86.6 and 120.4 were detected, but not identified. Especially the peak at 86.6 was interesting, since it was the only compound detected with dithiazine in the final reaction mixture, and could therefore very well be linked to the precipiatation. To identify these peaks, a MS MS analysis of the peaks could be made. The resulting fragmentation spectrum could then be used to find the structure of the compounds.

The fouling was found to consist of both volatile and non-volatile matter. To get additional information about the chemistry of the fouling, differential scanning calorimetry could be used to investigate at which temperatures compounds are lost from the fouling.

Another set of experiments should also have a larger focus on how to solve the problem. In chapter 11, suggestions for solutions were given, and further experiments could be based on these. First of all it would be necessary to develop a method for measuring the concentration of spent scavenger in the crude oil. Two possible solutions could be to use Raman spectroscopy, where the concentration dependency is found with the use of chemometrics, or to extract scavenger products into an aqueous phase, which is then analysed with an LC ESI-MS. For the latter a sampling procedure must be developed. Such a method of analysis could be used to investigate if the build-up of fouling is linked to the concentration of spent scavenger in the oil. It would be most interesting, if a lower limit for spent scavenger concentration that leads to fouling deposition could be found. It could be that at sufficiently low concentrations, the amount of fouling created would not be sufficient to deposit in the system.

Finally, a cost benefit study comparing the triazine method with alternative amine solutions could be made to evaluate at which point a change of method would be beneficial.

Appendices

Appendix A

X-ray diffraction

In X-ray diffraction, the scattering of X-rays may be used to study the crystallographic structure of solids. X-ray diffraction has been used in two main areas: fingerprint characterization of crystalline materials, and determination of the structure of crystalline materials. Each crystalline solid has a unique characteristic X-ray pattern, which may be used as a fingerprint for its identification. Besides the crystal structure, it is possible with X-ray diffraction experiments to gain information about the average spacing between the crystallographic planes, the orientation of single crystals, and the size, shape and internal stress of small crystalline regions [7].

When X-rays are incident upon a particle, they will be scattered randomly in all directions; however, when incident upon a solid crystalline material, some of these randomly scattered beams may interfere constructively to produce diffracted beams. This can be seen by examining an atomic lattice with light incident on it. In figure A.1 a situation with two planes is illustrated. The light scattered by the second plane will have travelled further than the light scattered by the first plane depending on the distance, d, between the planes. If this extra distance equals an integer number of wavelengths, the two light beams will be in phase, and can interfere constructively. In figure A.1 it is seen that the additional distance travelled by the second light beam is $|AB| + |BC|$. By applying trigonometry, this extra distance may be found from the angle θ and d.

$$\sin(\theta) = \frac{|AB|}{d} \Updownarrow \tag{A.1}$$

$$|AB| = d\sin(\theta) \tag{A.2}$$

And since $|AB| = |BC|$

$$|AB| + |BC| = 2d\sin(\theta) \tag{A.3}$$

This additional distance has to be equal to an integer number of wavelengths for the light beams to be in phase; therefore, we can write

$$n\lambda = 2d\sin(\theta) \tag{A.4}$$

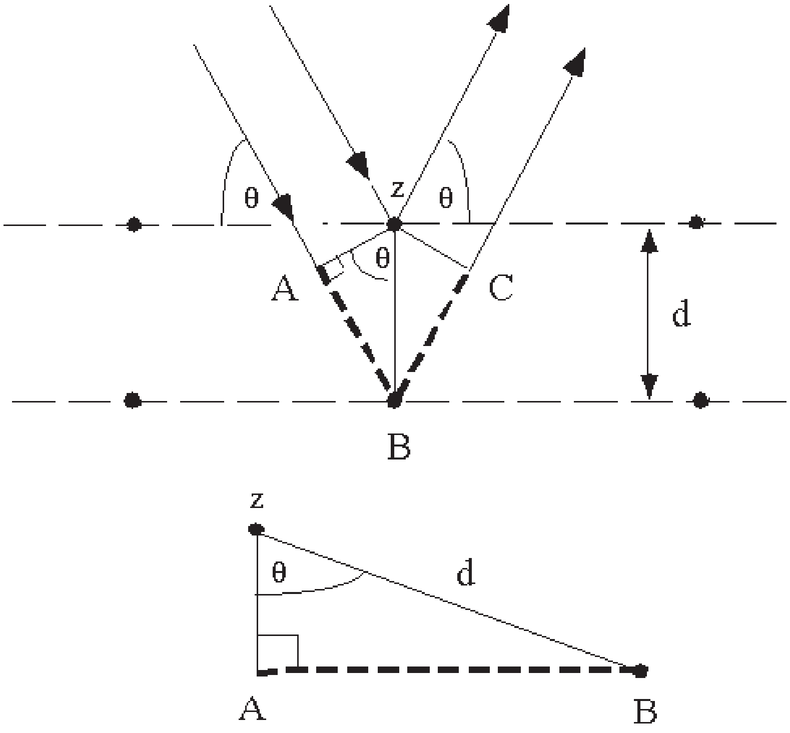

Figure A.1: Diffraction of light leading to constructive interference

Physically, n is the order of diffraction. Equation A.4 is known as Bragg's law, and it describes how an interference pattern from light scattering by particles depends on both the wavelength and the angle with which the light is diffracted. The latter can be seen by realising that 2θ is actually equal to the diffraction angel*, see figure A.1. From Bragg's law it is seen that a particular material containing a number of planes with different d, will give diffraction at several values of θ. The law also predicts several values of θ for each value of d because Bragg's law describes a pure interference spectrum, where diffraction for each value of d is possible at several values of θ of equal intensity. However at diffraction, the intensity of the peaks will decrease with increasing order of diffraction ($|n|$). For pure diffraction, the resulting curve describing the intensity is called an envelope curve, and by multiplying this with the pure interference pattern from Bragg's law, a diffraction pattern is produced where each peak will have smaller neighbouring peaks resulting from higher order of diffraction. In practice, the peaks for higher order diffraction are rarely seen in the spectrum because the intensity is very low in comparison with the peak for zero order diffraction.

If the lattice system of the sample is known, an XRD analysis can be used to find the specific lattice of the sample. This is possible because the interplanar spacing, d, will be related to the lattice vectors (a, b and c) and the Miller indices of the planes depending on the lattice system.

Miller indices are the reciprocal values of a given plane's intersection with the lattice vectors, and are commonly designated h, k and l. Putting these values in round brackets, (hkl), describes a certain plane. A result of this, is that a (hkl) Miller plane will be the first plane from the origin which makes intercepts with the axis at a/h, b/k and c/l. With this information, the interplanar spacing can be found by calculating the distance from the origin to the plane. If we consider a plane that intersects all three lattice vectors, see figure A.2, the distance between two planes, d$_{hkl}$, will be the same as the perpendicular distance from a point in the plane, P, to the origin, O. The line OP will

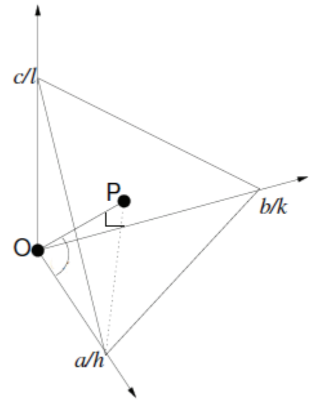

Figure A.2: Distance from origin to Miller plane

form an angle to all three lattice vectors α, β and γ, and by using trigonometry we can write:

$$\cos\alpha = \frac{d_{hkl}}{a/h} = d_{hkl}\frac{h}{a} \tag{A.5}$$

$$\cos\beta = \frac{d_{hkl}}{b/k} = d_{hkl}\frac{k}{b} \tag{A.6}$$

$$\cos\gamma = \frac{d_{hkl}}{c/l} = d_{hkl}\frac{l}{c} \tag{A.7}$$

Because the three lattice vectors for a square lattice are orthogonal we have: $\cos^2\alpha + \cos^2\beta + \cos^2\gamma = 1$. This can be found by applying Pythagoras theorem. By inserting the values for $\cos^2\alpha$, $\cos^2\beta$ and $\cos^2\gamma$ we get:

$$\left(\frac{h}{a}\right)^2 d_{hkl}^2 + \left(\frac{k}{b}\right)^2 d_{hkl}^2 + \left(\frac{l}{c}\right)^2 d_{hkl}^2 = 1 \Updownarrow \tag{A.8}$$

$$\frac{1}{d_{hkl}^2} = \frac{h^2}{a^2} + \frac{k^2}{b^2} + \frac{l^2}{c^2} \tag{A.9}$$

This is the interplanar spacing for an orthorhombic lattice. In table A.1 the interplanar distance for this and three other lattice systems are given. Other lattice systems include trigonal, monoclinic and triclinic. These will have more complicated equations. By knowing the lattice system, the equation for the interplanar distance can be inserted into

Table A.1: Interplanar spacing d_{hkl} for different lattice systems and their dependency on Miller indices hkl. Parameters a, b and c give the length of the crystallographic unit cell, while α, β and γ specify the angels [7].

Lattice system	Constraints	$\frac{1}{d_{hkl}^2} =$
Cubic	$a = b = c$ $\alpha = \beta = \gamma = 90°$	$\frac{h^2+k^2+l^2}{a^2}$
Tetragonal	$a = b$ $\alpha = \beta = \gamma = 90°$	$\frac{h^2+k^2}{a^2} + \frac{l^2}{c^2}$
Orthorhombic	$\alpha = \beta = \gamma = 90°$	$\frac{h^2}{a^2} + \frac{k^2}{b^2} + \frac{l^2}{c^2}$
Hexagonal	$a = b$ $\alpha = \beta = 90°$ $\gamma = 120°$	$\frac{4}{3}\frac{h^2+hk+k^2}{a^2} + \frac{l^2}{c^2}$

the Bragg equation, i.e. if the lattice is cubic, the Bragg equation for the fundamental order of diffraction can be rewritten to:

$$\sin^2\theta = \frac{\lambda^2}{4a^2}(h^2 + k^2 + l^2) \tag{A.10}$$

In determining the crystal lattice, a spectrum is recorded, and the diffraction angle for each peak can be used to calculate $\sin^2\theta$. If the lattice is cubic, these values can then be multiplied with a constant to give nearly integer values for all the $h^2+k^2+l^2$ values. The length of the unit cell, a, can be found from the constant. At this point, it should be noted that the Bragg equation was derived by considering a simple cubic lattice, where there is only one atom per unit cell. However, the majority of solids are found in more complicated lattice structures. The majority of one-elemental metals are for example found in either face-centred cubic (fcc), body-centred cubic (bcc) or hexagonal close-packed (hcp) structure. In these structures, the presences of neighbouring atoms in the unit cell may give rise to destructive interference between some of the scattered X-rays. Therefore, some of the planes will not give a diffraction pattern. These planes can be found by evaluation of the structure factor*of the sample [7]. For fcc structures this means that only planes where all the Miller indices are either odd or even (i.e. 111 or 222) will give diffraction patterns, and for bcc structures, only planes where the sum of the Miller indices give an even number will allow constructive interference. We can therefore say that the Bragg equation is a necessary, but not sufficient condition for X-ray diffraction to occur [7]. By knowing these selection rules, the detected planes can be compared with the planes that can be expected to occur for specific crystal lattices.

A more practical way of using X-ray diffraction as a qualitative technique, is to compare the recorded spectrum with a library of known structures.

Appendix B

IR spectroscopy

In IR spectroscopy, infrared radiation is used to excite molecules into vibrational states of higher energy. The resulting spectrum will indicate which functional groups are present in the molecule, and be a fingerprint for the specific molecule.

In figure B.1 an energy diagram for a diatomic molecule is seen. The curve has the shape of a Lennard-Jones potential, where the equilibrium bond length, R_e, is found at the minimum point. It is clear that the potential is not symmetrical, but as long as we are close to R_e, the potential will resemble a harmonic oscillator, which may therefore be used as a starting point for a discussion about vibrational motion.

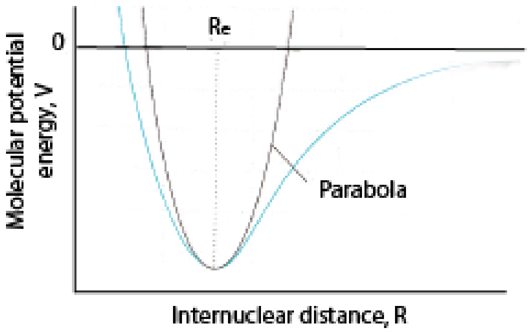

Figure B.1: Molecular potential energy curve approximate with parabola [4]

For a harmonic oscillator, the potential will have the form of a parabola, with the formula indicated in equation B.1.

$$V = \frac{1}{2}kx^2 \quad , \quad x = R - R_e \tag{B.1}$$

Since we are not interested in the absolute potential energy, but rather the change in potential energy, $V(0) = 0$. k is the force constant, giving the stiffness of the bond. With this expression for the potential energy, the Hamiltonian for a harmonic oscillator becomes [4]:

$$H = -\frac{\hbar}{2m}\frac{d^2}{dx^2} + \frac{1}{2}kx^2 \tag{B.2}$$

There is however a complication that needs to be taken into account; namely that the atoms joined in the bond move, which means that m cannot be used as a representation for the mass. Instead, it is necessary to use the effective mass, μ[1].

Therefore, the Hamiltonian is rewritten and m is replaced with μ. Only the relative motion of the two particles are of concern, and the translational term can be neglected, giving a Schrödinger equation, as seen in equation B.7.

$$-\frac{\hbar}{2\mu}\frac{d^2\psi}{dx^2} + \frac{1}{2}kx^2\psi = E\psi \tag{B.7}$$

To solve this Schrödinger equation, creation and annihilation operators, **a** and $\mathbf{a}^{+}$, are used [3], but first some appropriate substitutions is made so that equation B.7 is rewritten.

$$\lambda = \frac{E}{\hbar\omega/2} \quad y = \left(\frac{\mu\omega}{\hbar}\right)^{\frac{1}{2}} \quad \omega = \left(\frac{k}{\mu}\right)^{\frac{1}{2}} \tag{B.8}$$

$$\left(\frac{d^2}{dy^2} - y^2\right)\psi = -\lambda\psi \tag{B.9}$$

The left hand side can be factorised by noticing that:

$$\left(\frac{d}{dy} + y\right)\left(\frac{d}{dy} - y\right)\psi = \left(\frac{d^2}{dy^2} - y^2 - 1\right)\psi \tag{B.10}$$

$$\left(\frac{d}{dy} - y\right)\left(\frac{d}{dy} + y\right)\psi = \left(\frac{d^2}{dy^2} - y^2 + 1\right)\psi \tag{B.11}$$

---

[1] For two particles moving in free space, the Hamiltonian is: $H = -\frac{\hbar}{2m_1}\frac{d^2}{dx_1^2} - \frac{\hbar}{2m_2}\frac{d^2}{dx_2^2}$. It can be shown that this expression can be rewritten to depend on the centre of mass and the effective mass

$$\frac{1}{m_1}\frac{d^2}{dx_1^2} + \frac{1}{m_2}\frac{d^2}{dx_2^2} = \frac{1}{m}\frac{d^2}{dx_{cm}^2} + \frac{1}{\mu}\frac{d^2}{dx^2} \tag{B.3}$$

Where $m = m_1 + m_2$ and $\mu = \frac{m_1 m_2}{m_1 + m_2}$. The Schrödinger equation for this system becomes:

$$-\frac{\hbar}{2m}\frac{d^2}{dx_{cm}^2}\psi_{cm} - \frac{\hbar}{2\mu}\frac{d^2}{dx^2}\psi = E_{total}\psi \tag{B.4}$$

This equation can be separated into two equations, one concerning the motion of the centre of mass, and one for the relative motion of the particles.

$$-\frac{\hbar}{2m}\frac{d^2}{dx_{cm}^2}\psi_{cm} = E_{cm}\psi_{cm} \tag{B.5}$$

$$-\frac{\hbar}{2\mu}\frac{d^2}{dx^2}\psi = E\psi \tag{B.6}$$

With $E_{total} = E_{cm} + E$. We see that the first of these equations describes the translational motion of a free particle, and it can be neglected in the expression for the vibrational energy, since we are only concerned with the relative motion of the particles here [3].

With this in mind the two operators are introduced:

$$\mathbf{a} = \frac{1}{\sqrt{2}}\left(y + \frac{d}{dy}\right) \quad \mathbf{a}^{+} = \frac{1}{\sqrt{2}}\left(y - \frac{d}{dy}\right) \tag{B.12}$$

These two operators can now be used to rewrite equation B.9 to depend on the operators.

$$\left(\frac{d^2}{dy^2} - y^2\right)\psi = -(2\mathbf{a}\mathbf{a}^{+} - 1)\psi = -(2\mathbf{a}^{+}\mathbf{a} + 1)\psi \tag{B.13}$$

This means that the Schrödinger equation may be written in either two forms:

$$\mathbf{a}\mathbf{a}^{+}\psi_\lambda = \tfrac{1}{2}(\lambda + 1)\psi_\lambda \tag{B.14}$$

$$\mathbf{a}^{+}\mathbf{a}\psi_\lambda = \tfrac{1}{2}(\lambda - 1)\psi_\lambda \tag{B.15}$$

By subtracting the two equations from one another, and dividing with the wavefunction corresponding to the energy equivalent to λ, a simple equation arises.

$$\mathbf{a}\mathbf{a}^{+} - \mathbf{a}^{+}\mathbf{a} = 1 \tag{B.16}$$

From this it is seen that $\mathbf{a}$ and $\mathbf{a}^{+}$ commute, $[\mathbf{a}, \mathbf{a}^{+}] = 1$, and this can be used to find the energy levels of the harmonic oscillator. This is done by multiplying equation B.15 with $\mathbf{a}$, and by using that $\mathbf{a}\mathbf{a}^{+} = \mathbf{a}^{+}\mathbf{a} + 1$.

$$\mathbf{a}\mathbf{a}^{+}\mathbf{a}\psi_\lambda = \tfrac{1}{2}(\lambda - 1)\mathbf{a}\psi_\lambda \Updownarrow \tag{B.17}$$

$$(\mathbf{a}^{+}\mathbf{a} + 1)\mathbf{a}\psi_\lambda = \tfrac{1}{2}(\lambda - 1)\mathbf{a}\psi_\lambda \Updownarrow \tag{B.18}$$

$$\mathbf{a}^{+}\mathbf{a}\mathbf{a}\psi_\lambda = \tfrac{1}{2}(\lambda - 1)\mathbf{a}\psi_\lambda - \mathbf{a}\psi_\lambda \Updownarrow \tag{B.19}$$

$$\mathbf{a}^{+}\mathbf{a}\mathbf{a}\psi_\lambda = \tfrac{1}{2}(\lambda - 3)\mathbf{a}\psi_\lambda \tag{B.20}$$

Then by comparing with equation B.15, which states that $\mathbf{a}^{+}\mathbf{a}\psi_{\lambda-2} = \frac{1}{2}(\lambda - 3)\psi_{\lambda-2}$, a proportionality is seen

$$\mathbf{a}\psi_\lambda \propto \psi_{\lambda-2} \tag{B.21}$$

From this it is seen that $\mathbf{a}$ indeed is an annihilation operator since when it is used on the wavefunction corresponding to an energy λ, the result is the wavefunction corresponding to an energy state $\lambda - 2$. This means that we step down in energy when applying $\mathbf{a}$ to a wavefunction. Because the energy cannot be negative, a lower limit, λ_{min} must eventually be reached, from where continued application of the annihilation operator will have no effect, meaning that $\mathbf{a}\psi_{\lambda_{min}} = 0$. If the creation operator is applied to this equation we get $\mathbf{a}^{+}\mathbf{a}\psi_{\lambda_{min}} = 0$, and from here the energy levels may be derived, by using that $\mathbf{a}^{+}\mathbf{a}\psi_{\lambda_{min}} = \frac{1}{2}(\lambda_{min} - 1)\psi_{\lambda_{min}}$ [3].

$$0 = \tfrac{1}{2}(\lambda_{min} - 1)\psi_{\lambda_{min}} \Updownarrow \tag{B.22}$$

$$\lambda_{min} = 1 \tag{B.23}$$

It is seen that the minimum value of λ is 1, and it follows from here that the allowed values are 1, 3, 5, ..., or $\lambda = 2\upsilon + 1$ with $\upsilon = 0, 1, 2, \ldots$. From this it may be concluded that the allowed energies are:

$$E = \frac{2\upsilon + 1}{\hbar\omega/2} = (\upsilon + \tfrac{1}{2})\hbar\omega \quad \upsilon = 0, 1, 2, \ldots \tag{B.24}$$

A more practical expression can be obtained by converting the frequency ω to wavenumbers, since this is the unit often used in infrared spectroscopy.

$$E_\nu = (\upsilon + \tfrac{1}{2})\hbar c\tilde{\nu} \tag{B.25}$$

Earlier it was assumed that the potential energy could be represented as a parabola; however, when the vibrations bring the molecules sufficiently far from each other, the vibrations will not be harmonic, but anharmonic due to the shape of the potential energy well. One approximation that accounts for this behaviour is the use of a Morse potential, and by solving the Schrödinger equation when this potential is used, energy levels that better fit experimental values are achieved.

$$V(x) = hcD_e\left(1 - e^{-ax}\right)^2 \quad , \quad a = \left(\frac{k}{2hcD_e}\right)^{\frac{1}{2}} \qquad \text{Morse potential} \tag{B.26}$$

$$E_\nu = (\upsilon + \tfrac{1}{2})\hbar\omega - (\upsilon + \tfrac{1}{2})^2\hbar\omega x_e \quad , \quad x_e = \frac{a^2\hbar}{2\mu} \tag{B.27}$$

D_e is the depth of the minimum of the curve and x_e is called the anharmonicity constant. As υ becomes large, the Morse potential subtracts from the harmonic expression, which results in decreasing difference in energy between the levels. A feature of this, is that there will be and upper level for the excited states. The Morse potential is still only an approximation, and a better approximation can be achieved by letting the equation for the energy levels consist of an expanding series of anharmonicity constants, where the next term will be raised to the power of three and so on [3].

A molecule consisting of N atoms has 3N degrees of freedom since each atom may move along any of the three perpendicular axes. In three of these modes the atoms move in the same direction, so their relative distance to each other remains unchanged, and only the centre of mass is moving. This molecular translational motion does not relate to vibrational motion, and the three modes can therefore be subtracted from the total degrees of freedom. Furthermore, to describe the orientation of a non-linear molecule in a three dimensional space, three angles are necessary. As a result, three additional degrees of freedom describe rotation of the molecule along one of the axis; hereby changing the spatial orientation of the molecule, but not the relative distance between the atoms. Therefore, we may also subtract these degrees of freedom from the total, leaving 3N - 6 degrees of freedom for a non-linear molecule, which are the fundamental vibrational modes. For a linear molecule, like carbon dioxide, only two angles are needed, which gives a total of 3N - 5 fundamental vibrational modes [4]. However, not all of these modes may actually vibrate. Some may be infrared inactive due to selection rules for vibrational transitions. These can be deduced from the transition dipole moment.

In infrared spectroscopy the excitation energy is not large enough to promote changes in the electronic state; therefore, the transition dipole moment for $\upsilon' \leftarrow \upsilon$ may be written as $\langle \epsilon, \upsilon' | \boldsymbol{\mu} | \epsilon, \upsilon \rangle$. By using the Born-Oppenheimer approximation, we can separate electronic and nucleic motion, and write $\boldsymbol{\mu}_{\upsilon'\upsilon} = \langle \upsilon' | \boldsymbol{\mu} | \upsilon \rangle$. The charge distribution, and therefore the dipole moment, in a molecule depends on the internuclear distance, and it can be expressed as a Taylor series:

$$\boldsymbol{\mu} = \boldsymbol{\mu}_0 + \left(\frac{d\boldsymbol{\mu}}{dx}\right)_0 x + \frac{1}{2}\left(\frac{d^2\boldsymbol{\mu}}{dx^2}\right)_0 x^2 + \cdots \tag{B.28}$$

Where $\boldsymbol{\mu}_0$ is the dipole moment of the molecule for zero displacement. Applying this to the transition dipole moment we get:

$$\langle \upsilon' | \boldsymbol{\mu} | \upsilon \rangle = \boldsymbol{\mu}_0 \langle \upsilon' | \upsilon \rangle + \left(\frac{d\boldsymbol{\mu}}{dx}\right)_0 \langle \upsilon' | x | \upsilon \rangle + \frac{1}{2}\left(\frac{d^2\boldsymbol{\mu}}{dx^2}\right)_0 \langle \upsilon' | x^2 | \upsilon \rangle + \cdots \tag{B.29}$$

Because the states υ' and υ correspond to two different energy states $\upsilon' \neq \upsilon$, and because these states may be described with Hermite polynomials when the potential well is approximated to a harmonic oscillator, the states are orthogonal and therefore $\langle \upsilon' | \upsilon \rangle = 0$. With this, the Taylor series simplifies to:

$$= \left(\frac{d\boldsymbol{\mu}}{dx}\right)_0 \langle \upsilon' | x | \upsilon \rangle + \frac{1}{2}\left(\frac{d^2\boldsymbol{\mu}}{dx^2}\right)_0 \langle \upsilon' | x^2 | \upsilon \rangle + \cdots \tag{B.30}$$

We can draw a very important conclusion from this derivation; namely that the transition matrix is non-zero only when the dipole moment changes with displacement. The reason for this is that when electromagnetic radiation is incident on a molecule, it must interact with the molecule to promote a transition. When it does this, it will affect the electromagnetic field of the molecule, hereby creating a transition dipole moment. From this we have that the gross selection rule*for vibrational spectra is:

> *The electric dipole moment of a molecule must change during displacement of nuclei to show a vibrational spectrum.*

This means that homonuclear diatomic molecules, like H_2 and N_2 become infrared inactive, because the electron density is evenly distributed on both atoms, and a vibrational motion will not create a dipole moment. Heteronuclear diatomic molecules, like HCl and CO, which have a dipole moment that changes during a vibration, will be infrared active. By following this analogy, polyatomic molecules may also have specific vibrational modes that are infrared inactive, because the vibration causes no change in the dipole moment [3]. An example of this is the symmetrical vibration of CO_2 where the bonds to the two oxygen atoms contract and lengthen. It can be shown that the specific selection rule*is:

$$\Delta \upsilon = \pm 1 \tag{B.31}$$

At room temperature, most molecules will be in their ground state initially, and the most important transition therefore becomes $\upsilon = 0 \rightarrow \upsilon = 1$ [25].

The vibrational modes of molecules may be divided in two main groups, with several subgroups associated: stretching and bending/deformation motion. Stretching vibration are more energy demanding compared to bending, because of the attractive forces between the two nuclei and their electrons, and these vibrational modes will be found at higher wavenumbers in the vibrational spectrum. However, stretching motion for one group, i.e. C-S, may be lower in energy than bending motion for another group, i.e. C-H. This is because, the frequency required to promote a transition decreases when the mass of the atoms increase. Likewise, the frequency will increase when the stiffness of the bond, k, increases. Stretching motion can be described as being either symmetric or antisymmetic, and bending motion can be described as scissoring, rocking, twisting, or wagging [25]. The vibrational modes can be seen in figure B.2.

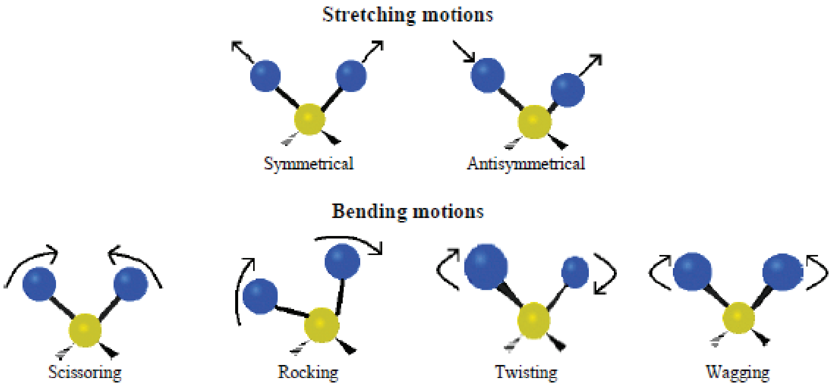

Figure B.2: Vibrational motions

The dependency on the atoms in the bond makes the absorption peaks very specific for different functional groups. Some functional groups may absorb in the same IR region, but because of the different vibrational modes, each functional group may have several peaks in a spectrum and by comparing all peaks, functional groups can be differentiated. The assignment of peaks in a spectrum to specific functional groups are especially useful at wavenumbers above 1350 cm^{-1}.[2] In this region the vibrational modes of a functional group can be regarded as being independent of the remaining part of the molecule. The region below, 1350 cm^{-1}, is called the fingerprint region. Here it is more difficult to assign specific peaks to certain functional groups because the vibrational modes should be view as a whole-molecule vibration. It is not impossible to assign peaks to functional groups, but care must be taken. On the other hand, this offers an incredible useful feature for identification of unknown substances since the region will be very specific for a particular molecule; hence the name fingerprint region. Of course this requires a library, where the collected spectrum can be compared with existing spectra of known compounds.

The intensity of a peak depends on the magnitude of the transition dipole moment; the larger the transition dipole moment, the more intense the peak will be. The intensity

---

[2] This is not a fixed value.

of a peak also increases with the number of times the functional group is present in the molecule [25].

ATR-FTIR

The instrument used to obtain the infrared spectra in this project is an Attenuated Total Reflection Fourier Transform Infrared (ATR-FTIR) spectrometer. In an ATR module, an infrared beam is directed at a crystal with a high refractive index, at such an angle that it causes total reflexion internally in the crystal, as described by Snell's law. The crystal is in contact with the sample and, the principle is then to measure how much of the light is absorbed by the sample. When the infrared light is reflected in the crystal, an evanescent wave that extends beyond the crystal is formed. It is this wave that interacts with the sample, but because the wave only protrudes a very short distance (0.5 - 5 μm) beyond the crystal, this technique requires very good contact between sample and crystal. In figure B.3 an illustration explaining the technique can be seen. Another restriction to the use of ATR is that the sample must have a refractive index significantly lower than the crystal, otherwise total reflection will not take place. As seen in figure B.3, multiple reflections occur in the crystal. Because scattering will happen for each reflection, the light absorbance cannot be used for quantitative measurements. The advantage of multiple reflections is that the observed absorbance will become stronger due to the multiple points where the radiation and sample can interact [10].

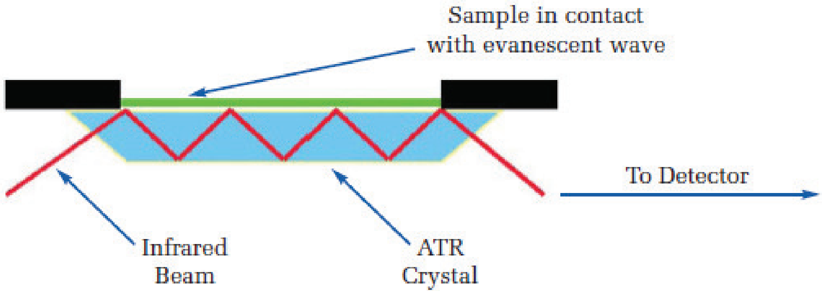

Figure B.3: Principle behind ATR [10]

After an IR spectrum has been collected with an ATR module, the spectrum has to be post processed with ATR correction. The reason for this is that the depth of penetration of the radiation depends on the wavelength.

$$d = \frac{\lambda}{2\pi\sqrt{n_1^2 sin(\theta)^2 - n_2^2}} \tag{B.32}$$

Where n_1 and n_2 are the refractive indexes of the crystal and the sample, θ is the angle of the incoming radiation, and λ is the wavelength of the radiation. Radiation of lower wavelengths, higher wavenumbers, will penetrate the sample to a less extent compared to less energetic radiation.

Appendix C

Electrospray ionisation mass spectrometry

A mass spectrometer is a device capable of measuring masses of atoms and molecules or fragments of molecules, which means it can be used to study the composition of the reaction mixture during the scavenging process. To obtain a spectrum, the species are ionised and then separated according to their mass to charge ratio, m/z. An ion with a +2 charge will as such have a m/z value equal to half the mass of the ion.

There are generally two ways of performing the ionisation: electron ionisation and chemical ionisation. Electron ionisation charges the species by bombarding them with electrons that have been accelerated through an electric field. Because the energy of the electrons is greater than the energy in the molecular bonds, electrons will be removed from the molecule, leaving it in an unstable state from where it breaks into fragments. By analysing the fragments, the nature of the molecule can be determined.

Chemical ionisation is a milder ionisation technique. Here chemical species such as CH_4 or NH_3 are converted into strong proton donors by electron bombardment.

$$\mathrm{CH_4 + e^- \rightarrow CH_4^{+\bullet} + 2e^-} \tag{C.1}$$

$$\mathrm{CH_4^{+\bullet} + CH_4 \rightarrow CH_5^+ + CH_3^\bullet} \tag{C.2}$$

$$\mathrm{CH_4^{+\bullet} \rightarrow CH_3^+ + H^\bullet} \tag{C.3}$$

$$\mathrm{CH_3^+ + CH_4 \rightarrow C_2H_5^+ + H_2} \tag{C.4}$$

These positively charged species can then protonate the analyte without extensive fragmentation.

At the detector, the ions and fragments are converted into an electric signal, which the computer then usually depicts as a bar diagram with the m/z ratio along the abscissa and the intensity along the ordinate. This is the mass spectrum. In a mass spectrum for an electronic ionisation, the molecular ion, $M^{+\bullet}$, will be the ion with the highest m/z ratio, while for chemical ionisation it will be the protonated molecular ion, MH^+. The peaks with lower m/z ratios represent fragments of the molecular ion, and these will be found at distances relative to the molecular ion equal to probable mass losses. Examples are 15 (CH_3), 17 (NH_3 or OH), 18 (H_2O), 29 (C_2H_5) and 31 (OCH_3) [13].

Because ESI-MS is used in this project, minimum fragmentation is expected, and we will not look further into the interpretation of the fragmentation pattern. Instead we look at the molecular ion itself since this may also yield significant information about the structure of the ion.

The m/z value of the molecular ion shows whether the compound contains an even or odd number of nitrogen atoms. If a compound has an odd number of nitrogen atoms (1, 3, 5 $\cdots$), in addition to any number of C, H, halogens, O, S, Si and P atoms, then the nominal mass will also be odd. A compound with an even nominal mass will have an even number of nitrogen atoms (0, 2, 4 $\cdots$). This is called the nitrogen rule [13] Giving the fact that the scavenging reaction is a substitution of nitrogen atoms with sulphur atoms, this is very useful information.

Next to the molecular ion peak one or two smaller peaks will often be present. These are the result of heavier isotopes, i.e. for carbon 98.93 % of all carbon atoms are ^{12}C and 1.07 % are ^{13}C. Because of the distribution of isotopes, the intensity of the M+1 and M+2 peaks will be equal to a certain percentage of the molecular ion peak. Because of uncertainties and variations in the isotope distribution, a deviation between theoretical and experimentally found value of 10 % is accepted. In this way the intensity of the M+1 and M+2 peaks relative to the M peak can be used to check whether a given molecular formula fit the peaks [13].

Table C.1: Isotopes of selected elements [13]

Element	Mass number	Mass (Da)	Abundance (atom%)
H	1	1.007825	99.988
	2	2.01410	0.012
C	12	12	98.93
	13	13.00335	1.07
N	14	14.00307	99.632
	15	15.00011	0.368
O	16	15.99491	99.757
	17	16.99913	0.038
	18	17.99916	0.205
S	32	31.97207	94.93
	33	32.97146	0.76
	34	33.96787	4.29

The specific instrument used in this project is an electrospray ionisation mass spectrometer (ESI-MS). This type of mass spectrometer is often used in combination with liquid chromatography (LC), where the LC can be used to separate and quantify compounds, before they are characterised with the mass spectrometer. Chromatography is a high pressure technique producing huge amount of sample, while mass spectrometers operate in high vacuum. ESI is particular useful in this respect because of its ability to reduce the amount of sample, by removing solvent, so that analyte ions in vacuum are produced. An ESI-MS consists of three main parts.

1. Spray chamber
2. Glass capillary, skimmers, octopoles and lenses
3. Ion trap

These are designed to extract or produce ions from the solution, transport then from atmospheric pressure to vacuum, and then detect and measure amounts of specific m/z ratios. In general this process can be broken into four steps:

1. Ion formation
2. Nebulisation
3. Desolvation
4. Ion evaporation

In the ESI-MS, species are turned into either positively or negatively charged ions; however, by selecting prober solvents and buffer systems, ions may be produced prior to injection, and this may enhance the sensitivity of the MS. However, preformed ions are not a prerequisite for ESI-MS, the instrument will create ions on its own.

Nebulisation takes place in the spray chamber, and is a process where the sample solution is converted into a stream of aerosols. The sample solution enters the spray chamber through a very small grounded needle. Around this needle is placed a concentric tube where nebulising gas enters the spray chamber. The gas will affect the sample solution via shear forces, and in this way ease droplet formation. For positive ion mass spectrometry, the spray chamber is held at a negative potential relative to the needle. This creates a strong electric field, which attracts ions of one polarity to the surface of the droplets, turning the sample solution into a fine mist of charged aerosols; hence the name electrospray. Because the nebulisation occurs without heating, thermal decomposition is minimised ensuring that only very little fragmentation takes place.

To analyse the ions with the MS, it is necessary to remove solvent completely. This is down by introducing a counter flow of heated drying gas, which will cause evaporation of the solvent. Although the drying gas is heated, the energy is used to evaporate solvent, and the analyte will as such not be subject to a temperature increase. As solvent evaporates, the diameter of the aerosols decreases, which brings the charged species on the surface of the droplets closer together. This creates a Coulombic repulsion, and when the force of repulsion equals the surface tension of the droplet, known as the Rayleigh limit, the droplet will undergo a Coulomb explosion. This process repeats itself until the charge of the droplet surface reaches a certain limit, $\sim 10^8 \ \frac{V}{cm^3}$. At this point, the electrostatic field created by the ions at the surface will exceed the surface tension of the droplet, and ions are emitted directly from the droplets, ion evaporation. It is obvious that the ion generation can be greatly facilitated by choosing a solvent with low heat capacity, surface tension and dielectric constant. However, for ESI to function properly the solvent must be polar.

Actual instrument

The ESI-MS used in this project is not connected to a LC. Instead a syringe pump is used to transport sample solution into the spray chamber. From the spray chamber, ions are transported by a glass capillary towards the ion trap where analysis takes place. To ensure that only small amounts of sample is introduced into the MS, the capillary is placed at a right angle to the nebuliser spray. Around the entrance of the glass capillary is placed an end plate, which is held at an even more negative potential than the rest of the spray chamber. This attracts ions towards the glass capillary, hereby aiding the ion harvesting.

The drying gas is injected around the glass capillary, and will therefore heat the capillary. There is a small gap between the end plate and the entrance of the glass capillary, which ensures that the droplets encounters the drying gas before entering the capillary. Besides transporting ions from the spray chamber to the MS, the glass capillary also works as an effective barrier separating the atmospheric pressure in the spray chamber and the vacuum in the MS. The pressure difference will push the ions through the capillary once they have been attracted towards the entrance by the electrostatic potential.

After the capillary, skimmers that remove the bulk of the drying gas are placed. Behind the skimmers two octopoles are placed. These focuses and transports the ions to the focusing/exit lenses, which couples the focus and transport region to the ion trap, but they are also used to allow and block ions from the ion trap. This is done by controlling the electrostatic potential of the skimmers. When the trap is being filled, the skimmers are held at a potential, which will allow the ions to migrate towards the trap, and when filled, the potential shifts so that ions are repelled and hereby kept from entering the trap. The transport is carried out by creating a pressure gradient through the MS with four pumps. The pressure behind the glass capillary is approximately 1-2 mbar, and between the skimmers the pressure drops to 0.15 mbar. Between the second skimmer and the inlet to the ion trap the pressure is $1.6 \cdot 10^{-3}$ mbar, and in the final chamber surrounding the ion trap the pressure is held at $5.6 \cdot 10^{-5}$ mbar. The final part of the MS system is the ion trap and detector.

The trap consists of a ring electrode and two end caps. A constant frequency radio-frequency voltage is applied to the ring electrode, and this will send the ions into a stable trajectory in the trap. The stability of the trajectory depends on the amplitude of the ring electrode voltage, and by varying the amplitude, ions with specific m/z ratios will be brought into an unstable trajectory and be expelled from the trap. The ions are then focused onto a dynode, which creates a cascade of electrons that are measured, and gives the intensity of a certain m/z ratio. To increase the sensitivity of the ion trap, it is filled with helium prior to ion injection. The helium will lower the kinetic energy of the ions through collisions, which will ensure that more ions obtain a stable orbit in the trap. In comparison to a quadrupole MS, the ion trap will analyse the sample in batches instead of continuously, and during a scan the trap will therefore continuously fill and empty, making the final spectrum an average of the spectra for each entrapment. In figure C.1 an overview of the instrument is shown with all the discussed parts.

During operation the MS is set up with the parameters given in table C.2.

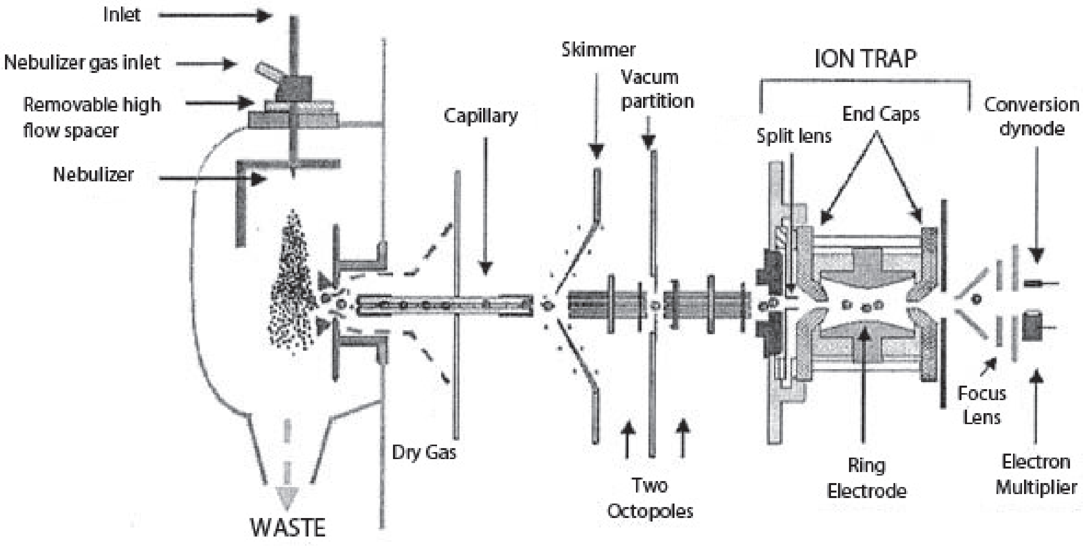

Figure C.1: ESI-MS [31]

Table C.2: ESI-MS set up

Parameter		Parameter	
Mass range mode	Std/normal	Skimmer	40.0 V
Ion polarity	Positive	Oct 1 DC	12.00 V
Ion source type	ESI	Oct 2 DC	1.70 V
Dry gas temperature	325 ℃	Scan begin	50 m/z
Nebulizer	15 psi	Scan end	2200 m/z
Dry gas flow	5.00 l/min	Averages	7 spectra
Trap drive	45.8	Max accu time	20000 μs
Octopole RF amplitude	135.6 Vpp	ICC target	-1
Capillary exit	107.4 V	Charge control	on

Appendix D

HSP

HSP is short for Hansen's Solubility Parameters, and is one of several methods for determining the solubility of a given solute in one or more solvents. For a solvent to dissolve a compound, the solvent must overcome the cohesive forces of the compound, and as a result, solubility parameters are also often called cohesion energy parameters. Cohesive forces are the forces between molecules, which hold a liquid together, and because of this, the magnitude of these forces can be measured as the energy required to bring the molecules from liquid to gas form; energy of evaporation. This approach also forms the basis of the fundamental definition of solubility parameters as given by Hildebrand. The Hildebrand solubility parameter is defined as the square root of the cohesive energy density [12].

$$\delta = \sqrt{\frac{E}{V}} \tag{D.1}$$

Where E is the measurable total energy of vaporization, and V is the molar volume of the pure solvent.

This solubility parameter can be used in a theoretical description of a mixing process. Thermodynamically, mixing of a system will occur if the free energy of mixing is zero or negative as given by equation D.2 [12].

$$\Delta G^M = \Delta H^M - T\Delta S^M \tag{D.2}$$

If only the non-combinatorial[1] Gibbs energy is considered, then it can be calculated from the solubility parameter of the solvent and solute [12].

$$\Delta G^M_{noncomb} = \phi_1 \phi_2 V_M (\delta_1 - \delta_2)^2 \tag{D.3}$$

Where ϕ_1 and ϕ_2 are the volumes fractions of the solvent and solute. Equation D.3 shows that the when the solvent and solute have identical solubility parameters, ΔG^M is zero. This can be used to predict the maximum difference in solubility parameters for dissolution to occur. Since mixing always results in an increase in entropy, the TΔS

---

[1] Without entropy effects

term will contribute negatively to the total free energy. As the difference in solubility parameters between solvent and solute increase, the non-combinatorial Gibbs energy will become increasingly positive. The limit for solubility can therefore be seen as the point where the difference in solubility parameters cancels the increase in entropy [12].

$$\Delta G^{M}_{noncomb} = T\Delta S^{M}_{comb} \tag{D.4}$$

However, the use of the Hildebrand solubility parameter is limited since it is defined for regular solutions, where only dispersion forces hold the molecules together. In most cases there will also be contributions from two other intermolecular forces, dipole dipole forces and hydrogen bonding.

Dispersion forces are atomic forces occurring for all molecules. They occur because the electron distribution in a molecule is determined by probabilities, and therefore at a given moment the electron distribution in a molecule may be skewed. This gives the molecule a momentary dipole, which may induce a dipole in a neighbouring molecules and so on, hereby creating attraction between the molecules. The size of the dispersion forces depends on the size and geometry of the molecule. The more electrons available for displacement in the molecule, the more effective the induced dipoles. Furthermore, dispersion forces are very short ranged and decay with the distance between molecules to the power of six ($\Delta E = \frac{1}{r^6}$). Molecules with a large contact surface, such as straight chained hydrocarbons, therefore have more efficient dispersion forces than molecules with a low contact surface, such as branched hydrocarbon chains.

Dipole dipole forces are also present in most molecules. They occur because of permanent dipoles in the molecule, according to which the molecules in the liquid will arrange themselves. The dipoles occur because atoms in the molecular structure have different electron affinities, which will create a shift in the electron distribution. The strength of the dipole depends on the distance between the atoms that create the distortion in the electron distribution, and the difference in electron affinity of the atoms.

Hydrogen bonds are the result of electron exchange processes between small electronegative atoms, mainly oxygen, nitrogen and flour, with a hydrogen atom. The bond exists because the hydrogen atom on one of these atoms will be attracted by lone pairs on adjacent small electronegative atoms. Molecules with hydrogen atoms bonded to these atoms, such as alcohols and amines, can make active hydrogen bonds, whereas molecules with no hydrogen atom, such as ketones and aldehydes, only can make passive hydrogen bonds with other molecules capable of donating a hydrogen atom. Because of the electron/proton exchange, these bonds resembles intramolecular bonds, and are also much more energetic than the two other intermolecular forces. This makes them very important in determining the affinity between solute and solvent.

The difference between the Hildebrand and Hansen solubility parameters, is that in HSP all three of the intermolecular forces are accounted for. Hereby we can write the energy density as consisting of three terms, and see that the squared total solubility parameter (or Hildebrand solubility parameter) may be considered as the sum of the three individual energy contributions [12].

$$E = E_D + E_P + E_H \tag{D.5}$$

$$\frac{E}{V} = \frac{E_D}{V} + \frac{E_P}{V} + \frac{E_H}{V} \tag{D.6}$$

$$\delta^2 = \delta_D^2 + \delta_P^2 + \delta_H^2 \tag{D.7}$$

A fourth factor that will influence the affinity between solvent and solute is the size of the molecule, expressed by the molar volume. It has been found that smaller molecules such as acetone and methanol tend to be more readily soluble, and will show improved abilities as solvents compared to larger molecules with similar solubility parameters. The size of molecules is also important for permeation and diffusion, which may also affect the solubility ability of a given molecule, since molecules, which move more easily and which are better for penetrating the structure of the solute, will be better solvents. Thermodynamically, a small molar volume will favour lower ΔG^M, explaining the improved solubility abilities. As a result, molecules with small molar volumes may incorrectly appear as being outliers in a HSP analysis [12].

To estimate the affinity between a solvent and a solute the RED number can be calculated.

$$RED = \frac{R_A}{R_0} \tag{D.8}$$

Here R_0 is the radius of the solubility sphere for the solute, and R_A is the solubility parameter distance developed by Skaarup.

$$R_A^2 = 4(\delta_{D2} - \delta_{D1})^2 + 4(\delta_{P2} - \delta_{P1})^2 + 4(\delta_{H2} - \delta_{H1})^2 \tag{D.9}$$

This equation has been developed from experimental data, where the solubility data has been plotted to give a sphere encompassing the solvents capable of dissolving the solute, see more of this further down. The constant, 4, is a result of wanting a sphere rather than a spheroidal. To achieve this, it is necessary to double the scale of the dispersion forces compared to the two other parameters. In this way, the constant represents the difference between the atomic forces (dispersion) and the molecular forces (dipole dipole and H-bonding). A RED number of 0 is equal to identical solubility parameters between solvent and solute. Numbers below 1 indicates high affinity, while solvents with numbers close to 1 are close to the solubility boundary [12].

There are several methods that can be used to determine the solubility parameters of a molecule, both empirical and theoretical. One theoretical method is the group contribution method. This can be used when the structure of the molecule is known. Here table values of the solubility parameters of the functional groups of the molecule are used to calculate the total solubility parameters. The general idea behind the method is that the properties, F, of a molecule can be estimated by addition of contributions from each group [12].

$$F = \sum_i n_i F_i \tag{D.10}$$

As an example, a propane molecule will in this case consist of two methyl groups and one methylene group. The method employed by Hansen, determines the dispersion and dipole forces along with the total cohesive energy of the liquid. The dispersion forces can be determined from knowledge of the molar volume and critical temperature. The critical temperature can be used to calculate the relative temperature and from plots of the relative temperature and the molar volume, the dispersion energy can be read. It is necessary to distinguish between, straight chained, cyclic and aromatic compounds. Furthermore, since the dispersion forces depends on the number of electrons, compounds which consist of heavy atoms like chlorine, bromine and sulphur demand the use of a correction factor. The polar forces can be estimated by equation D.11.

$$\delta_P = 37.4 \frac{DM}{\sqrt{V}} \tag{D.11}$$

Where DM is the dipole moment and V the molar volume. Finally, with knowledge of the dispersion and dipole forces, the hydrogen bonding forces can be estimated by subtracting the other two parameters from the total cohesive energy. Should any of these parameters be difficult to determine, e.g. difficulties in determining the dipole moment of the molecule, then the group contribution method can be used [12].

The solubility parameters for a given solute can also be determined experimentally by dissolving the solute in several solvents with known HSP values. From visual observations the degree of solubility can then be determined by noting which solvents are capable of dissolving the solute completely, which solvents that only interacts with the solute and which of the solvents in which the solute in insoluble. By plotting the results in a coordinate system with the three intermolecular forces as the axes, a sphere can be constructed so that it encompasses all the solvents where the solute is completely dissolved, and with the solvents causing interaction laying at the edge of the sphere. The centre of the sphere will then represent the solubility parameters of the solute, and the radius will be R_0 used in calculations of the RED number.

$$R_0^2 = (\delta_D - \delta_{D(solute)})^2 + (\delta_P - \delta_{P(solute)})^2 + (\delta_H - \delta_{H(solute)})^2 \tag{D.12}$$

A general weakness of this method is that it is the solvents that causes the least solubility (interaction) that are used to determine the solubility parameters of the solute, instead of the solvents which are capable of completely dissolving the solute [12].

Appendix E

Density of hydroxyethyl-triazine solution

The density of the hydroxyethyl-triazine solution is found by weighing the mass of three 10 ml volumetric flasks filled with triazine. In table E.1 the results are found.

Table E.1: Density of hydroxyethyl-triazine solution

Nr	$m_{flask}(g)$	$m_{flask+triazine}$ (g)	Diff (g)
1	12.6015	23.6921	11.0906
2	12.6295	23.6759	11.0464
3	12.6320	23.7107	11.0787
Average			11.0719 g
Density			1.1072 g/ml

Appendix F

Mass lists for MS spectra

This appendix contains the mass lists for the MS spectra presented in the report. They are divided into the experiments in which they occur.

MS spectra of basis chamicals

Table F.1: Mass list for spent scavenger with and without 1 M NaCl

	Spent scavenger		+ 1 M NaCl	
m/z	Intensity	I %	Intensity	I %
62.8	30447	9.6	99747	9.9
74.7	35006	11.0	56881	5.6
86.6	193051	60.7	255540	25.3
88.6	43940	13.8	67828	6.7
120.4	264882	83.3	455382	45.0
121.3	14844	4.7	27078	2.7
122.4	26533	8.3	46349	4.6
166.2	254135	79.9	244303	24.2
167.2	18848	5.9	-	-
168.2	23820	7.5	-	-
188.2	11946	3.8	339537	33.6
189.2	-	-	30576	3.0
190.2	-	-	29875	3.0
193.2	318158	100.0	582534	57.6
194.2	29909	9.4	51103	5.1
195.2	16268	5.1	35490	3.5
215.2	16144	5.1	1011076	100.0
216.2	-	-	78983	7.8
217.2	-	-	62545	6.2
218.3	77525	24.4	106332	10.5
236.2	-	-	158286	15.7
237.2	-	-	46066	4.6
242.3	-	-	287408	28.4
244.3	49967	15.7	42664	4.2
317.3	84384	26.5	75595	7.5

Table F.2: Mass list for pure hydroxyethyl-triazine

m/z	Intensity	Intensity %
62.8	22056	45.9
115.3	4781	10.0
117.3	4380	9.1
118.4	48042	100.0
133.3	4354	9.1
135.2	6078	12.7
151.3	5961	12.4
156.2	5120	10.7
171.1	4533	9.4
173.2	3945	8.2
175.2	4655	9.7
177.2	4616	9.6
201.2	4579	9.5
203.2	4629	9.6
218.2	3886	8.1
219.2	5613	11.7
257.3	7578	15.8
279.2	7212	15.0
285.3	4364	9.1
317.3	4484	9.3
331.3	4846	10.1
344.4	4142	8.6
365.3	4271	8.9
381.2	5183	10.8
391.3	7709	16.0
404.3	3958	8.2
409.3	3909	8.1
424.3	10356	21.6
425.2	4206	8.8
452.3	5349	11.1

Table F.3: Mass list for MEA with and without 1 M NaCl

MEA			MEA + 1 M NaCl		
m/z	Intensity	I %	m/z	Intensity	I %
62.8	154013	55.9	81.5	355289	58.7
133.4	27800	10.1	83.5	112846	18.6
147.3	275713	100.0	129.2	127646	21.1
208.2	68888	25.0	139.2	106273	17.6
218.3	26902	9.8	141.2	591779	97.7
225.2	35002	12.7	197.0	368495	60.9
243.2	38611	14.0	199.0	347925	57.5
245.2	55672	20.2	201.0	123229	20.4
268.2	65001	23.6	254.9	455926	75.3
279.2	23238	8.4	256.9	605451	100.0
284.3	39955	14.5	258.9	306089	50.6
306.2	28563	10.4	261.0	65695	10.9
328.2	23134	8.4	312.9	208135	34.4
344.3	55944	20.3	314.9	395242	65.3
348.2	23634	8.6	316.9	267211	44.1
350.2	21797	7.9	318.9	91413	15.1
374.3	23854	8.7	370.8	284254	46.9
388.4	94939	34.4	372.8	558933	92.3
390.3	25147	9.1	374.8	461930	76.3
392.3	22812	8.3	376.8	183263	30.3
404.3	30779	11.2	428.8	197324	32.6
424.3	34309	12.4	430.8	480469	79.4
432.4	121783	44.2	432.8	491834	81.2
433.4	32843	11.9	434.8	266930	44.1
434.2	25228	9.2	436.8	77620	12.8
452.3	24270	8.8	486.8	76061	12.6
476.5	100120	36.3	488.8	195413	32.2
477.4	28270	10.3	490.8	245602	40.6
520.5	65343	23.7	492.8	158202	26.1
564.6	31894	11.6	548.8	87559	14.5

MS analysis of reaction system, HS^- ions

Table F.4: Mass lists for first three hours of the scavenging reaction

	Start		1 hour		2 hours		3 hours	
m/z	Intensity	I %	Intensity	I %	Intensity	I %	Intensity	I %
62.8	400196	3.7	38154	4.8	35387	19.8	31409	11.3
74.7	-	-	32135	4.0	17158	9.3	21483	7.7
86.6	-	-	155803	19.5	115546	62.7	152378	54.9
88.6	-	-	42167	5.3	17610	9.6	26418	9.5
120.4	180772	1.7	305170	38.3	108692	59.0	154862	55.8
121.3	-	-	18404	2.3	-	-	-	-
122.4	-	-	31531	4.0	11775	6.4	15442	5.6
166.2	-	-	58482	7.3	118490	64.3	159971	57.6
167.2	-	-	-	-	10116	5.5	11121	4.0
168.2	-	-	-	-	16295	8.8	16593	6.0
182.2	-	-	-	-	30505	16.6	39307	14.2
188.2	-	-	151293	19.0	184181	100.0	277572	100.0
189.2	-	-	15616	2.0	15626	8.5	22419	8.1
190.2	-	-	18347	2.3	19813	10.8	28760	10.4
191.2	-	-	48259	6.1	37495	20.4	30285	10.9
193.2	167907	1.6	394331	49.5	124863	67.8	185750	66.9
194.2	-	-	35315	4.4	14363	7.8	15152	5.5
195.2	-	-	30615	3.8	11649	6.3	13620	4.9
204.2	-	-	71560	9.0	159010	86.3	182868	65.9
205.2	-	-	-	-	15997	8.7	18633	6.7
206.2	-	-	-	-	17734	9.6	20800	7.5
215.2	4127444	38.6	797355	100.0	53353	29.0	106551	38.4
216.2	329588	3.1	69324	8.7	-	-	11305	4.1
217.2	228029	2.1	44769	5.6	-	-	-	-
218.3	1147106	10.7	-	-	-	-	-	-
219.3	155296	1.5	-	-	-	-	-	-
236.2	6335827	59.3	92367	11.6	72349	39.3	78744	28.4
237.2	770355	7.2	35810	4.5	14240	7.7	15267	5.5
238.2	349493	3.3	-	-	-	-	-	-
242.3	10685500	100.0	-	-	-	-	-	-
243.3	1159402	10.9	-	-	-	-	-	-
244.3	109911	1.0	-	-	-	-	-	-
385.1	-	-	-	-	22929	12.4	24478	8.8
449.1	2121862	19.9	-	-	-	-	-	-
450.1	549043	5.1	-	-	-	-	-	-
451.1	236047	2.2	-	-	-	-	-	-
461.3	1593751	14.9	-	-	-	-	-	-
462.3	346750	3.2	-	-	-	-	-	-

Table F.5: Mass list for final part of scavenging reaction

	4 hours		24 hours		72 hours		192 hours	
m/z	Intensity	I %	Intensity	I %	Intensity	I %	Intensity	I %
62.8	21523	6.6	46132	4.5	59718	4.0	116091	6.9
74.7	21335	6.5	23295	2.3	21390	1.4	22215	1.3
86.6	168290	51.3	215243	20.8	153960	10.2	159268	9.5
88.6	21471	6.5	21157	2.0	17699	1.2	12719	0.8
120.4	119909	36.5	69060	6.7	44302	2.9	21841	1.3
121.3	-	-	-	-	-	-	-	-
122.4	11043	3.4	-	-	11775	6.4	-	-
166.2	198252	60.4	457336	44.3	595367	39.5	611876	36.6
167.2	17039	5.2	36908	3.6	47258	3.1	53466	3.2
168.2	22236	6.8	47410	4.6	59514	3.9	54097	3.2
182.2	51073	15.6	43612	4.2	-	-	-	-
188.2	328368	100.0	1033300	100.0	1507858	100.0	1673314	100.0
189.2	25982	7.9	71937	7.0	111347	7.4	114250	6.8
190.2	32457	9.9	104801	10.1	136496	9.1	152466	9.1
191.2	23437	7.1	25798	2.5	12479	0.8	15369	0.9
193.2	136088	41.4	83858	8.1	49234	3.3	25886	1.5
194.2	13507	4.1	-	-	-	-	-	-
195.2	10109	3.1	-	-	-	-	-	-
204.2	209123	63.7	338196	32.7	19951	1.3	-	-
205.2	18483	5.6	32320	3.1	-	-	-	-
206.2	25182	7.7	32063	3.1	-	-	-	-
215.2	62890	19.2	53192	5.1	20174	1.3	-	-
216.2	-	-	-	-	-	-	-	-
217.2	-	-	-	-	-	-	-	-
218.3	-	-	-	-	-	-	-	-
219.3	-	-	-	-	-	-	-	-
236.2	62631	19.1	213626	20.7	219850	14.6	666355	39.8
237.2	11208	3.4	33665	3.3	36913	2.4	87850	5.3
238.2	-	-	-	-	12616	0.8	36422	2.2
242.3	-	-	-	-	-	-	-	-
243.3	-	-	-	-	-	-	-	-
244.3	-	-	-	-	-	-	-	-
385.1	26701	8.1	54490	5.3	-	-	-	-
449.1	-	-	30283	2.9	35965	2.4	227120	13.6
450.1	-	-	-	-	12942	0.9	62737	3.7
451.1	-	-	-	-	-	-	31713	1.9
461.3	-	-	-	-	-	-	-	-
462.3	-	-	-	-	-	-	-	-

Actual scavenging - triazine and H_2S

Table F.6: Mass lists for scavenger solution after reaction with H_2S in the ratios H_2S to scavenger: start, 1:2, 1:1 and 3:2

	Start		Ratio 1:2		Ratio 1:1		Ratio 3:2	
m/z	Intensity	I %	Intensity	I %	Intensity	I %	Intensity	I %
56.9	40598	2.4	53239	5.0	59056	3.0	67485	2.6
74.7	45713	2.7	105296	9.9	163747	8.4	187980	7.3
86.6	12042	0.7	375080	35.4	692503	35.6	883893	34.5
88.6	-	-	114922	10.8	188049	9.7	266490	10.4
120.4	-	-	826450	78.0	1548059	79.5	2054420	80.1
121.3	-	-	50701	4.8	79779	4.1	104447	4.1
122.4	-	-	83680	7.9	148253	7.6	178694	7.0
166.2	-	-	-	-	31591	1.6	40396	1.6
193.2	-	-	1059738	100.0	1947887	100.0	2565634	100.0
194.2	-	-	96072	9.1	188722	9.7	249664	9.7
195.2	-	-	66644	6.3	99078	5.1	136903	5.3
215.2	-	-	160524	15.1	490814	25.2	443967	17.3
216.2	-	-	-	-	53150	2.7	44170	1.7
217.2	-	-	-	-	28651	28651	-	-
218.3	34124	2.0	73820	7.0	108704	5.6	87573	3.4
242.3	968114	57.5	824151	77.8	771549	39.6	256516	10.0
243.3	104738	6.2	79960	7.5	83709	4.3	28096	1.1
244.3	77812	4.6	50886	4.8	30182	1.5	23173	0.9
258.3	123819	7.4	117269	11.1	67193	3.4	38749	1.5
461.3	1684073	100.0	623942	58.9	365625	18.8	67380	2.6
462.3	380942	22.6	137409	13.0	87224	4.5	-	-
463.3	133935	8.0	41802	3.9	-	-	-	-

Table F.7: Mass lists for scavenger solution after reaction with H_2S in the ratios H_2S to scavenger: 2:1, 5:2, 3:1 and 4:1

	Ratio 2:1		Ratio 5:2		Ratio 3:1		Ratio 4:1	
m/z	Intensity	I %	Intensity	I %	Intensity	I %	Intensity	I %
56.9	50071	2.2	-	-	11673	1.4	16755	0.8
74.7	166920	7.4	115348	1.8	43116	5.2	63441	2.9
86.6	786860	35.0	528044	8.4	261813	31.4	544090	25.0
88.6	233819	10.4	97533	1.6	36002	4.3	53167	2.4
120.4	1629562	72.5	677031	10.8	187169	22.4	87504	4.0
121.3	85793	3.8	-	-	9172	1.1	-	-
122.4	162807	7.2	55907	0.9	17956	2.2	-	-
166.2	641284	28.5	1168477	18.6	833763	100.0	2173466	100.0
167.2	47504	2.1	108951	1.7	66246	7.9	158316	7.3
168.2	56082	2.5	130412	2.1	76626	9.2	212223	9.8
188.2	29269	1.3	2025311	32.3	380977	45.7	649356	29.9
189.2	-	-	160434	2.6	26981	3.2	43591	2.0
190.2	-	-	209472	3.3	29964	3.6	55559	2.6
193.2	2248453	100.0	904912	14.4	241033	28.9	91649	4.2
194.2	214075	9.5	84393	1.3	22351	2.7	8778	0.4
195.2	126462	5.6	-	-	14502	1.7	9447	0.4
204.2	-	-	-	-	-	-	17800	0.8
215.2	393880	17.5	6271843	100.0	393725	47.2	37161	1.7
216.2	33753	1.5	559782	8.9	38804	4.7	-	-
217.2	-	-	334135	5.3	20773	2.5	-	-
242.3	172300	7.7	4334507	69.1	195039	23.4	-	-
243.3	-	-	469091	7.5	24613	3.0	-	-
244.3	-	-	49349	0.8	9640	1.2	-	-
258.2	36087	1.6	-	-	-	-	-	-
461.3	53476	1.7	1285867	20.5	33981	4.1	-	-

Spent scavenger reaction with H_2S

Table F.8: Mass list for spent scavenger reaction with H_2S

m/z	Intensity	I %
62.8	34748	2.4
74.7	56802	3.9
86.6	508857	34.8
87.6	23162	1.6
88.6	40906	2.8
120.4	54505	3.7
166.2	1463913	100.0
167.2	105906	7.2
168.2	149831	10.2
182.2	99607	6.8
188.2	154461	10.6
189.2	17201	1.2
190.2	14971	1.0
193.2	58023	4.0
204.2	33559	2.3
243.3	20682	1.4
244.3	52978	3.6
315.3	31183	2.1
317.3	87254	6.0
318.3	18602	1.3
333.3	20686	1.4
360.3	19653	1.3
387.3	15079	1.0
388.4	21668	1.5
389.3	15396	1.1
402.3	16999	1.2
432.4	26095	1.8
476.5	19420	1.3

Effects of heating on spent scavenger

Table F.9: Mass list for spent scavenger after heating

m/z	Intensity	I %
62.8	33394	10.7
74.7	32291	10.3
86.6	144987	46.3
88.6	37035	11.8
120.4	249731	79.7
122.4	25139	8.0
141.3	38752	12.4
152.3	22781	7.3
166.2	194322	62.0
168.2	21642	6.9
193.2	313190	100.0
194.2	31730	10.1
215.2	24965	8.0
244.3	117607	37.6
245.3	21655	6.9
298.3	26640	8.5
304.3	54550	17.4
315.3	24590	7.9
317.3	212149	67.7
318.3	49951	15.9
331.3	57896	18.5
332.3	21970	7.0
333.3	77004	24.6
360.3	60261	19.2
371.3	43728	14.0
387.3	41410	13.2
389.4	21411	6.8
390.4	27716	8.8
444.4	21586	6.9

Appendix G

Characterisation of oil from Maersk

During the investigation of the fouling problem, crude oil from Maersk was characterised with GC-MS and by measuring the sulphur content.

The initial purpose with the GC-MS analysis was to investigate if the spent scavenger products could be detected in the oil; however, due to the low solubility of the scavenger products in oil, and because of the huge dilution of the spent scavenger in the oil, this was not possible. Instead the GC-analyses serve as a description of the composition of the oil.

Since the purpose of the scavenging process is to remove H_2S, and therefore sulphur, from the raw oil, the first approach was to measure the sulphur content of the oil and spent scavenger at different points in the oil processing.

This appendix describes the two experiments and holds the results achieved. In figure G.1, a picture of the samples can be seen, and in figure G.2, the two phase system of the spent scavenger solution can be seen. To ease the referring to the different samples, they have been given tags to identify them. These are found in table G.1.

Figure G.1: Maersk samples

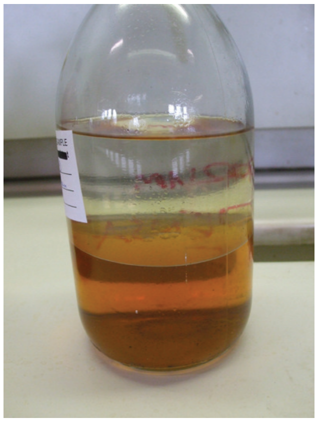

Figure G.2: Spent scavenger solution

Table G.1: Sample tags

Tag	Sample
1	Oil from three phase separator at Dan
2	Oil from three phase separator at Dan
3	Oil from three phase separator at Dan
4	Oil ready to be sent to Shell
5	Spent scavenger oil phase
6	Spent scavenger aqueous phase

Method

GC-MS

The samples were stirred for homogenisation, and then 2 ml was extracted and transferred to 10 ml test tubes. 2 ml of pentane was added to the samples, a lid was put on, and the test tubes were shaken to ensure mixing. For all the oil samples and the oil phase from the spent scavenger solution, the mixing was complete; whereas, the water phase from the spent scavenger gave a two phase system. This was to be expected, but more importantly, the colouring compounds remained in the water phase, see figure G.4. In figure G.3, all the samples can be seen. Each measurement was double determined.

Figure G.3: Pentane treated samples

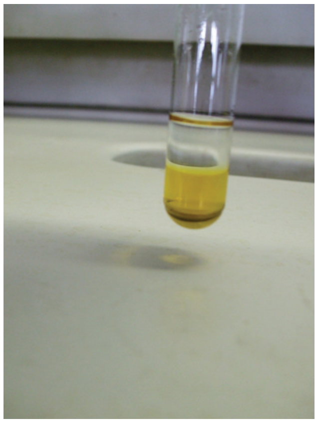

Figure G.4: Spent scavenger water phase mixed with pentane

The pentane phase was transferred with Pasteur pipettes to vials, which were then put in the GC-MS autosampler and analysed.

Sulphur content

To measure the sulfur content of the oil and the spent scavenger aqueous phase, the samples were analysed with ICP AES. To ensure that suitable amounts of oil and water were used in the experiment, three amounts were weighed; 0.5, 1.0 and 1.5 g. With three oil samples from the three phase separator, one from the oil send to Shell, and two samples from the spent scavenger separator, a total of 18 samples were produced. The samples were weighed into 150 ml autoclave bottles, and to open the oil matrix, 20 ml of 7 M HNO_3 was added to the oil. This was done by first adding 10 ml dem. water, and then 10 ml concentrated HNO_3. The bottles were then autoclaved for 30 minutes at 200 kPa and 120 ℃. After autoclaving, the solutions were filtrated to remove the remaining particles. This was done with filtering paper, and the filtrate was collected in 50 ml volumetric flasks, which were then filled up with dem. water.

The ICP AES was calibrated with four standard sulphur solutions with concentrations of 1, 2, 10 and 20 $\frac{mg}{L}$. After calibrations the twelve solutions were placed in the ICP's autosampler and measured.

Results

GC-MS

In figure G.5 a GC spectrum of oil sample 3 can be seen. Because of difficulties with identifying specific hydrocarbons in the GC spectrum, reference analyses have been made on pure C-12, C-15, C-16, C-17, C-18 and C-20. The computer then cross checks with these spectra, and identifies the peaks in the oil spectrum. In our spectrum the C-17 and C-18 peak have been labelled.

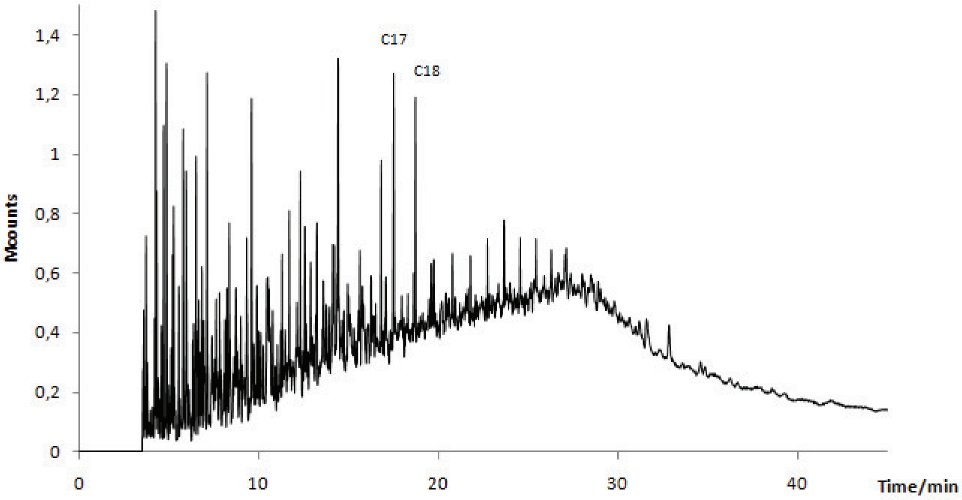

Figure G.5: Oil from three phase separator

Up to C-18, significant amounts of most of the hydrocarbons are found; for the higher mole weight hydrocarbons, the concentrations are lower. The large number of peaks is due to branching of the carbon chains. No peaks for spent scavenger compounds are found.

In figure G.6 a GC spectrum of the oil send to Shell, sample 4, is shown. As expected, the spectrum is very equal to the spectrum of the oil from the three phase separator, and also here no spent scavenger products are detected.

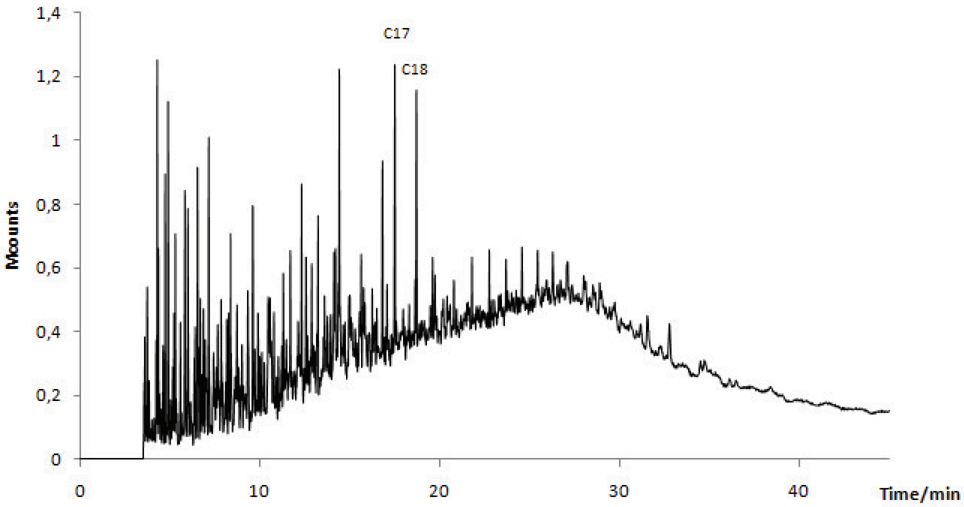

Figure G.6: Oil to Shell

In figure G.7 a GC spectrum of the oil phase from the spent scavenger separator is seen. The spectrum shows that hydrocarbons below C-12 constitute the solution, which is also to be expected since it is the condensate from the gas phase separated in the three phase separator. Even in this oil phase, where the spent scavenger products

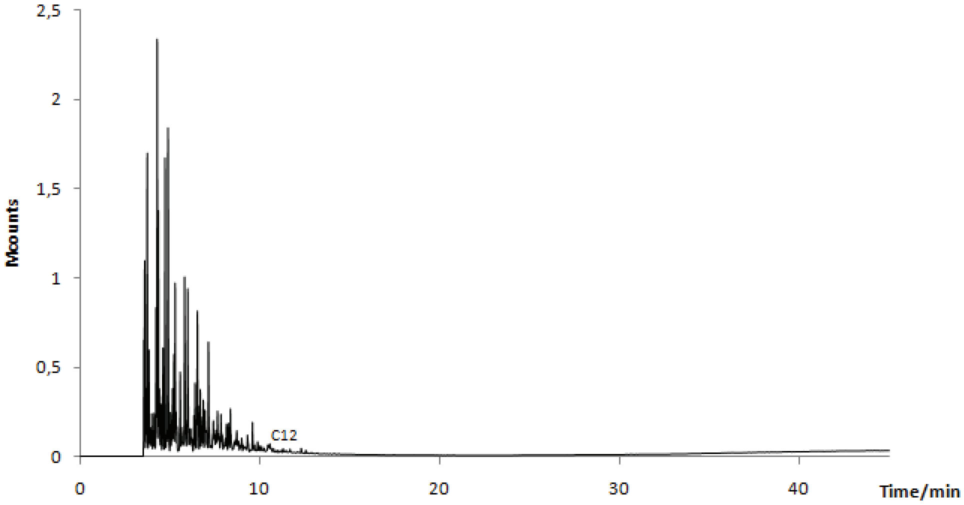

Figure G.7: Oil phase from spent scavenger separator have the highest concentration, no such compounds are detected with the GC-MS. The aqueous phase is also investigated, but no scavenger compounds are transferred to the pentane phase, and a completely flat spectrum is obtained.

Sulphur content

In table G.2 the data for the calibration curve can be seen.

Table G.2: Calibration data

c(S) (mg/L)	Intensity
1	238.0
2	475.5
10	2312.1
20	4662.5

The best fit for these data are equation G.1.

$$\begin{aligned} I &= 232.79 \cdot c(S) \\ R^2 &= 1 \end{aligned} \tag{G.1}$$

In table G.3 the results from the determination of the sulphur content of the oil samples and the aqueous spent scavenger phase can be seen. The amount of sulphur in each

Table G.3: Sulphur content of oil

Sample	m_{sample}	c(S) (mg/L)	S in sample (mg)	S in samples (mg/g)	Average
1	0.4933	8.531	0.427	0.865	
1	1.0066	13.04	0.652	0.648	0.734
1	1.4962	20.61	1.031	0.689	
2	0.5006	7.265	0.363	0.865	
2	0.9993	15.38	0.769	0.648	0.725
2	1.5006	20.41	1.021	0.680	
3	0.4937	7.265	0.363	0.736	
3	1.0049	16.04	0.802	0.798	0.747
3	0.4947	20.17	1.059	0.708	
4	0.5107	9.661	0.483	0.946	
4	1.0044	15.35	0.768	0.764	0.824
4	1.5008	22.89	1.145	0.763	
5	0.5160	0.576	0.029	0.056	
5	1.0500	0.701	0.035	0.033	0.040
5	1.5000	0.891	0.045	0.030	
6	0.5190	51.82	2.591	4.992	
6	1.0102	88.61	4.431	4.386	4.987
6	1.5050	168.0	8.400	5.581	

sample is calculated by multiplying the concentration with the volume of the volumetric flasks. Then the amount of sulphur in the oil can be found by dividing with the weighed amount of oil.

$$S_{oil} = \frac{c(S) \cdot V}{m_{oil}} \tag{G.2}$$

Where V is 50 ml. The amounts of sulphur measured in the oil indicate a lower concentration than for general DUC oil (2.61 mg/g), for which Maersk has supplied information. The investigated oil may therefore be low on sulphur, but it is also possible that some sulphur has been lost during the sample treatment. The results also indicate a slightly higher sulphur concentration in the oil sent to Shell, which could indicate the presence of spent scavenger products. However, with the standard deviation for the average values and general uncertainties in the analysis taken into account, the numbers must be said to be indifferent. The sulphur found in the analyses are probably mercaptans and other sulphur containing compounds of organic origin dissolved in the oil.

It is also seen that the sulphur concentration is 125 times higher in the aqueous spent scavenger phase compared to the oil phase from the spent scavenger. This is in coordinance with equilibrium data supplied by Maersk, which states that close to 99 % of the spent scavenger products should be dissolved in the aqueous phase. The amounts of sulphur led back to the oil is therefore very small, and explains why it does not alter the sulphur concentration of the oil. Due to high background signal of sulphur in the oil, a measurement of the sulphur content can probably not be used as an indication of the amounts of spent scavenger in the oil.

Bibliography

[1] Sigma Aldrich. Available: 14/4-2011, `http://www.sigmaaldrich.com/catalog/ProductDetail.do?lang=en&N4=T88404|ALDRICH&N5=SEARCH_CONCAT_PNO|BRAND_KEY&F=SPEC`.

[2] K. Andersen. Chemical Engineer, Maersk Oil and Gas, Chemistry and Environment.

[3] P. Atkins and R. S. Friedmann. *Molecular Quantum Mechanics*, volume 4th Edition. Oxford University Press, 2008.

[4] P. Atkins and J. Paula. *Elements of Physical Chemistry*, volume 4th Edition. Oxford University Press, 2007.

[5] J. Bakke and J Buhaug. Hydrogen sulfide scavenging by 1,3,5-triazinanes. comparison of the rates of reaction. *Industrial and Engineering Chemistry Research*, 43, 2004.

[6] J. Bakke, J. Buhaug, and J. Riha. Hydrolysis of 1,3,5-tris(2-hydroxyethyl)-hexahydro-s-triazine and its reaction with H_2S. *Industrial and Engineering Chemistry Research*, 40, 2001.

[7] M. Birkholz. *Principles of X-ray Diffraction, in Thin Film Analysis by X-ray Scattering*, volume 1st Edition. Wiley-VCH Verlag GmbH and Co, 2006.

[8] D. S. Breslow and H. Skolnik. *Multi-Sulfur and Sulfur and Oxygen Five- and Six-membered Heterocycles - Part Two*, volume 1st Edition. Interscience publishers, 1966.

[9] F. Egebjerg. Production Technologist, A/S Dansk Shell.

[10] Perkin Elmer. Available: 28/4-2011, `http://las.perkinelmer.com/content/TechnicalInfo/TCH_FTIRATR.pdf`.

[11] H. S. Fogler. *Elements of Chemical Reaction Engineering*, volume 4th Edition. Pearson Education Inc., 2008.

[12] C. M. Hansen. *Hansens Solubility Parameters - A User's Handbook*, volume 2nd Edition. CRC Press - Taylor and Francis Group, 2007.

[13] D. C. Harris. *Quantitative Chemical Analysis*, volume 7th Edition. W. H. Freeman and Company, 2007.

[14] R. L. Horton, R. Stoker, and P. Davis. Process for preventing or remediating trithiazine deposition in high H_2S wells, 2010. United States Patent, M-I LLC Houston TX.

[15] National Toxicology Program interagency program under the US goverment. Toxicological data for DMEA, Available: 18/5-2011, `http://ntp.niehs.nih.gov/ntp/htdocs/Chem_Background/ExSumPdf/DMAE_update_110002.pdf`.

[16] M. A. Kelland. *Production Chemicals for the Oil and Gas Industry*, volume 1st Edition. CRC Press, 2009.

[17] P. Klaboe. The vibrational spectra of 1,4-dithiane and 1,3,5-trithiane. *Spectrochimica Acta*, 25A, 1969.

[18] A. Kohl and R. Nielsen. *Gas Purification*, volume 5th Edition. Gulf Publishing Company, 1997.

[19] R. Krishnaswamy, R. Lacerda, I. Slobodcicov, and E. Campagnolo. Modelling and simulation of hydrogen sulfide removal from petroleum production lines by chemical scavengers. *Chemical Engineering Communications*, 196, 2011.

[20] W. C. Lyons and G. J. Plisga. *Standard Handbook of Petroleum and Natural Gas Engineering*, volume 2nd Edition. Elsevier Inc., 2005.

[21] Kemikalier og Sikkerhed. `www.kemikalier-og-sikkerhed.dk.zorac.aub.aau.dk`, Available: [2011, 16/2].

[22] Maersk Oil. Available: 13/4-2011, `www.maerskoil.com/GlobalOperations/Denmark`.

[23] Geoff Rayner-Canham and Tina Overton. *Descriptive Inorganic Chemistry*, volume 4th Edition. W. H. Freeman and Company, 2006.

[24] Sikkerhedsstyrelsen. Bekendtgørelse nr 4009, gasreglementet - afsnit a. Available: 15/2-2011, https://www.retsinformation.dk/Forms/R0710.aspx?id=55462.

[25] G. Socrates. *Infrared and Raman Characteristic Group Frequencies: Tables and Charts*, volume 3rd Edition. Wiley-VCH Verlag GmbH and Co, 2003.

[26] T. W. Graham Solomon and Craig B. Fryhle. *Organic Chemistry*, volume 8th Edition. Wiley, 2004.

[27] J. G. Speight. *The Chemistry and Technology of Petroleum*, volume 4th Edition. CRC Press, 2007.

[28] Dansk Standard. Determination of total residue and total fixed residue in water, sludge and sediment, 1980.

[29] D. S. Sulivan, A. R. Thomas, J. M. Garcia, and P. Yon-Hin. Method of treating sour gas and liquid hydrocarbon, 1998. United States Patent, Nalco/Exxon Energy Chemicals L.P.

[30] G. N. Taylor and R. Matherly. Structural elucidation of the solid byproduct from the use of 1,3,5-tris(hydroxyethyl)hexahydro-s-triazine based hydrogen sulfide scavengers. *Industrial and Engineering Chemistry Research*, 50, 2011.

[31] Agilent Technologies. Operational manual for Agilent 1100 Series LC/MSD Trap, Esbjerg Institute of Technology - Aalborg University.

[32] Wiley. *Kirk-Othmer Encyclopedia of Chemical Technology*, volume 5th Edition. Wiley-VCH, 2007.

[33] Wiley. *Ullmann's Encyclopedia of Industrial Chemistry*, volume 7th Edition. Wiley-VCH, 1997.

Nomenclature

Aprotic	Aprotic solvents cannot make active hydrogen bonds. Polar aprotic solvents, like aldehydes and ketones, may still take part in hydrogen bonding though. Because of the inability to form hydrogen bonds, aprotic solvents are very poor at dissolving anions, but polar aprotic solvents are still good at dissolving cations, leaving the anions very reactive.
Asphaltenes	Large aromatic molecules, average of around 750 μ, where the aromatic rings are linked by chains of aliphatic and/or naphthenic aromatic ring systems. They are usually defined as the part of the crude oil which is insoluble in n-heptane, but soluble in toluene.
Clastic rock	Rock type composed of pre-existing rock fragments (clasts).
Debye	Non-SI metric unit for electric dipole moment. $1\ \mathrm{D} = 10^{-18}$ statC·cm.
Diffraction angle	The diffraction angle is the angle between the incident and the diffracted light beam.
Gross selection rule	A gross selection rule describes the general features that a molecule must posses if it is to have a spectrum of some kind.
Nominal mass	The nominal mass of a molecule is the sum of the integer mass of the most abundant isotope of the constituent atoms. For example is ^{12}C the most abundant carbon isotope. This is different from the molecular mass, which is the sum of atomic masses found in the periodic table, which is a weighted average of the mass of all the isotopes.
Protic	Forms hydrogen bonds to the dissolved nucleophile, hereby encumbering it and limiting its ability to participate in nucleophilic substitution reactions.
Sedimentary rock	One of three main types of rocks, the other two being igneous and metamorphic rocks. Sedimentary rocks are formed by

	pressure and temperature exerting on sedimentary particles produced by weathering and erosion of the Earth's crust.
Shale	A very fine grained clastic sedimentary rock that is composed of clay minerals and silt sized particles of minerals like quartz and calcite.
sp^3 hybridised	To explain bond angles in molecules, the atomic orbitals may be mixed to form hybrid orbitals. A sp^3 orbital is a hybrid of the s- and all three p-orbitals, which will result in a tetrahedral shape, consisting of four bonds with a bond angle of 109.5 °.
Specific selection rule	A specific selection rule states which change in quantum number may be expected to occur in a transition described by a gross selection rule.
Struture factor	The structure factor is given by $S_{hkl} = \sum_j f_j e^{i(\vec{\rho_j} \cdot \vec{G_{hkl}})}$. Here f_j is the atomic form factor, which gives the scattering amplitude of a wave by an isolated atom. For X-rays the scattering amplitude increases with atomic number. $\vec{\rho_j}$ is the position vector for the atoms in the basis of the lattice. Simple cubic lattices have a one atom basis, bcc lattices have a two atom basis and fcc lattices have a four atom basis. Finally $\vec{G_j}$ is the reciprocal lattice vector.
VSEPR	Valence Shell Electron Pair Repulsion. A theory that is used to predict the geometric structure of molecules based on the principle that valence electrons will arrange themselves in such a way as to maximise the distance between them to achieve least repulsion.